Pilot Reuse in Distributed Massive MIMO Systems

A Thesis Submitted to The University of Kent

For The Degree of Doctor of Philosophy

In Electronic Engineering

By

Ramiz Sabbagh

March, 2019

Supervisor

Professor Jiangzhou Wang

Dedication

I dedicate this work to my beloved wife, Reem, who has been a constant source of support and encouragement during the challenges of my Ph.D. studies, and for all the sacrifices she makes everyday. I am truly grateful for having you in my life.

I wish to express my heartfelt love to my beautiful daughters, Alma and Anna, whose existence has given me the extra strength and motivation to get things done during the course of my study.

This work is also dedicated to my great mother, for her endless love, affection, encouragement and prayers. I would much prefer it if you were well enough to share with me this success.

Acknowledgements

First, I would like to express my sincere gratitude to my supervisor, Prof. Jiangzhou Wang, for the continuous support throughout my Ph.D. studies and related research, and for his patience, motivation, and immense knowledge. His guidance helped me in all the time of research. I learned much from his insight. I would like to thank you very much for your support and understanding over these past four years.

I would also like to thank my co-supervisor, Dr. Huiling Zhu, for her help, advice, insightful questions and constructive feedback on my research. I have benefited tremendously from her enthusiasm and invaluable comments. She deserves many thanks for her continued interest and guidance throughout my work.

I would like to thank Dr. Cunhua Pan from Queen Mary University of London, for his feedback and cooperation on my research work. I am also deeply grateful to Dr. Emil Björnson from Linköping University for his unfailing support to me and to all researchers everywhere. I am grateful for the constructive and valuable comments provided by Ruth Keene when helping me with the editing of my work. Furthermore, I would like to express my gratitude to Prof. Martin Ridout and Dr. Stella Hadjiantoni from the School of Mathematics, Statistics and Actuarial Science for their valuable support and assistance.

I am also very grateful to all the teaching and research staff of the school of Engineering

and Digital Arts, who have taken some time to discuss and enrich my work. I would like to thank all past and current Ph.D. colleagues at the Communication Research Group, particularly to mention: Wael Ali, Ali Mahbas, Asaad Daghal, Hind Albasry, Osama Alluhaibi, Kenan Al-Hares, for the wonderful time. I have enjoyed many discussions with them on various technical and non-technical topics. In addition, a warm word for my great friend and colleague in Ninevah University, Qusai Sultan, who has always been a major source of support when things would become a bit discouraging. Thank you all for making my years of study a wonderful experience.

I gratefully acknowledge the Iraqi government, Ministry of Higher Education and Scientific Research and Ninevah University for their financial support. Without it, I would not have been able to study abroad and complete my Ph.D. program.

A very special word of thanks goes to my parents, sisters and brothers, for their unconditional love, support and cooperation throughout my life. You deserve my wholehearted thanks. I would not be who am I today without you all.

My deepest gratitude and love belongs to my wife Reem, for her tremendous understanding, patience, care, and love through the process of researching and writing this thesis. This accomplishment would not have been possible without her.

Above all, to the Great Almighty, the author of knowledge and wisdom, for his countless love, strength and encouragement He has given me, and for being always there for me. Thank you for letting me succeed through all the difficulties.

List of Publications and Submissions

1. R. Raoof, C. Pan, H. Zhu and J. Wang, "Dynamic Pilot Reuse in Distributed Massive MIMO Systems," 2017 IEEE 85th Vehicular Technology Conference (VTC Spring), Sydney, NSW, 2017, pp. 1-5.

2. R. Sabbagh, H. Zhu and J. Wang, "Pilot Allocation and Sum-Rate Analysis in Distributed Massive MIMO Systems," 2017 IEEE 86th Vehicular Technology Conference (VTC-Fall), Toronto, ON, 2017, pp. 1-5.

3. R. Sabbagh, C. Pan and J. Wang, "Pilot Allocation and Sum-Rate Analysis in Cell-Free Massive MIMO Systems," 2018 IEEE International Conference on Communications (ICC), Kansas City, MO, 2018, pp. 1-6.

4. R. Sabbagh, H. Zhu, W. Ali and J. Wang, "User-Centric Based Pilot Assignment for Cell-free Massive MIMO Systems," Submitted to IEEE Transactions on Wireless Communications.

Abstract

Distributed massive multi-input multi-output (MIMO) is an attractive technology to meet the vast growth in the requirements for huge data rates in future wireless communication systems. To realise the gains of the distributed massive MIMO, the central processing unit (CPU) typically needs to estimate the channels between the remote radio heads (RRHs) and the user-equipments (UEs) from mutually orthogonal pilots sent by UEs. The channel coherence is limited in time as well as frequency, causing a trade-off between the resources spent on pilots and those allocated for data symbols. The reuse of pilots is needed to reduce the pilot overhead, when a large number of UEs are being simultaneously served. This, in turn, introduces pilot interference in the channel estimation phase. In this thesis, the problem of pilot allocation is investigated, with the aim to smartly and efficiently reuse the pilots among UEs in different distributed massive MIMO scenarios by utilising the user-centric clustering approach.

Within the cellular distributed massive MIMO (DM-MIMO), a novel dynamic pilot reuse (DPR) scheme is proposed by assuming the pilot reuse inside the same cell of a dense DM-MIMO network. Since the pilot reuse directly affects the UEs' data-rate, the DPR scheme is developed with the objective of maximising the uplink sum-rate by allowing two UEs separated by a sufficient distance and satisfying a particular signal-to-interference-plus-noise ratio (SINR) constraint to share the same pilot. In order to achieve the objective, an expression of the SINR is firstly derived for any UE sharing its pilot with another. A novel low-complexity algorithm is then presented to reuse the pilots based on the separation distance between UEs. The iterative grid search (IGS) method is also employed to find the optimum SINR threshold with the aim to maximise the sum-rate. The simulation results have demonstrated the superiority of the DPR scheme over other

reuse schemes based on the uplink sum-rate performance.

Another novel user-centric based pilot assignment scheme is presented in the cell-free (CF) massive MIMO network to minimise the maximum estimation error for UEs subject to some practical constraints. This scheme depends on allocating pilots with fewer reuse times to the UEs with the weakest channel conditions, while the UEs with good channel qualities adopt pilots with higher reuse times. Two novel low-complexity algorithms are developed to perform the two stages of this pilot reuse scheme. Furthermore, a novel problem is addressed considering the effect of pilot allocation on the satisfaction of UE's quality of service requirements, in terms of SINR. The problem is solved by utilising another two algorithms to minimise the number of pilots and the average channel estimation error subject to a specific SINR threshold. The simulation results reveal the superiority of the proposed scheme over the existing ones, and its average channel estimation error performance approaches that of the exhaustive search with much lower complexity. Furthermore, increasing the number of pilots initially improve the SINR, but when the number of pilots is significantly increased, this does not improve the SINR further.

Contents

List of Figures

List of Tables

Abbreviations

2G ..... Second Generation

3G ..... Third Generation

4G ..... Fourth Generation

5G ..... Fifth Generation

AP ..... Access Point

AWGN ..... Additive White Gaussian Noise

AoA ..... Angle of Arrival

CF ..... Cell-free

CPU ..... Central Processing Unit

CSI ..... Channel State Information

C-RAN ..... Cloud Radio Access Network

CAS ..... Co-located Antennas System

CoMP ..... Coordinated Multipoint

CDF ..... Cumulative Distribution Function

DFT ..... Discrete Fourier Transform

DAS ..... Distributed Antennas System

DM-MIMO . Distributed Massive MIMO

DPR ..... Dynamic Pilot Reuse

EB ..... Exabytes

FDD ..... Frequency-division Duplexing

i.i.d ..... Independent and Identically Distributed

IoT ..... Internet of Things

IGS ..... Iterative Grid Search

LS ..... Least-squares

LTE ..... Long Term Evolution

M2M ..... Machine to Machine

MRT ..... Maximum-ratio Transmission

MMSE ..... Minimum Mean Squared Error

MIMO ..... Multiple-input-multiple-output

NMSE ..... Normalized Mean Square Error

QoS ..... Quality of Services

RRH ..... Remote Radio Head

RU ..... Resource Unit

SINR ..... Signal-to-interference-plus-noise Ratio

SVD ..... Singular Value Decomposition

SE ..... Spectral Efficiency

3GPP ..... Third Generation Partnership Project

TDD ..... Time-division Duplexing

UE ..... User-equipment

ZF ..... Zero Forcing

List of Symbols

$\mathbb{B}$ ..... Number of RRH Tiers in a DM-MIMO Cell

N ..... Number of RRHs in the Cell/CF System

$\mathcal{N}$ ..... Set of RRHs in the Cell/CF System

$\mathbb{N}$ ..... Number of Serving RRHs per UE

N_k ..... Set of RRHs Serving UE k

N_i ..... Set of UEs Served by RRH i

$\bar{K}$ ..... Total Number of UEs in the Cell/CF System

$\bar{\mathcal{K}}$ ..... Set of All UEs in the Cell/CF System

K ..... Number of Admitted UEs in the Cell/CF System

$\mathcal{K}$ ..... Set of Admitted UEs in the Cell/CF System

$\mathcal{K}_\pi$ ..... Group of UEs Sharing the π^{th} Pilot Sequence

M ..... Number of Antennas per RRH

$\mathcal{M}_i$ ..... Set of Antennas per RRH

S ..... Number time-frequency RUs per Coherence Interval

B ..... Number RUs for Pilot Signalling per Coherence Interval or Number of Available Pilots

$\mathcal{Q}$ ..... Available Pilot Index Set

$\mathbf{Q}$ ..... Available Orthogonal Pilot Signals Set

$\mathcal{P}(\mathcal{K}, \mathcal{Q})$ ..... Arbitrary Pilot Reuse Scheme

$g_{k,i,m}$ ..... Uplink Estimation Response for the k^{th} UE to the m^{th} Antenna in the i^{th} RRH

$\alpha_{k,i}$ ..... Large-scale Fading Coefficient Between the k^{th} UE to the i^{th} RRH

$\mathbf{g}_{k,i}$ ..... Uplink Estimation Response from the k^{th} UE to the i^{th} RRH

$\mathbf{Y}_i$ ..... Received Signal Matrix of Pilots at the i^{th} RRH

$\mathbf{N}_i$ ..... Uplink Pilot Transmission AWGN

ρ_p ..... Transmit Power During Pilots Uplink Transmission

$\mathbf{y}_{p,k,i}$ ..... CPU Observation of the Uplink Estimation from the k^{th} UE to the i^{th} RRH

$\tilde{\mathbf{g}}_{k,i}$ ..... MMSE Estimation Error of $\mathbf{g}_{k,i}$

$\mathbf{y}_{d,i}$ ..... Received Data Signal Vector for the i^{th} RRH

ρ_d ..... Transmit Power for Data Uplink Transmission

$\mathbf{z}_{d,i}$ ..... Uplink Data Transmission AWGN

x_k ..... Uplink Transmitted Data Signal from the k^{th} UE

$\hat{\mathbf{G}}_i$ ..... Estimated Uplink Estimation Response Matrix from All UEs to the i^{th} RRH

$\mathbf{Z}_i$ ..... Covariance Matrix of the Uplink Estimation Estimation Errors for the i^{th} RRH

$\hat{\mathbf{a}}_{k,i}$ ..... MMSE Detection Vector for the k^{th} UE at i^{th} RRH

R_T ..... Uplink Ergodic Achievable Sum-rate

$\mathbf{SINR}_{\langle k,k' \rangle}$ ... Uplink SINR of the k^{th} UE When Its Pilot is Shared with the k'^{th} UE

$\mathbf{SINR}_k$ ..... Uplink SINR of the k^{th} UE Without Pilot Reuse

ω ..... Number of Times of Pilot Reuse in the DPR Scheme

$\mathbb{F}$ ..... Number of UE Pairs the DPR Scheme

γ_{th} ..... SINR Threshold

$\mathbb{N}_b$ **and** $\mathbb{T}$ .... IGS Method Parameters

Δ ..... Subinterval of IGS Method

$\gamma_{max}^{(n)}$ ..... Maximum Threshold of n^{th} Iteration the of IGS Method

$\gamma_{min}^{(n)}$ ..... Minimum Threshold of n^{th} Iteration the of IGS Method

γ_{min} ..... Minimum Threshold of the IGS Method

γ_{max} ..... Maximum Threshold of the IGS Method

$(\cdot)^T$ ..... Transpose of a Matrix

$(\cdot)^*$ ..... Conjugate of a Matrix

$(\cdot)^H$ ..... Hermitian Transpose of a Matrix

$\mathbb{E}\{\cdot\}$ ..... Expectation Operation

$\hat{a}$ ..... Estimated Value of a

$\mathbf{I}_N$ ..... $N \times N$ Dimensional Identity Matrix

$\mathbf{tr}(A)$ ..... Trace of A

$\mathbb{C}^{M \times N}$ ..... Set of Complex Matrices with M Rows and N Columns

$\mathbf{h}_{i,k}$ ..... Downlink Channel vector from RRH i to UE k

$\mathbf{w}_{i,k}$ ..... Precoding-vector from RRH i to UE k

s_k ..... Data Symbol for UE k Sent by the Serving Cluster of RRHs

$\rho_{i,k}$ ..... Transmit Power Assigned to UE k from RRH i

z_k ..... Downlink Data Transmission AWGN

y_k ..... Downlink Received Signal at an Arbitrary UE k

$\hat{\mathbf{h}}_{i,k}$ ..... MMSE Estimation of the Estimation $\mathbf{h}_{i,k}$

$\tilde{\mathbf{h}}_{i,k}$ ..... MMSE Estimation Error of $\hat{\mathbf{h}}_{i,k}$

$\theta_{i,k}$ ..... Variance of the MMSE Estimation ($\hat{\mathbf{h}}_{i,k}$)

$\psi_{i,k}$ ..... Variance of the MMSE Estimation Error ($\tilde{\mathbf{h}}_{i,k}$)

$NMSE_{i,k}$ .... Normalized Mean Square Error (NMSE) of the $\hat{\mathbf{h}}_{i,k}$

ξ_k ..... Aggregated NMSE per UE k

$\bar{\xi}$ ..... Average NMSE for All UEs in $\mathcal{K}$

$SINR_{k_{min}}$ .... Lower-bound SINR for UE k

P_i ..... Total Power Transmitted by RRH i

$R_{T_{min}}$ ..... Lower-bound of the Downlink Ergodic Achievable Sum-rate of All UEs

g_l ..... Number of Times the l^{th} Pilot Sequence, $l \in \mathcal{Q}$

G ..... Limit of the Number of Times of Reuse a Pilot

η_k ..... A Metric to Evaluate the Estimation Quality of the UE k

Υ_k ..... A Metric to Evaluate the Pilot Contamination Caused by UEs Sharing the Same Pilot Sequence with UE k

h ..... A Minimum Number of Pilots Needed to Serve All the UEs in the CF Network

$\mathcal{P}(\mathcal{K}, \mathcal{Q})$ ..... Arbitrary Pilot Reuse Scheme with UEs Set $\mathcal{K}$ and Pilot Set $\mathcal{Q}$

$\mathbf{\Lambda}$ ..... Binary Matrix to Show the Relationship Between UEs Based on (4.13b)

$\mathcal{Q}^{used}$ ..... Used Pilot Set in **Algorithm 4.1**

$\mathcal{Q}^{temp}$ ..... Temporary Pilot Set in **Algorithm 4.1**

$\mathcal{Q}^{un}$ ..... Unlinked Pilot Set in **Algorithm 4.1**

$\aleph_k$ ..... Number of Connections the UE k Adopts with Other UEs in the Undirected Graph

h_s ..... Minimum Number of Pilots Needed to Serve All the UEs in Problem $\mathcal{P}_e$

$\mathcal{V}$ ..... Set of UE Set Partitions

$\mathcal{L}_{v_f}$ ..... Subsets of ${v_f}^{th}$ Partition

$\left\{ \right\}$ ..... Stirling Number of the Second Kind

a_i ..... Distinct Numbers That Appear in the Partition

r_i ..... Number of Times That a_i is Repeated

$d_{i,k}$ ..... Distance Between the i^{th} RRH to the k^{th} UE Measured in km

$\wp_{i,k}$ ..... Shadow Fading Possessing a Lognormal Distribution

σ^2_{shad} ..... Shadow Fading Standard Deviation

R ..... Cell Radius

Chapter 1

Introduction

1.1 Motivation

The demands for high data rates and efficient use of different resources have been motivating the rapid evolutions in mobile networks. According to the Ericsson Mobility report, for the near future, the total mobile data traffic will experience a 43% annual increase from 2018 to 2023 to reach 107 Exabytes (EB) per month by the end of 2023 as shown in Figure 1.1 [1]. Meeting this growing amount of data traffic is a critical issue for wireless systems. While the fourth generation (4G) mobile systems have approached theoretical capacity, the fifth generation (5G) mobile networks is to be launched in 2020 to deal with growing expectations of quality of services (QoS) [3]. Another significant requirement that customers anticipate is the availability of equally good services anywhere [4]. The demand for wireless data connectivity is an additional challenge that will continue to increases in the near future. The fully networked society will be a feature of the 5G mobile networks, where all electronic devices are connected to the Internet as well as communications, such as machine-to-machine (M2M), Internet of things (IoT), etc, need to be supported beside personal communications [2]. Moreover, on the basis of

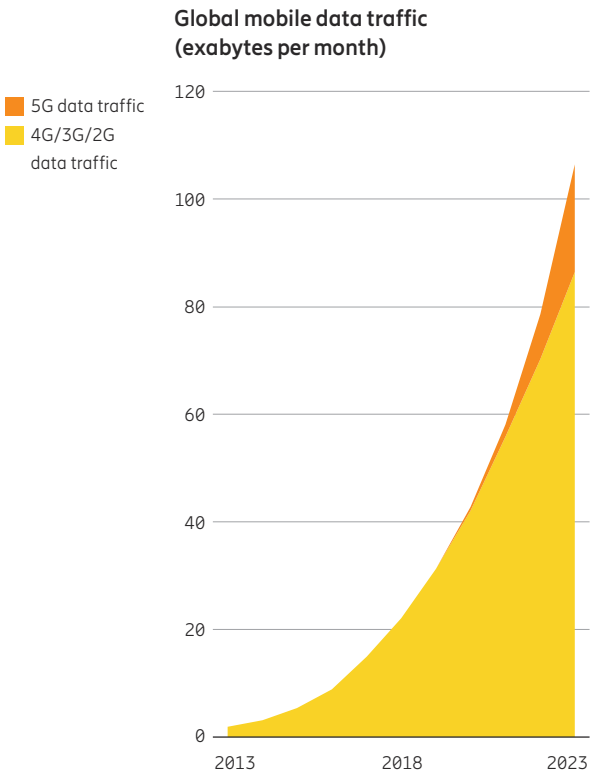

Figure 1.1: Global mobile data traffic (EB per month) (Source: Ericsson) [1].

the Ericsson Mobility Report [1], the number of connected devices including the IoT, and other devices such as mobile phones, is expected to reach 31.4 billion in 2023. Therefore, it is essential to deal with all these intense demands through designing new revolutionary wireless network technologies.

To deal with the above mentioned challenges in the forthcoming wireless networks, various new approaches have been proposed. One of the promising technologies is the distributed massive multi-input multi-output (DM-MIMO). The traditional DM-MIMO is implemented in a cellular structure [5–8]. In this thesis, the term DM-MIMO is used to refer to this traditional form with a cellular topology. The key idea with DM-MIMO is to allow a set of low-functionality remote radio heads (RRHs) to jointly serve the user-equipments (UEs) within the cell with less transmission distance, so that better coverage,

power saving and capacity merits than a co-located massive MIMO are obtained [9–13]. The RRHs in each cell are linked to a central processing unit (CPU) where the signal processing and resource allocation operations are achieved. Each UE in the cell is only served by the RRHs in that cell. In DM-MIMO, scaling up the number of antennas equipped with RRHs brings the benefits of the massive MIMO, such as delivering high performance in terms of spectral and energy efficiency [14–16].

In the cellular topology in which the DM-MIMO is implemented, a cell covers a limited number of UEs [5, 6, 16]. As previously mentioned, future wireless networks have to handle billions of devices, human UEs and machine-type communications. More practical networks are needed to manage the resources more efficiently than the cellular systems, and to be able to meet the huge demand for wireless connectivity [15]. Thus, a new form of DM-MIMO has been proposed under the name of cell-free (CF) massive MIMO where the concept of cells is not considered [15, 17–20]. CF massive MIMO network is designed to cover a large geographical area by utilising a CPU and a number of RRHs distributed within the coverage area to jointly serve the UEs. Similarly to the conventional DM-MIMO, the baseband signal processing operations in the CF network are performed in the CPU. A set of RRHs can be utilised to provide equally good service for all UEs in the network. In addition, high-bandwidth low-latency fronthaul links, such as fibre optic, are employed to connect the RRHs to the CPU in the network. Owing to its architecture and the centralised signal processing ability, CF massive MIMO can adapt to non-uniform loaded scenarios and manage the resources more efficiently than the traditional cellular systems. It is necessary to clarify here the relationship between the cloud radio access network (C-RAN) and the CF massive MIMO. In C-RAN, the baseband processing is moved from the access points to the cloud. CF massive MIMO means that many distributed access points are serving the UEs by coherent joint transmission. These two methods can

be used together, but C-RAN can be also used with conventional base stations and/or cell-free without C-RAN [21].

The computational complexity in the CPU is a challenge due to the huge signal processing and resources allocation operations that need to be performed there. Therefore, an efficient clustering method called user-centric is invoked in this thesis to achieve low-complexity in the CF massive MIMO and DM-MIMO networks [22–24]. In this method, each UE is served by a set of the nearest RRHs based on the fact that the far away RRHs contribute little to the UE's signal quality. This may result in that the clusters serving different UEs might be overlapped.

The local channel state information (CSI) approach is assumed in this thesis, as described in [25], in order to avoid dealing with huge quantity of CSIs. This approach includes measuring the CSI between any UE to only its serving cluster and this is called the intra-cluster CSI. On the other hand, only the large-scale fading can be provided for RRHs outside UE cluster set, and this is named the inter-cluster CSI. The acquisition of the large-scale fading can be obtained easily in practice due to the slow rate at which it varies compared to the small-scale fading.

1.2 Challenges

As the CSI is required to be known at the transmitter, massive MIMO systems generally exploit the channel reciprocity. This can be fulfilled with the help of the time-division duplex (TDD) protocol. When the CSI is measured through pre-defined orthogonal pilot signals transmitted by UEs in the uplink in every coherence interval, the CSI will also be valid during the downlink transmission due to the channel reciprocity. The obtained channel estimates are utilised to perform data detection in the uplink and to beamform

data to the UEs in the downlink. The channel estimation needs to be achieved within each coherence interval, which is limited in specific time and frequency intervals. Assigning orthogonal pilot sequences to UEs becomes challenging as unaffordable pilot resources are required and that increases linearly with the number of UEs. Hence, it is necessary to allow some UEs to share the same pilot especially when the number of UEs is high and that is to be expected in the future networks, as explained earlier. The reuse of pilot signals incurs what is known as pilot contamination when a RRH receives a superposition of undesired UEs' pilot signals and this leads to a corrupted CSI estimation and sizeable estimation error. Therefore, a smart pilot assignment scheme should be developed to reduce the pilot overhead, while guaranteeing the quality of service (QoS) for UEs to be satisfied.

1.3 Contribution of the Thesis

The key contributions of this thesis are summarized as follows:

1. A novel dynamic pilot reuse (DPR) scheme is proposed to allow a pair of UEs to share a single pilot sequence within the same cell of the dense DM-MIMO system with adopting the user-centric approach. Specifically, the proposed reuse scheme achieves the objective of maximising the uplink achievable sum-rate subject to UEs' signal-to-interference-plus-noise ratio (SINR) requirements and pilot resources constraints. Under the proposed pilot reuse scheme, the SINR expression is derived for any UE sharing its pilot with another UE by utilising both minimum mean squared error (MMSE) detection and channel estimation. A low-complexity algorithm is then developed to allow reusing the pilots based on the separation distance between UEs. The iterative grid search (IGS) method is also employed to find the threshold

that can be utilised in the proposed algorithm to maximise the sum-rate. Finally, simulation results are presented to show the effectiveness of the DPR scheme with the optimised threshold in terms of the uplink achievable sum-rate.

2. Another novel user-centric based pilot assignment scheme is proposed in the CF massive MIMO network to deal with the UEs suffering low channel quality and with a high probability of delivering a bad rate performance due to the high estimation error when pilots with high pilot reuse are allocated to them. The pilot allocation scheme is developed to minimise the maximum channel estimation error with the constraints of a limited number of pilot reuse times and allocating different pilots to the UEs served by at least one common RRH. The design of this scheme includes two stages. The first one aims to find the minimum number of pilots required to serve all UEs in the system when the aforementioned constraints are applied. This stage relies on the the graph colouring after applying the Dsatur algorithm [26]. UE selection is adopted here to remove some UEs when the minimum number of pilots needed is higher than the number of available pilot sequences. In the second stage, pilots are allocated to satisfy the objective of minimising the maximum estimation error. The allocation of pilots depends on assigning pilots with fewer pilot reuse times to UEs with the worst channel quality. Two algorithms are additionally proposed to perform both the initial stage and the pilot assignment in the second stage. The downlink sum-rate analysis is also included when the impact of the proposed allocation scheme is taken into account along both the local CSI and the user-centric approaches.

3. By utilising the same idea of the proposed pilot allocation scheme of the CF massive MIMO network, a second problem has been presented to link the channel estima-

tion error with the sum-rate performance which, to the author's best knowledge, has not been investigated before for the user-centric based CF massive MIMO. In this problem, both the number of pilots and the average channel estimation error are minimised subject to a particular SINR threshold per UE in addition to the constraints of the first problem. Furthermore, another two algorithms are presented to satisfy this objective with the constraints.

1.4 Thesis Outline

The structure of this thesis is based on five chapters and an appendix as follows:

In Chapter 1, the motivation and the challenges of the CSI acquisition are discussed. The main contributions of this thesis are summarised, and the thesis contents are outlined.

In Chapter 2, a brief introduction about the wireless channel is given. After that, massive MIMO, and specifically both DM-MIMO and CF massive MIMO networks are described. The pilot-based channel estimation together with the issue of pilot contamination are then discussed. The state of the art on pilot assignment design in both the DM-MIMO and the CF massive MIMO networks are finally listed.

In Chapter 3, the system model of a single cell DM-MIMO network is first introduced. The DPR scheme is then proposed along analysing the sum-rate performance when the pilot reuse is taken into consideration. Finally, simulation results in terms of the uplink achievable sum-rate are included to evaluate the performance of the DPR scheme.

In Chapter 4, the signal transmission model of the CF massive MIMO network is introduced in addition to the channel estimation for intra-cluster CSI and the downlink sum-rate performance. The proposed pilot allocation scheme in CF massive MIMO is then presented. After that, the channel estimation error minimisation problem is developed

while a SINR threshold is satisfied. Different algorithms are presented to solve these problems. The complexity analysis of the proposed algorithms are further discussed. Finally, extensive simulation results are produced to assess the proposed algorithms and to show the impacts of various parameters on the performance of the proposed schemes.

In Chapter 5, the conclusions of this thesis are drawn, and future research directions are discussed.

In Appendix A, the explicit formulas of the parameters of equations (3.13) and (3.14), and the derivation of equation (4.10) are all included.

A list of the related publications to this work is provided on page v.

Chapter 2

Theoretical Background and Literature Review

This chapter provides many of the basic concepts related to wireless channels, massive MIMO system and pilot-based channel estimation in this system. These concepts will be utilised in other parts of this thesis. A description of the wireless propagation environment is initially introduced in Section 2.1. After this, it is observed in Section 2.2 that the channel can be seen as approximately constant within a particular time and frequency intervals. An overview of the concept of massive MIMO system is discussed in Section 2.3, with a focus on both the traditional cellular distributed massive MIMO (DM-MIMO) and the cell-free (CF) massive MIMO. Section 2.4 provides insights into the user-centric approach. The channel estimation in massive MIMO with a distributed setup is explained in Section 2.5 including the challenges of high pilot overhead and pilot contamination which are the main motivations of this thesis. Finally, Section 2.6 includes some of the works related to the pilot allocation design and pilot overhead reduction.

2.1 The Wireless Channel

A signal propagating through space is highly affected by the environment. Propagating the radio signal with distance causes the signal power to be attenuated. Further impacts that the outdoor channels include are the scattering, diffraction and reflection which all influence the radiated energy. Such phenomena arise from different interfering objects in the environment, for instance buildings and trees. These objects lead to what is known as Multi-path Propagation where the transmitted signal arrives at the destination through several different paths, with each path differs from the others in both the delay spread and the attenuation [27].

2.1.1 Path-loss

When a signal is propagated through an ideal free space, the signal power is attenuated due only to the Free-space Path-loss. Far from the transmitting antenna, the signal suffers an inverse square law power loss which indicates that the power density of the signal is reduced with a square of the propagating distance from the transmitter. In addition, free-space path-loss is proportional to the square of the frequency of the radio signal[1]. In the case of mobile networks, where the signal is transmitted over a ground plane, a part of the transmitted signal is reflected by the ground's surface and might be destructively interfered with the primary path. The power density in such a scenario experiences a path-loss exponent of 4. However, the path-loss exponent value is normally in the range of 2.5 to 6 in real urban environments based on the terrain and different environmental factors - for instance the foliage [27, 28].

[1]In Chapter 3, a simple large-scale fading coefficient formula is used that does not include the effect of the frequency on the path-loss. In Chapter 4, another formula is utilised for the large-scale fading that works in the range from 2 to 6 GHz.

2.1.2 Shadow Fading

Radio signals can be significantly attenuated due to large objects such as a hill or large building, positioned between the transmitter and receiver. These obstacles create shadow zones that occupy an area exceeding the wavelength of the signal carrier. The large scale attenuation is created due to shadow fading for the period in which the terminal exists in the shadow region of the object. Even when the main signal is completely obscured, some parts of the signal power can still reach the terminal when the radio signal experiences diffraction at the edges of the scatterer. Shadow fading is more likely to arise in urban environments where many large objects can exist. It has been found that the logarithm of attenuation generated by shadow fading due to various shadowing effects of building and natural features approaches the normal distribution. Therefore, this kind of fading is also described as lognormal fading [27, 28].

2.1.3 Small-scale Fading

Scattering and other factors such as reflection and diffraction that the propagating signal undergoes while travelling through a radio channel cause the multi-path propagation. This implies that the signal reaches the receiving antenna along various paths, each adopting different attenuation and phase shift as mentioned earlier. These multi-path signals can be combined constructively or destructively at the destination, creating another type of fading called Small-scale Fading. It represents the short term variation of the received signal power level. In the environments where no line of sight and a large number of uncorrelated scattered components exist, and this is usual in the urban areas, then the in-phase and quadrature components of the received signal can be assumed to follow independent zero-mean Gaussian processes, and this is known as Rayleigh fading [27, 28].

2.1.4 Doppler Effect

Another effect that the transmitted signal might experience is the Doppler shift, which particularly appears when the terminal is in motion relative to the transmitting antenna. This mobility produces a Doppler shift in the frequency of the corresponding multi-path signals. The quantity of Doppler shift is determined by both the velocity of the terminal with respect to the incoming signal and the carrier frequency. The combined impact of the Doppler shifts from different multi-path components causes the expansion of the received signal spectrum, and this is known as frequency dispersion. The channel response due to frequency dispersion varies with time, and this effect is referred to as the time-selective fading. The aggregated impact of all of the path-loss, large- and small-scale fading, and Doppler shift can be considered as the main factors that influence the signal transmitted over a radio channel [27, 28].

2.2 Channel Coherence

The multi-path components mentioned above generate small-scale fading due to the constructive and destructive interference of these components at the receiver, based on their path lengths. In multi-path channels, the phase shift of multi-path signals changes with frequency, resulting in frequency-varying small-scale fading. In this case, the Coherence Bandwidth can be defined as the frequency interval over which the channel is approximately constant. The frequency selective channel describes the case when the signal bandwidth is larger than the coherence interval, otherwise the channel is said to be frequency flat. Due to Doppler shift, the channel can suffer a time-selective fading too as explained earlier. Similarly, the time in which the channel is viewed as time-invariant is the Coherence Time. The propagation channels in outdoor environments experience

both frequency- and time-selective fading. Within the block of coherence time interval and frequency coherence interval, the channel response can be considered as constant and flat-fading. It is therefore necessary to perform the channel estimation via training in each coherence interval to measure the channel effects, that discussed in Section 2.1, on the transmitted signals. For communication systems, a coherence block consists of a number of time-frequency resource units (RUs). As an example, a single RU in the Long-Term Evolution (LTE) downlink grid comprises of duration 71.4 μs and a bandwidth of 15 kHz [2, 27, 28].

Three parameters determine the size of a coherence block: UE speed, carrier frequency and phase differences in the multi-path propagation. Each UE has its own coherence bandwidth and coherence time. However, in practice, the worst condition of the propagation scenario should be considered in deciding the size of the coherence block. In addition, when the coherence bandwidth and coherence time of a UE is much greater than the coherence block, it is not necessary to measure the channel estimate in every block [2]. In this thesis, and for the sake of simplicity, it is assumed that all UEs need to estimate that channel in each coherence block.

2.3 Massive MIMO System

Massive MIMO is a scalable version of multi-user MIMO, which originally appeared in [14]. In the massive MIMO, hundreds or thousands of base station antennas are deployed to serve tens of UEs simultaneously. This technique provides promising gains in both spectral and energy efficiencies over the conventional multi-user MIMO systems. The serving antennas can be employed either in a compact co-located form or in a distributed manner. However, the focus now is on the co-located massive MIMO as illustrated in

Figure 2.1(a). The distributed massive MIMO will be discussed later in Subsections 2.3.1 and 2.3.2.

All UEs in massive MIMO utilise the full time-frequency resources simultaneously in both the uplink and downlink transmissions. That significantly increases the spectral efficiency over current systems. On the uplink of massive MIMO, the signals transmitted by the UEs are detected by the base station. The base station on the downlink works on ensuring that each UE delivers only its own signal. The multiplexing and de-multiplexing signal processing operations at the base station can be possibly performed with the availability of a large number of antennas along the CSI information. The base stations are designed to deal with the burden of processing complexity aiming to achieve high rate performance at UEs even if they utilise cheap and single antennas terminals [28–30].

Employing more antennas in the massive MIMO system produces a large number of degrees of freedom, which enables the base station to form sharp beams focusing toward the UEs by using simple linear processing techniques. Increasing the number of antennas in base stations makes the UEs' channel directions asymptotically orthogonal to a significant extent, and this is known as the Favourable Propagation. Thus, simple signal processing can work nearly optimally with the linear combining/precoding schemes in the uplink/downlink transmissions, respectively. The availability of narrow beams to each UE facilitates mitigating intra-cell interference between these UEs. However, the impact of pilot contamination on the channel estimates due to pilot reuse is still the dominant inherent limitation of massive MIMO [2,14,29]. This will be further discussed in Subsection 2.5.1.

An additional consequence of increasing the number of antennas is that the power can be sharply focused onto the UEs, and thereby the radiated power can be reduced. Therefore, higher energy efficiency by an order or more of magnitude can be achieved.

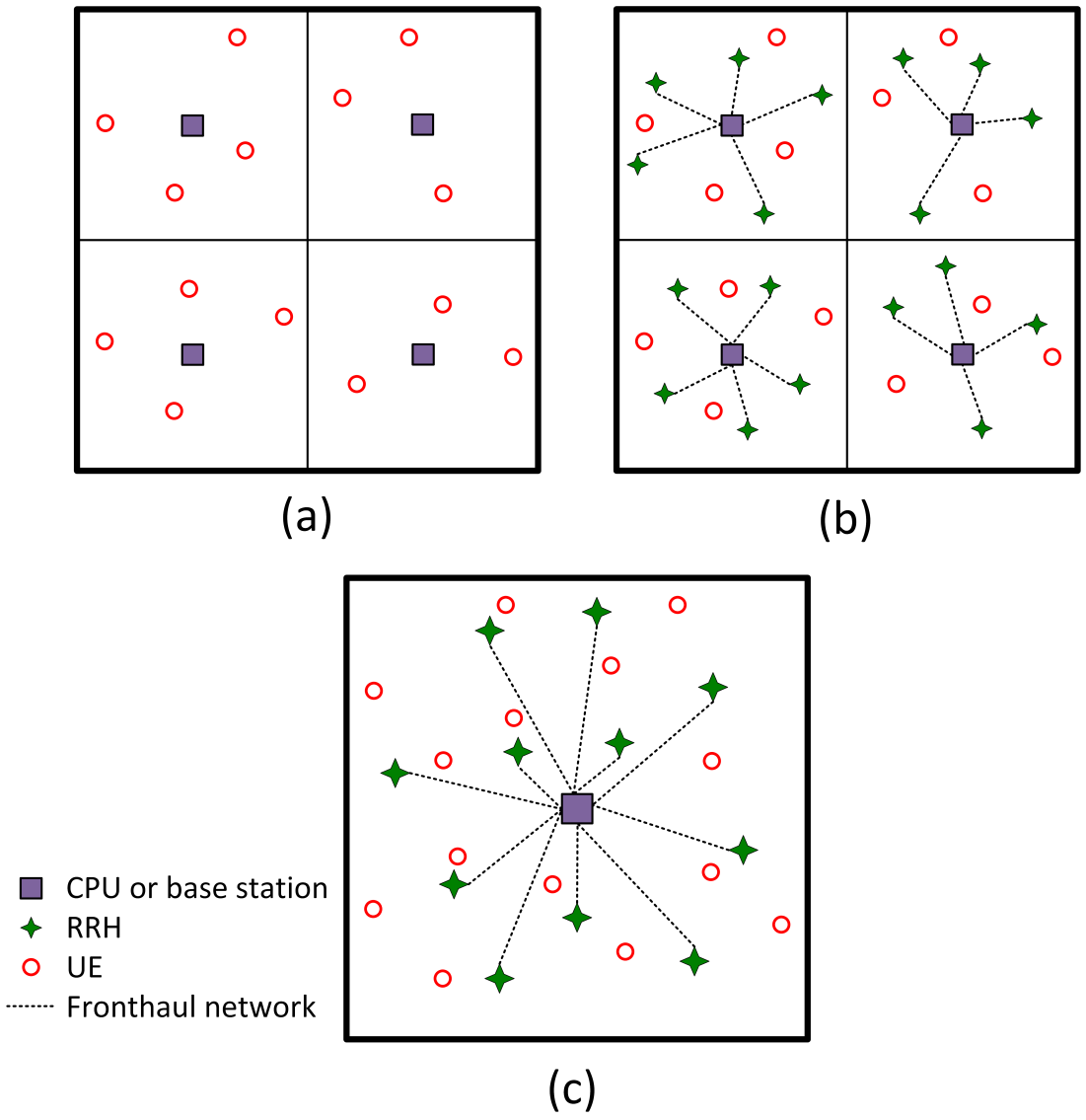

Figure 2.1: Structure of different massive MIMO systems: (a) Co-located Massive MIMO, (b) DM-MIMO and (c) CF Massive MIMO.

Low-cost amplifiers can be further employed to serve the UEs instead of the conventional high-output power amplifiers [2, 29]. Furthermore, in massive MIMO, the base station benefits what is known as Channel Hardening. This means that when a signal is beamformed by a large number of antennas, the fading multi-antenna channel behaves almost as deterministic scalar channel as a result of the law of large numbers. Hence, this alleviates the impact of the small-scale fading and improves the downlink channel gain estimation [15, 18, 30].

2.3.1 Distributed Massive MIMO (DM-MIMO)

The massive antenna arrays exploited at the base stations can be placed in a distributed setup to form what is entitled the Distributed Massive MIMO (DM-MIMO). DM-MIMO can be viewed as a combination of the distributed antennas system (DAS) and the massive MIMO technology. This combination brings all the benefits of these two concepts. The spatially separated antennas in DAS provide low-path-losses and a high degree of macro-diversity, thereby having power saving, coverage and capacity merits over a co-located antenna system (CAS). In addition, adopting large antenna arrays yields the previously mentioned advantages of the co-located massive MIMO. That will be, unfortunately, at the cost of high backhaul requirements. In the cellular DM-MIMO networks, the architecture of a single cell includes replacing the base station with a set of low-functionality remote radio-heads (RRHs) spreading out over the cell to perform radio signals transmission/reception as illustrated in Figure 2.1(b). These RRHs are connected through high-bandwidth low-latency fronthaul links, optical fibres for instance, to a central processing unit (CPU) where the signal processing operations are achieved. In addition to that DM-MIMO inherits the idea of DAS, DM-MIMO has a similar concept to that of the network MIMO and the coordinated multipoint (CoMP) as RRHs perform joint transmis-

sion. However, each UE in DM-MIMO is served by a large number of antennas [5,6,16,18].

2.3.2 Cell-free (CF) Massive MIMO

Subsection 2.3.1 described the conventional DM-MIMO based on cellular topologies, in which a limited number of UEs can be served in each cell [5–7]. In the future, wireless networks have to handle a huge number of UEs, human UEs and machine-type communications as discussed in Section 1.1. Therefore, the DM-MIMO has reproduced under the name of Cell-free (CF) Massive MIMO, where the concept of cells or cell boundaries are eliminated as illustrated in Figure 2.1 (c), to be more convenient in such scenarios [15, 17–20]. CF massive MIMO is a new and scalable network architecture where a number of RRHs are distributed over a large area and jointly cooperated to serve a set of UEs. In the architecture of CF massive MIMO, the baseband signal processing can take place in the CPU as well. However, in the conventional DM-MIMO, RRHs located in a particular cell only serve the UEs within that cell. The set of low-cost RRHs can be deployed to provide uniformly good service within the coverage area of the CF network. CF massive MIMO has the ability to manage the resources efficiently due to the centralised signal processing capabilities of the CPU, thus it can work better in the non-uniform loaded scenarios than the cellular DM-MIMO. In addition to the inter-cell interference efficient mitigation through the centralised signal processing and CoMP technique, CF massive MIMO can improve the energy efficiency via RRH selection [20]. It also provides better coverage compared with using uncoordinated small cells where each UE is served by a single RRH [18].

2.4 User-Centric Approach

One of the challenges in the CF massive MIMO is the high computational complexity in the CPU owing to the huge signal processing and resources allocation operations that need to be performed there. An efficient method entitled user-centric can be utilised to achieve low-complexity and scalable channel acquisition in the CF massive MIMO network [22–24, 31]. This method depends on each UE individually choosing its serving RRH cluster from the set of closest RRHs or strongest channels, as distant RRHs do not make a significant contribution to its signal quality due to the severe path-loss. This assumes that a UE's serving RRH cluster may overlap with other UEs' clusters. Forming clusters in practice depends on the large-scale fading, where the average channel gains of UEs are measured and sent to the CPU. After that, the CPU determines the cluster associated with each UE based on the measured channel gains, which vary slowly [32]. Different cluster formation methods can be employed in the CPU. However, for simplicity purposes, clusters are formed in this thesis based on the distance only where each UE is associated with the nearest set of RRHs. The savings on the capacity of the backhaul obtained from adopting the user-centric method is discussed in [23]. For instance, in the downlink transmission, and by assuming K UEs, N RRHs equipped with M antennas, the CPU needs to transmit, at each symbol interval, NM times the K data symbol in the case when the user-centric approach is not utilised. This means that the overhead per symbol interval is NMK in this case. However, that can be reduced to $\mathbb{N}MK$ in the user-centric CF massive MIMO by supposing that each UE is served by a set of $\mathbb{N}$ RRHs [23].

2.5 Channel Estimation in D-/CF Massive MIMO Systems

To achieve the full potential of both the DM-MIMO and CF massive MIMO systems previously explained, the CPU has to measure the channel state information (CSI) from the active UEs to the RRHs within the current coherence interval. These CSIs are utilised by the CPU to jointly precode data for the UEs in the downlink transmission, and to jointly detect the UE signals in the uplink transmission. A common method for measuring the channel response is to transmit pre-known pilot sequences and to evaluate how the channel impacts, that discussed in Section 2.1, affect these pilots at the receiver side. In order to obtain accurate CSIs, orthogonal pilot sequences are generally adopted. The columns of a pilot book $\mathbf{Q} \in \mathbb{C}^{B \times B}$ can be employed to generate B orthogonal pilots, and this book should satisfy $\mathbf{Q}^H \mathbf{Q} = \mathbf{I}_B$. In the case of DM-MIMO network, it is recommended for each CPU in each cell to allocate different orthogonal pilots among the UEs in its cell. Two examples of pilot books are the Walsh-Hadamard matrix and the discrete Fourier transform (DFT) matrix. The Walsh-Hadamard matrix can be generated with dimensions of a power of two: $B = 2^n$ for $n = 0, 1, \cdots$. On the other hand, the DFT matrix can be generated with an arbitrary dimension, so it does not need to be a power of 2 [2].

2.5.1 Pilot Contamination

The channel estimates obtained from pilot signals are valid within the coherence block, after which it is necessary to measure the channel again as aforementioned in Section 2.2. Due to the limited size of the channel coherence blocks, it is not always possible to guarantee that the number of mutually orthogonal pilot sequences is larger than the number of UEs in the cell/system. Thus, it is essential to reuse the pilot sequences among

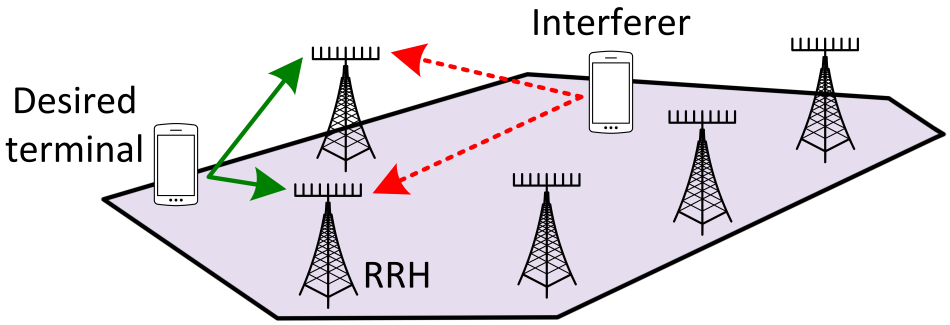

Figure 2.2: Contamination of uplink pilot signal when a pilot is shared by two UEs [2].

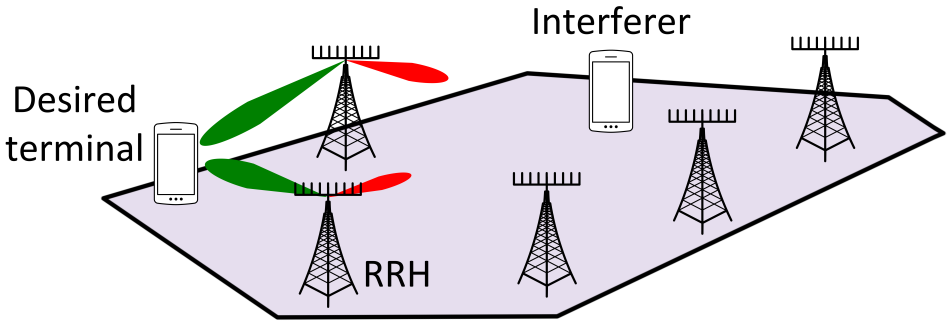

Figure 2.3: Effect of pilot contamination on downlink data transmission [2].

UEs in different cells in the DM-MIMO or among a set of UEs in the CF massive MIMO resulting a pilot coherent interference. This interference causes the channel estimation quality of the UEs sharing the same pilot to be degraded and this can not be improved by adding more antennas. The phenomenon of pilot interference on the received pilot signal is known in the literature as Pilot Contamination. For the scenario shown in Figure 2.2, two UEs are transmitting their pilots simultaneously, and the CPU then receives a superposition of their signals, in which the desired pilot sequence is contaminated. The channel estimates at the CPU unintentionally include a superposition of the channels from both the desired UE and the interferer [2, 29].

During uplink data transmission, the CPU is aimed at coherently detecting the re-

ceived signals by different RRHs through utilising the previously estimated CSIs. Part of the interfering signal is then unintentionally detected along the UE's desired signal. That is more harmful in the case of adopting a large number of antennas at RRHs where the high array gain increases the power of both the desired signal and the interference signal. In the downlink transmission, the RRHs beamform the downlink signals in the direction of the desired UE, but parts of these signals are unintentionally directed toward the location of the interferer UE. This is clarified in Figure 2.3. Considerable efforts have been made to limit the effect of pilot contamination. That includes allocating the pilots effectively, and this is the focus of this thesis.

2.5.2 Time-Division Versus Frequency-Division Duplexing

In massive MIMO systems, the channel can be generally measured by utilising the received pilot sequences. Alternatively, the channel estimation can use the feedback from the receiver to the transmitter, or both the feedback and the received pilots. That depends on which duplexing mode is employed, the time-division duplexing (TDD) or the frequency-division duplexing (FDD) which both are shown in Figure 2.4 [2].

1. In TDD, the uplink transmission and the downlink transmission are separated in time. Thus, the channel responses are reciprocal, which indicates that the channel response is the same in both the uplink and the downlink. The CPU performs the channel estimation through uplink pilots. Due to channel reciprocity, the estimates in the uplink are valid for the downlink too. As a result, the pilot signals needed depend only on the number of UEs, and the number of RRH antennas do not affect the number of required pilots. That is attractive for D-/CF massive MIMO systems as the total number of antennas in the cell/system is much higher than the number

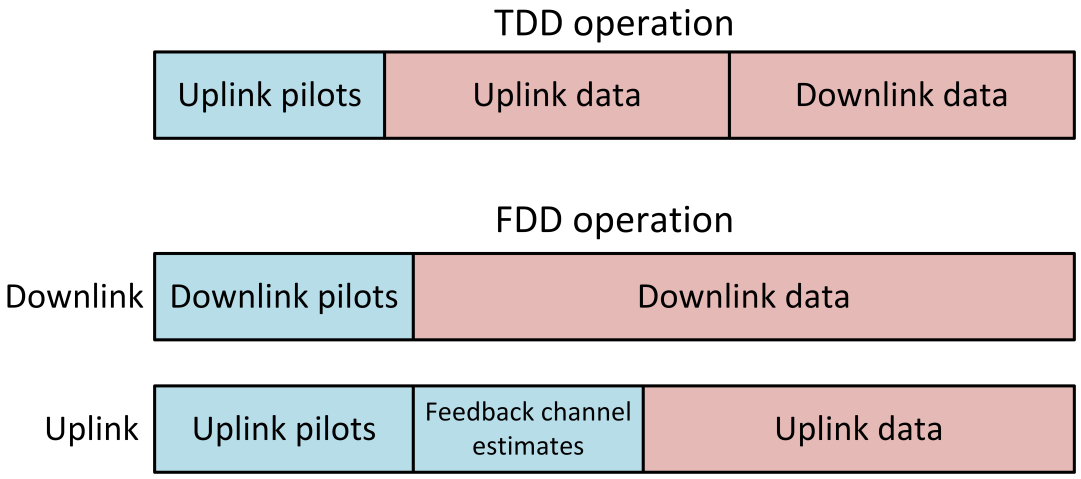

Figure 2.4: Slot structure for FDD and TDD operation modes.

of UEs. Therefore, TDD protocol is assumed throughout this thesis.

2. In FDD, the uplink transmission and the downlink transmission are separated in frequency. The uplink and downlink channels are always different and it is not possible to benefit the reciprocity in this case. The UEs, in FDD operation, measure the channel from the pilots sent by the RRHs, these estimated CSIs are fed back to the CPU through a control channel to enable the downlink precoding computation. In order to obtain the uplink channel estimates, the CPU relies on the pilots received from the UEs by the RRHs [2, 29].

2.5.3 MMSE Channel Estimation

The minimum mean squared error (MMSE) channel estimator exploits knowing the channel statistics to perform the channel estimation. Although it has high complexity compared with other estimators such as the least-squares (LS) estimator, the MMSE estimator has been widely implemented in the literature due to its good performance. It employs the spatial information of a UE included in its channel covariance matrix to improve

the channel estimation. Specifically, the MMSE estimator amplifies the signal from the direction of the desired UE and attenuates the signals from the direction of interferers [33].

To clarify how the MMSE estimator works, a CF massive MIMO network is assumed with K single-antenna UEs and N RRHs, each equipped with M antennas. The set of UEs is denoted as $\mathcal{K} = \{1, 2, \cdots, K\}$. The channel response between the k^{th} UE and the i^{th} RRH is symbolised as $\mathbf{g}_{i,k}$, where $\mathbf{g}_{i,k} = [g_{1,i,k}, g_{2,i,k}, \cdots, g_{M,i,k}]^T$, and $g_{m,i,k}$ is the channel coefficient between the k^{th} UE and the m^{th} antenna at the RRH i. The $M \times M$ channel covariance matrix $\mathbf{R}_{i,k}$ is then represented as $\mathbf{R}_{i,k} = \mathbb{E}\{\mathbf{g}_{i,k}\mathbf{g}_{i,k}^H\}$. This covariance matrix will be exploited by the MMSE estimator as it includes the spatial information of a UE [28].

It is further assumed that the set of orthogonal pilot signals are denoted as $\mathbf{Q} = \{\mathbf{q}_1, \mathbf{q}_2, \cdots, \mathbf{q}_b, \cdots, \mathbf{q}_B\} \in \mathbb{C}^{B \times B}$. It is additionally considered that $\mathcal{K}_b = \{k : b_k = b\}$ is the group of UEs sharing the b^{th} pilot sequence. During the uplink training phase, each UE needs to transmit its assigned pilot to the RRHs to measure the CSIs. Given the pilot reuse scheme, the received signal at RRH i arranged in a structure of size $M \times B$, is given by

$$\mathbf{Y}_i = \sum_{k \in \mathcal{K}} \sqrt{\rho_p}\, \mathbf{g}_{i,k}\mathbf{q}_{b_k}^H + \mathbf{N}_i, \tag{2.1}$$

where ρ_p is the transmit power for pilots, while $\mathbf{N}_i$ is the additive noise matrix received during the training phase with entries having the distribution $\mathcal{CN}(0, \sigma_p^2)$.

To estimate the channel-vector $\mathbf{g}_{i,k}$, where $i \in \mathcal{I}_k$, $\mathbf{Y}_i$ is first projected into $\mathbf{q}_{b_k}$, yielding

$$\begin{aligned} \mathbf{y}_{i,k} &= \frac{1}{\sqrt{\rho_p}}\mathbf{Y}_i\mathbf{q}_{b_k}, \\ &= \mathbf{g}_{i,k} + \sum_{l \in \mathcal{K}_{b_k} \setminus \{k\}} \mathbf{g}_{i,l} + \mathbf{n}_i, \end{aligned} \tag{2.2}$$

where $\mathbf{n}_i = \frac{1}{\sqrt{\rho_p}}\mathbf{N}_i\mathbf{q}_{b_k}$. The minimum mean square error (MMSE) estimate of channel $\mathbf{g}_{i,k}$

is given by [2]

$$\hat{\mathbf{g}}_{i,k} = \mathbf{R}_{i,k}\Big(\sum_{l \in \mathcal{K}_{b_k}} \mathbf{R}_{i,l} + \hat{\sigma_p}^2\Big)^{-1}\mathbf{y}_{i,k}, \tag{2.3}$$

where $\hat{\sigma_p}^2 = \sigma_p^2/\rho_p$.

In order to estimate $\mathbf{g}_{i,k}$, the CPU should perform the multiplications shown in both (2.2) and (2.3) with having the pilot sequence of UE k. However, if two UEs sharing the same pilots, the estimates of their channels will be correlated. This is a consequence of the inability of the CPU to separate UEs that have transmitted the same pilot signal and have the same spatial characteristics [2, 28]. Therefore, efficient pilot allocation schemes are needed to reuse the pilots with meeting UEs' quality of service (QoS).

2.6 Related Works

This section discusses the previous works that have addressed the pilot assignment design or pilot overhead reduction in both CF massive MIMO and DM-MIMO networks. In addition, an overview of the history of the user-centric method is finally discussed.

2.6.1 The Scenario of CF Massive MIMO

Several papers [7, 18, 34–36] have discussed the problem of pilot allocation in CF massive MIMO. In [34], non-orthogonal pilot codes were proposed. In this pilot design, each RRH can detect the pilot collision when more than one UE in its area utilises the same pilot dimensions. After this, RRHs can be turned on or off to prevent pilot collisions which may reduce system performance, especially when the number of RRHs is not high. A downlink pilot scheme appeared in [35] based on the fact that less channel hardening can be expected in the single-antenna access points (APs) CF massive MIMO than that of a co-located massive MIMO. However, [35] does not take into account the effect of pilot reuse

which is impractical assumption in a CF massive MIMO network with a large number of UEs. A greedy pilot assignment scheme was investigated in [18], along a power allocation optimisation problem, aiming to mitigate pilot contamination when non-orthogonal pilot sequences are utilised. In this scheme, pilots were allocated randomly to UEs in the initial stage, then the pilot allocation was iteratively improved by updating the pilot of the UE with the worst downlink rate so minimum pilot contamination can be obtained. This will be repeated a particular number of times. However, the user-centric approach was not included in this work, also, single-antenna APs were considered in [18]. RRHs or APs can adopt multiple antennas to increase the array gains and to reduce the backhaul requirements. The authors in [36] adopted the user-centric method and a precoding strategy was investigated to balance between inter-cluster interference and signal with the objective of maximising the sum-rate, also solving a power allocation problem was included. Nonetheless, a perfect CSI was additionally assumed in [36]. In [7], a novel pilot allocation scheme has been proposed for the scenario of CF massive MIMO by allocating one pilot for a pair of UEs satisfying a specific SINR ratio. However, it is necessary to reuse the pilots more than only once in the large networks. In addition, the problem investigated in the CF massive MIMO network in this thesis focuses on the UEs with bad channel conditions which is not the case in [7]. Therefore, the problem in this thesis differs from that in [7] not only in its objective but also in its constraints.

Pilot reuse design has been extensively studied in both co-located and distributed massive MIMO [37–41] due to the significance of CSI acquisition in massive MIMO systems. In the proposed reuse schemes, identical pilots are generally assigned to the UEs with different angles or least channel correlations depending on the special features of massive MIMO. Some of these works [37–39] adopted cell-based approaches where the pilots are reused among the cells. These approaches are not applicable in the CF scenarios due to

the lack of cells. Other approaches included, for instance, data-aided channel estimation with superimposed training design as in [40], and blind channel estimation based on singular value decomposition (SVD) as in [41]. However, such approaches suffered from high computational complexity when applied to the CF massive MIMO with a large network. In [32], a novel pilot allocation scheme was presented to maximise the number of admitted UEs with a fixed number of pilot sequences in the dense cloud radio access (C-RAN) networks based on the graph colouring algorithm. Although this scheme can be extended to work in the CF massive MIMO scenario, it did not consider any quality of service (QoS) requirements when pilots were reused among UEs; a dual transmit antennas setting was also considered at each RRH in [32] which means it was not a massive MIMO system. In Chapter 4 of this thesis, the design of pilot assignment scheme is addressed in the CF massive MIMO with the joint impacts of the pilot contamination and the user-centric approach.

2.6.2 The Scenario of Traditional Cellular DM-MIMO

In the literature, many approaches have been introduced to mitigate pilot contamination for different architectures of massive MIMO systems, including co-located massive MIMO [38, 42, 43], Network MIMO [44] and small cells scenarios [45]. In these approaches, UEs in the same cell adopt different orthogonal pilot signals, meanwhile the same group of pilots are reused among cells. However, in the case when the number of pilots is much less than the number of UEs in the cell, it might be necessary for more than one UE to share the same pilot within a single cell. By following this approach, the angle of arrival (AoA)-based methods [46, 47] have assumed pilot reuse within the same cell in the co-located massive MIMO to further reduce the pilot overhead. In these methods, the UEs with non-overlapping AoAs do not contaminate each other when they adopt the same

pilot. However, the assumption of the small AoA spread is not always feasible in practice.

The aforementioned pilot assignment approaches [18, 34] that have been designed for CF massive MIMO networks can be applied to reuse the pilots within a single cell DM-MIMO network. However, the previously mentioned limitations of these works are still valid here, as the user-centric clustering is considered in the scenario of DM-MIMO of this thesis along multiple antennas RRHs. Thus, in the next chapter, a novel pilot allocation scheme is presented to reuse the pilots within the same cell of the user-centric based DM-MIMO system with the objective of maximising the sum-rate under the constraint that the SINR for each UE is not less than a specific threshold where the impacts of pilot contamination are taken into account.

2.6.3 User-centric Approach

In the literature, the user-centric clustering method has appeared to mange the coordination in multi-cell scenarios as an alternative way to the disjoint clustering scheme. In the disjoint clustering scheme, the entire network is divided into non-overlapping clusters and the UEs in each cluster are jointly served by only the base stations or RRHs within the coverage area. Although the disjoint clustering scheme can be considered as an efficient method to mitigate the inter-cell interference [48, 49], UEs at the cluster edge still experience significant out-of-cluster interference. Alternatively, the user-centric clustering employs dynamic and flexible multi-cell coordination [44, 50, 51]. In user-centric clustering, each UE is served by an individually selected subset of neighbouring BSs or RRHs and different clusters for different UEs may overlap. The main benefit here is that such a method does not include any explicit cluster edge. The impact of the geographical location of UEs was discussed in [44], however the desirable cooperation and coordination vary with time depending on different parameters, such as mobility of UEs, and macroscopic

conditions, such as congestion in specific areas [22].

The user-centric approach has been also applied in CF massive MIMO in different works [23, 52] where UEs can be associated with multiple nearby RRHs without cell boundaries. In [23], the CF massive MIMO architecture, when each UE is served by all the RRHs, was contrasted with the user-centric approach. It has been shown in [23] that the user-centric method generally provides better data-rate performance except for UEs with bad channel conditions. In [52], the user-centric based CF massive MIMO was investigated when both UEs and RRHs were equipped with multiple antennas. A channel-inverting beamforming scheme was proposed that does not need channel estimation at the UEs.

Chapter 3

Pilot Reuse in a Single Cell DM-MIMO System

This chapter describes the proposed pilot allocation design that assumes the pilot reuse within the same cell of the dense DM-MIMO network. The dynamic pilot reuse (DPR) scheme is developed to deal with the case when the number of UEs in the target cell is larger than the number of available pilot sequences. In Section 3.1, the system model and the channel model are introduced. Following this, in Section 3.2, the uplink sum-rate performance is discussed and analysed by considering the pilot contamination, and the problem formulation of pilot assignment is then presented. A low-complexity algorithm aiming to solve this problem is developed in Section 3.3, where the pilots in this algorithm are allocated based on the proposed reuse scheme. The computational complexity of the pilot allocation algorithm is further analysed in this section. Finally, Section 3.4 presents the simulation results in terms of the uplink sum-rate to evaluate the performance of the proposed reuse scheme.

3.1 System Model

A dense single cell DM-MIMO network consisting of $\mathbb{S}$-tier hexagonal topology structure with $N = 3\mathbb{S}^2 + 3\mathbb{S} + 1$ RRHs [45] and $\bar{K}$ UEs is considered as shown in Figure 3.1. Each RRH and each UE are equipped with M antennas and a single antenna, respectively. The set of RRHs and UEs are denoted as $\mathcal{N} = \{1, \cdots, N\}$ and $\bar{\mathcal{K}} = \{1, \cdots, \bar{K}\}$, respectively. It is supposed that K UEs are admitted in this network and the set of these UEs is expressed as $\mathcal{K} \subseteq \bar{\mathcal{K}}$. In addition, the set of antennas of the i^{th} RRH is denoted as $\mathcal{M}_i = \{1, \cdots, M\}$. It is also assumed that UEs are randomly distributed within the cell. Furthermore, RRHs are physically connected to the CPU through high-speed links, where the CPU performs the joint detection of the received signals from multiple RRHs.

TDD mode is adopted in this scenario, which indicates that the CSI is the same for both uplink and downlink transmissions. The channel estimation of the uplink channels is executed in the CPU with the received pilot signals. It is assumed that S time-frequency resource units (RUs) are allocated within one coherence block. Within these S RUs, B RUs are reserved for pilot sequences in each block. The remaining $(S - B)$ RUs are dedicated for uplink and downlink data transmission.

By assuming that the whole pilot resources are utilised for pilot signalling, the available pilot set is denoted as $\mathcal{Q} = \{1, \cdots, b, \cdots, B\}$, and the corresponding orthogonal pilot sequences as $\boldsymbol{Q} = \{\mathbf{q}_1, \cdots, \mathbf{q}_b, \cdots, \mathbf{q}_B\} \in \mathbb{C}^{B \times B}$, where each $\mathbf{q}_b \in \mathbb{C}^{B \times 1}$ in set $\boldsymbol{Q}$ is mutually orthogonal with each other, that is $\boldsymbol{Q}^H \boldsymbol{Q} = \mathbf{I}_B$ [6, 53]. By using the orthogonal pilot assignment scheme, only B UEs are able to send their pilots without interfering with each other [53]. In order to serve more UEs, a pilot reuse scheme is required. An arbitrary pilot reuse scheme is denoted as $\mathcal{P}(\mathcal{K}, \mathcal{Q}) = (k, b_k) : k \in \mathcal{K}, b_k \in \mathcal{Q}$, where (k, b_k) denotes that the k^{th} UE is allocated with the pilot sequence $\mathbf{q}_{b_k}$.

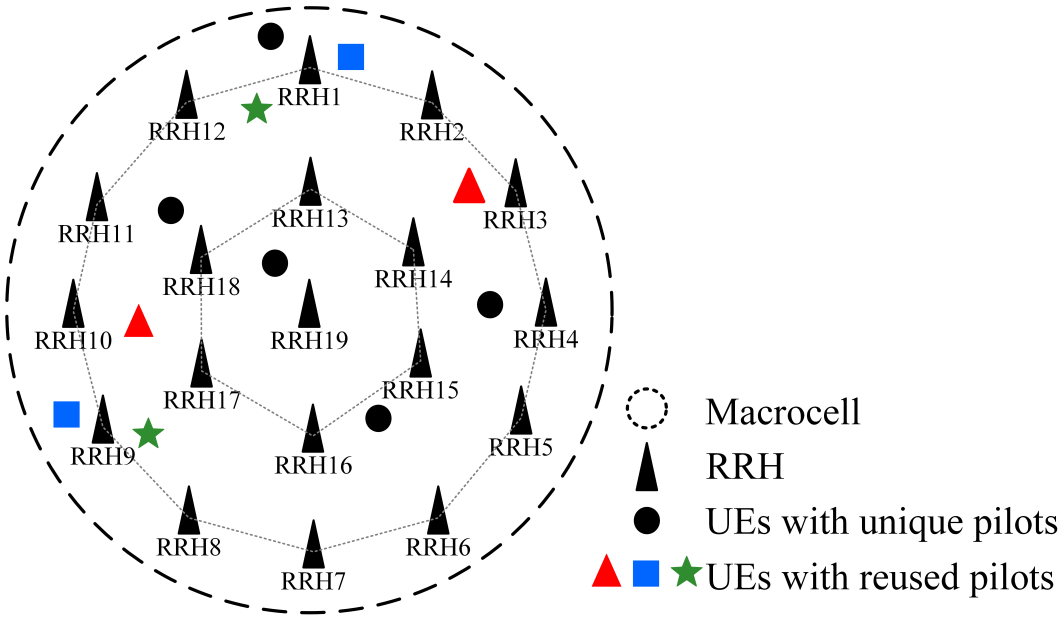

Figure 3.1: Structure of a single cell dense DM-MIMO with $N = 19$, i.e. $\mathbb{S} = 2$, and an illustration of the proposed DPR scheme by supposing $B = 8$ and $\bar{K} = 11$. Unique pilots are allocated for UEs with circle shapes, and a single pilot is allocated for a pair of UEs with any one of the following shapes: square, triangle and star.

The uplink channel response for the k^{th} UE to the m^{th} antenna in the i^{th} RRH is given by [38]:

$$g_{k,i,m} = \alpha_{k,i}^{1/2} h_{k,i,m}, \tag{3.1}$$

where $\alpha_{k,i}$ represents the large-scale fading coefficient between the k^{th} UE to the i^{th} RRH, which consists of both the path-loss and the shadow fading. $\alpha_{k,i}$ is assumed to be the same between the k^{th} UE and all M antennas of any RRH. In addition, $h_{k,i,m}$ is assumed to be the small-scale fading coefficient between the k^{th} UE to the m^{th} antenna in the i^{th} RRH, and it is further supposed that each element of $h_{k,i,m}$ is an i.i.d. complex Gaussian variable with zero mean and unit variance. The channel response $M \times 1$ vector from the k^{th} UE to the i^{th} RRH is given by [5]

$$\mathbf{g}_{k,i} = \alpha_{k,i}^{1/2} [h_{k,i,1}, h_{k,i,2}, \cdots, h_{k,i,M}]^T. \tag{3.2}$$

By assuming a synchronous pilot transmission from all UEs, the received signal matrix of pilots at the i^{th} RRH is

$$\mathbf{Y}_{p,i} = \sqrt{\rho_p} \sum_{k \in \mathcal{K}} \mathbf{g}_{k,i} \mathbf{q}_{b_k}^H + \mathbf{N}_i \in \mathbb{C}^{M \times B}, \tag{3.3}$$

where ρ_p is the transmit power for pilots. $\mathbf{q}_{b_k}$ is the pilot transmitted by the k^{th} UE, where $\mathbf{q}_{b_k} \in \boldsymbol{Q}$. Also, $\mathbf{N}_i \in \mathbb{C}^{M \times B}$ is complex additive white Gaussian noise with zero mean and unit covariance matrix[1]. The CPU has the following observation of the channel from the k^{th} UE to the i^{th} RRH [6, 47]

$$\mathbf{y}_{p,k,i} = \frac{1}{\sqrt{\rho_p}} \mathbf{Y}_{p,i} \mathbf{q}_{b_k} \in \mathbb{C}^{M \times 1}. \tag{3.4}$$

3.2 Sum-rate Analysis

In this chapter, the scenario that $\bar{K}$ is larger than the number of available pilot sequences B in the dense cell of DM-MIMO is discussed. Thus, the DPR scheme is proposed to allow a pair of UEs to share one pilot within the same cell and different pilots are assigned to different pairs. In this section, given the pairs of UEs using the same pilot according to the proposed DPR scheme, the achievable sum-rate for data transmission is analysed. Based on the analytical results and the target of maximising the sum-rate, an algorithm for the dynamic pilot reuse is proposed in the next section.

After reusing the pilots for some UE pairs, no pilot reuse is considered for the rest of the UEs, and unique pilot sequences are allocated to them. As illustrated in Figure 3.1, ($B = 8$) and ($\bar{K} = 11$) are considered. This means that three pilots ($\bar{K} - B$) are required to be reused in order to serve all the UEs in Figure 3.1 ($K = \bar{K}$). The UEs with unique pilot sequences are represented with the black circles, and the pair of UEs using the same

[1]This indicates that the noise is assumed to have a unit variance.

pilot sequence is represented by one of the following shapes: square, triangle and star. As a result, two groups of UEs will be created: UEs with unique pilot sequences, and UEs with reused pilot sequences. In order to obtain the channel estimation for these UEs, the equation (3.4) for any UE should be expanded as [6, 47]

$$\mathbf{y}_{p,k,i} = \sum_{k \in \mathcal{I}} \mathbf{g}_{k,i} + \frac{\mathbf{N}_i \mathbf{q}_{b_k}}{\sqrt{\rho_p}} \ \forall k \in \mathcal{K}, i \in \mathcal{N}, \tag{3.5}$$

where $\mathcal{I}$ is the set that includes the pair of UEs $\{k, k^{'}\}$ in the case of pilot reuse where the two UEs share the same pilot, or $\mathcal{I}$ includes only the k^{th} UE in the case of no reuse. Based on [54], CPU computes the MMSE estimation of the k^{th} UE[2]

$$\hat{\mathbf{g}}_{k,i} = \alpha_{k,i}(\sum_{k \in \mathcal{I}} \alpha_{k,i} + \frac{1}{\sqrt{\rho_p}})^{-1} \mathbf{y}_{p,k,i} \ \forall k \in \mathcal{K}, i \in \mathcal{N}, \tag{3.6}$$

where $\hat{\mathbf{g}}_{k,i} \sim \mathcal{CN}(0, \theta_{k,i}\mathbf{I}_M)$ and $\theta_{k,i}$ is given by

$$\theta_{k,i} = \alpha_{k,i}^2(\sum_{k \in \mathcal{I}} \alpha_{k,i} + \frac{1}{\sqrt{\rho_p B}})^{-1} \ \forall k \in \mathcal{K}, i \in \mathcal{N}. \tag{3.7}$$

The channel $\mathbf{g}_{k,i}$ can be decomposed as $\mathbf{g}_{k,i} = \hat{\mathbf{g}}_{k,i} + \tilde{\mathbf{g}}_{k,i}$, where $\tilde{\mathbf{g}}_{k,i}$ is the channel estimation error and it is statistically independent of $\hat{\mathbf{g}}_{k,i}$ due to the orthogonal property of MMSE estimation and the joint Gaussianity of both vectors, the covariance of $\tilde{\mathbf{g}}_{k,i}$ is $((\alpha_{k,i} - \theta_{k,i})\mathbf{I}_M)$.

During the uplink data transmission, the received data signal vector for the i^{th} RRH is

$$\mathbf{y}_{d,i} = \sqrt{\rho_d} \sum_{k \in \mathcal{K}} \mathbf{g}_{k,i} x_k + \mathbf{z}_{d,i} \in \mathbb{C}^{M \times 1}, \tag{3.8}$$

where ρ_d is the transmit power for data and all UEs have the same transmit power, $\mathbf{z}_{d,i} \in \mathbb{C}^{M \times 1}$ is complex additive white Gaussian noise with zero mean and unit covariance matrix. x_k is the transmitted data signal from the k^{th} UE, $k \in \mathcal{K}$.

[2]The large-scale fading can be estimated blindly or can be obtained from the statistical measurements [21].

It is assumed that the MMSE detection is applied in the CPU for recovering UE data. The detector $M \times 1$ vector for the k^{th} UE at i^{th} RRH is given as [54]

$$\hat{\mathbf{a}}_{k,i} = (\hat{\mathbf{G}}_i \hat{\mathbf{G}}_i^H + \mathbf{Z}_i + \frac{1}{\rho_d}\mathbf{I}_M)^{-1} \hat{\mathbf{g}}_{k,i}, \tag{3.9}$$

where $\hat{\mathbf{G}}_i$ is the estimated channel response $M \times K$ matrix from all the UEs to the i^{th} RRH, and the k^{th} column of $\hat{\mathbf{G}}_i$ is $\hat{\mathbf{g}}_{k,i}$. In addition, $\mathbf{Z}_i = \sum_{k \in \mathcal{K}} \mathbb{E}(\tilde{\mathbf{g}}_{k,i} \tilde{\mathbf{g}}_{k,i}^H)$ is the covariance matrix of the channel estimation errors for the i^{th} RRH.

The user-centric cluster method, that mentioned in Section 2.4, is adopted here to reduce the computational cost for a dense single cell DM-MIMO. This means that UEs are only served by a cluster of the nearest RRHs since distant RRHs contribute little to the UE's signal quality due to the severe path-loss. The notation $\mathcal{N}_k$ is used to represent the group of RRHs serving the k^{th} UE. For a pair of UEs sharing the same pilot, the clusters of RRHs serving these two UEs should not overlap. In other words, the UEs served by at least one common RRH should be allocated with difference pilots. This is essential to enable the CPU to differentiate the CSIs for the UEs sharing a single pilot. Based on (3.9), the CSIs from all UEs to the i^{th} RRH are needed. However, for UEs with pilot reuse, the instantaneous CSIs that can be provided are only from a UE to its serving cluster of RRHs. For the CSI from the UE to the RRHs outside its cluster, only the large-scale fading (path-loss and shadowing) can be tracked. The assumption of the availability of the large-scale fading is valid because of the slow rate at which this parameter varies compared with the small-scale fading, thus it can be obtained at a much lower cost.

The MMSE detection is then applied in the CPU. The estimated data symbol for the

k^{th} UE is represented by

$$\hat{x}_k = \sum_{i \in \mathcal{N}_k} \hat{\mathbf{a}}_{k,i}^H \mathbf{y}_{d,i}. \tag{3.10}$$

The ergodic achievable sum-rate can be written as

$$\mathrm{R}_T = (1 - \frac{B}{S}) \sum_{k \in \mathcal{K}} \log_2(1 + \mathrm{SINR}_k). \tag{3.11}$$

The SINR for the k^{th} UE, whose pilot is reused with the k'^{th} UE, is given in (3.12). The numerator of (3.12) represents the signal power, while the first term in the denominator includes the effect of channel estimation error, the second term is the pilot contamination, the third term is the sum interference power from other UEs and the last term is the power of noise. For a UE with unique pilot, the SINR can still be obtained from (3.12) but the second term of the pilot contamination in the denominator of (3.12) should be neglected.

$$\mathrm{SINR}_{\langle k,k' \rangle} = \frac{\rho_d (\sum_{i \in \mathcal{N}_k} \hat{\mathbf{a}}_{k,i}^H \hat{\mathbf{g}}_{k,i})^2}{\rho_d [(\sum_{i \in \mathcal{N}_k} \hat{\mathbf{a}}_{k,i}^H \tilde{\mathbf{g}}_{k,i})^2 + (\sum_{i \in \mathcal{N}_k} \hat{\mathbf{a}}_{k,i}^H \mathbf{g}_{k',i})^2 + \sum_{\substack{q \in \mathcal{K} \\ q \neq k \\ q \neq k'}} (\sum_{i \in \mathcal{N}_k} \hat{\mathbf{a}}_{k,i}^H \mathbf{g}_{q,i})^2] + (\sum_{i \in \mathcal{N}_k} \hat{\mathbf{a}}_{k,i}^H \mathbf{z}_{d,i})^2} \tag{3.12}$$

In order to simplify the SINR in (3.12), the deterministic equivalent analysis from [54] is employed here. The results in [54] are asymptotic since the SINR formulas were derived by considering the number of antennas increases considerably. However, simulation results in [54] demonstrate that even for a small number of antennas, the fit between simulation and approximation is acceptable. According to ([54], Theorem 5), the SINR for MMSE detector is given in ([54], equation (25)). This formula is modified to match the single cell DM-MIMO scenario of this chapter as shown in (3.13) and (3.14), for a UE without pilot reuse and a UE with pilot reuse, respectively. The elements of the channel vector from

the k^{th} UE to the antennas of the base station in [54] are replaced by the channel vector from the UE to all the antennas of the serving set of RRHs ($\mathcal{N}_k$). In the denominator of both (3.13) and (3.14), the first term represents the power of noise, the second term is the sum interference power from other UEs and the third or the last term in (3.14) is the pilot contamination. The parameters of $\delta_k, \mu_{\langle q,k\rangle}, \vartheta_k$ and $\mathbf{T}^{'}$ can be calculated by using ([54], Theorem 1 and Theorem 2). These parameters depend on $\bar{\mathbf{Z}}$, which can be calculated from $\bar{\mathbf{Z}} = \sum_{k\in\mathcal{K}}(\bar{\mathbf{R}}_k - \bar{\mathbf{\Theta}}_k)$ [54]. $\bar{\mathbf{R}}_k$ is a diagonal matrix with the diagonal entries of $\alpha_{k,i,m}$ for all the antennas equipped with all the serving RRHs cluster $\mathcal{N}_i$, where $\alpha_{k,i,m} = \alpha_{k,i}$ for $m \in \mathcal{M}_i$, $\forall i \in \mathcal{N}_i$. Similarly, $\bar{\mathbf{\Theta}}_k$ is a diagonal matrix with the diagonal entries of $\theta_{k,i,m}$ for all the antennas equipped with all the serving RRHs cluster $\mathcal{N}_i$, where $\theta_{k,i,m} = \theta_{k,i}$ for $m \in \mathcal{M}_i$, $\forall i \in \mathcal{N}_i$. Then, ([54], Theorem 1, Theorem 2 and Theorem 3) can be employed to calculate the parameters[3] $\delta_k, \bar{\mathbf{T}}^{'}, \mu_{\langle q,k\rangle}$ and ϑ_k, which are all functions of $\bar{\mathbf{R}}_k$ and $\bar{\mathbf{\Theta}}_k$.

$$\mathrm{SINR}_k = \frac{\delta_k^2}{\frac{1}{\rho_d(NM)^2}\ \mathrm{tr}\ \bar{\mathbf{\Theta}}_k\bar{\mathbf{T}}' + \frac{1}{(NM)^2}\sum_{\substack{q\in\mathcal{K}\\ q\neq k}}\mu_{\langle q,k\rangle}} \tag{3.13}$$

$$\mathrm{SINR}_{\langle k,k'\rangle} = \frac{\delta_k^2}{\frac{1}{\rho_d(NM)^2}\ \mathrm{tr}\ \bar{\mathbf{\Theta}}_k\bar{\mathbf{T}}' + \frac{1}{(NM)^2}\sum_{\substack{q\in\mathcal{K}\\ q\neq k}}\mu_{\langle q,k\rangle} + |\vartheta_{k'}|^2} \tag{3.14}$$

3.2.1 Problem Formulation

In this chapter, the DPR scheme is developed to allocate the pilots with the objective of maximising the achievable uplink sum-rate in (3.11) under some practical constraints and

[3]The explicit formulas of these parameters are presented in Appendex A.1

by utilising the user-centric cluster method. Hence, this problem can be formulated as

$$\max_{\mathcal{P}(\mathcal{K},\,\mathcal{Q})} \mathbb{E}\{\mathrm{R}_T\}, \tag{3.15a}$$

$$s.t.\ \mathrm{SINR}_{\langle k,k'\rangle} \geq \gamma_{th}, \forall k, k^{'} \in \mathcal{K} \text{ when } \mathbf{q}_{b_k} = \mathbf{q}_{b_k'} \tag{3.15b}$$

$$\mathcal{N}_k \cap \mathcal{N}_{k'} = \emptyset, \forall k, k^{'} \in \mathcal{K}. \tag{3.15c}$$

It can be seen from (3.15) that the reuse of the pilots between pairs of UEs is considered. For any pair of UEs $\{k, k^{'}\}$, the following constraints are provided: First, the constraint (3.15b) means that each UE in a pair with the same pilot should satisfy a SINR threshold (γ_{th}). This threshold will be optimised in subsection 3.3.1 to satisfy the objective in (3.15a). No SINR constraint is considered for the UEs with unique pilots. Following that, constraint (3.15c) indicates that the two RRH clusters $\mathcal{N}_k$ and $\mathcal{N}_{k'}$ must not be overlapped, as explained earlier. It is assumed in this problem that only B pilots are available. Furthermore, the number of times of pilot reuse is denoted as ω, where ω is upper bounded by $\min(N_p, B)$, and

$$N_p = \begin{cases} \frac{K}{2}, & \text{if } K \text{ is even} \\ \frac{K}{2} - 1, & \text{if } K \text{ is odd.} \end{cases} \tag{3.16}$$

3.3 Algorithm for Dynamic Pilot Reuse

The optimal solution of the problem in (3.15a) can be obtained by the exhaustive search method, in which it is required to test all possible pilot allocation schemes and choose the one that satisfies the aim of maximising the sum-rate. However, the exhaustive search method may cost high complexity especially in the case of high number of UEs. Therefore, a low-complexity algorithm is presented in this section. The pseudocode of this algorithm is clarified in **Algorithm 3.1**. In this algorithm, two UEs separated by a large distance

can share the same pilot to ensure a marginal channel estimation error. The reuse is only allowed when the potential SINRs for the two UEs sharing the same pilot are still higher than the SINR threshold γ_{th}. The SINRs of these UEs can be calculated based on (3.14), which includes the effect of pilot contamination. Additionally, (3.14) depends on the UEs' large-scale fading coefficients $\alpha_{k,i}$. This means that it is required in **Algorithm 3.1** to have large-scale channel gains, which change very slowly and can be easily obtained. In **Algorithm 3.1**, no reuse will be permitted if no pair satisfies the required γ_{th}, and only B UEs will be served in this case. **Algorithm 3.1** should update the pilot allocation for UEs when the number of UEs K changes or the location of the UEs changes as this affects constraint (3.15c).

The selection of the pairs of UEs that are able to share the same pilot can be summarised in two stages: In the first stage, the UEs are classified into pairs, in a descending order, according to the separation distance. A search is then fulfilled within these pairs to determine which is able to cope with the reuse condition to assign the same pilot to its two UEs. The full explanation of **Algorithm 3.1** can be described as follows:

1. *Initialization:* In line 1, an initialization of the pilot allocation, the number of pairs of UEs that use the same pilots (v) and the pair index (f) is performed.

2. *UE Pairs Classification:* A search is achieved in line 2 for the possible configurations of UE pairs, where the serving sets of RRHs for the UEs in each pair should not be overlapped. The set of UE pairs are ordered descendingly in $[\theta_1, \cdots, \theta_f, \cdots, \theta_{\mathbb{F}}]$ according to the separation distance, where $\mathbb{F}$ is the number of acceptable pairs.

3. *UEs Selection:* In line 4, the pair θ_1 is initially chosen, and the two UEs of this pair are considered as $\{k, k^{'}\}$.

Algorithm 3.1: Dynamic pilot reuse algorithm

1 **INPUT:** System parameters: K, M, B, N, ω and γ_{th};

2 Large scale fading coefficients $\alpha_{k,i}$.

3 **OUTPUT:** Pilot allocation: $\mathcal{P}(\mathcal{K}, \mathcal{Q})$.

1: $\mathcal{P}(\mathcal{K}, \mathcal{Q}) = 0$, pilot reuse times ($v = 0$), iteration number ($f = 1$).
2: Form the UE pairs set $[\theta_1, \theta_2, \cdots, \theta_f, \cdots, \theta_{\mathbb{F}}]$, where $\mathbb{F}$ is the number of pairs.
3: **while** $v < \omega$ OR $f < \mathbb{F}$ **do**
4: **for** a pair of UEs $(k, k^{'})$ with order θ_f **do**
5: **if** $\text{SINR}_{\langle k,k' \rangle} \geq \gamma_{th}$ AND $\text{SINR}_{\langle k',k \rangle} \geq \gamma_{th}$ **then**
6: $\mathbf{q}_{b_k} = \mathbf{q}_{b_{k'}}$.
7: Increment number of reuse $v = v + 1$.
8: Increment pair index $f = f + 1$.
9: Go to line 4.
10: **else**
11: Increment pair index $f = f + 1$.
12: Go to line 4.
13: **end if**
14: **end for**
15: **end while**
16: **if** $v = \omega$ OR $f = \mathbb{F}$ **then**
17: Randomly allocate the rest of the pilots.
18: **end if**

4. *Pilot Reuse Condition:* For the pair of UEs $\{k, k^{'}\}$ selected in line 4, the potential values of $\text{SINR}_{\langle k,k' \rangle}$ and $\text{SINR}_{\langle k',k \rangle}$ are calculated based on equation (3.14) and compared with γ_{th}. If both of them are larger than or equal to γ_{th}, one pilot will be allocated for the two UEs as shown in line 6. Later, a new pair of UEs is selected and tested (lines 8-9 or 11-12).

5. *Pilot Reuse Termination:* As shown in line 3, the above procedures to reuse pilots will be repeated a number of times equal to ω or when all the pairs of UEs are tested ($f = \mathbb{F}$). The parameter v in line 7 counts how many pilots are reused. When v equals ω or when all pairs of UEs are tested, reusing pilots will be terminated. It is necessary here to allocate the remaining pilots, if there is, randomly to the rest of the UEs as shown in lines 16 and 17. If all pairs satisfy the SINR constraint and in the end some pilots are still available, the pairs with lowest average SINR will be dissociated and unique pilots will be allocated to each UE in these pairs.

3.3.1 Determining the Optimal SINR Threshold (γ_{th})

The value of γ_{th} utilised in **Algorithm 3.1** is calculated by considering a simple method called the iterative grid search (IGS) [38] to find the threshold that provides the objective of maximum sum-rate in (3.15a). In IGS method, it is first required to measure the minimum and maximum values of γ_{th}, i.e. γ_{min} and γ_{max}, respectively. In the extreme case when $\gamma_{th} \leq \gamma_{min}$, any pair of UEs can meet the SINR constraint in (3.15b) whatever the separation distance between them. In this case, maximum number of UEs can be served, but high pilot contamination is expected. On the other hand, when $\gamma_{th} \geq \gamma_{max}$, no pair is able to meet the SINR constraint. This case indicates that no reuse can be applied and the number of UEs that can be served is the same as the number of

pilots (B) with no pilot contamination. The near-optimal threshold should be located between [γ_{min} and γ_{max}] and can be found by sampling the interval [γ_{min} and γ_{max}] by $\mathbb{N}_b$ points with uniform subinterval $\Delta = (\gamma_{max} - \gamma_{min})/(\mathbb{N}_b - 1)$. At each point, the sum-rate is calculated, and the threshold that provides the maximum sum-rate value will be considered as $\gamma_{max}^{(1)}$. These procedures will be repeated by supposing that the new threshold interval is, $[\gamma_{max}^{(1)} - \Delta^{(1)}/2, \gamma_{max}^{(1)} + \Delta^{(1)}/2]$. These steps will be applied $\mathbb{T}$ times in an iterative way, where $\mathbb{T}$ is the number of iterations. The final near-optimal threshold will be $\gamma_{th} = \gamma_{max}^{(T)}$.

3.3.2 Complexity Analysis

The computational complexity of **Algorithm 3.1** is investigated in this subsection. The maximum number of the possible combinations of UE pairs that satisfy (3.15c) is $\mathbb{F} = \sum_{f=1}^{K-1} f$. Therefore, the highest complexity for **Algorithm 3.1** is achieved when it is required to search over all the combinations of UE pairs to find the pairs that can meet the pilot reuse condition based on a specific threshold γ_{th}. By including the pairs classification and the search over UE pairs, the complexity of **Algorithm 3.1** is $\mathcal{O}(2\sum_{f=1}^{K-1} f)$ in the case of using a fixed SINR threshold γ_{th}. Using the IGS method to find γ_{th} that provides the maximum sum-rate requires additional iterations equal to $(\mathbb{N}_b\mathbb{T})$. As a result, the upper bound of the total complexity when the optimised threshold is used will be $\mathcal{O}((\mathbb{N}_b\mathbb{T} + 2)\sum_{f=1}^{K-1} f)$.

3.4 Simulation Results

The uplink performance of the proposed pilot reuse scheme in a single cell dense TDD DM-MIMO network is evaluated in this section. The UEs are randomly and uniformly

placed in the cell, and the distribution of the RRHs follow the topology structure shown in Figure 3.1 with $\mathbb{S} = 2$, i.e., $N = 19$, The large-scale fading coefficient $\alpha_{k,i}$ can be calculated as $\alpha_{k,i} = \wp_{k,i}/(d_{k,i}/r_o)^{\alpha}$, where $\wp_{k,i}$ represents the shadow fading and it obeys a log-normal distribution, which is represented by, $10\log_{10}(\wp_{k,i}) \sim \mathcal{CN}(0, \sigma_{shad})$, and $d_{k,i}$ is the distance between the k^{th} UE to the i^{th} RRH [14]. The other simulation parameters are set as follows: Cell radius $R = 2000$m, decay exponent $\alpha = 3$, shadow fading standard deviation $\sigma_{shad} = 8$ dB, transmit power for both pilots and data $\rho_p = \rho_d = 40$ dBm, normalised radius $r_o = 100$m and the IGS parameters[4] are $\mathbb{N}_b = 5$ and $\mathbb{T} = 2$. For comparison purposes, the performance of the following pilot reuse schemes are included beside the DPR scheme with an optimised threshold:

1. Orthogonal pilot allocation: A unique orthogonal pilot is allocated for each UE in this scheme. Thus, the number of admitted UEs is equal to the number of pilots B.

2. Random pilot reuse: In this scheme, UE pairs are selected randomly to allocate the same pilot for them without taking into account any SINR constraint.

3. DPR scheme with no threshold: This scheme adopts the DPR algorithm as well but allocating the pilots to UE pairs is performed based only on the separation distance between the two UEs in each pair. This indicates that the SINR constraint will not be taken into account in this case too.

4. DPR scheme with a fixed threshold: The DPR algorithm is utilised here with a fixed SINR threshold which means that the IGS method is not adopted in this case.

To guarantee the fairness, the number of times of pilot reuse ω in the DPR scheme

[4]The value of $\mathbb{T}$ was chosen based on the simulation results. When $\mathbb{T}$ is bigger than 2, the same value of the SINR threshold γ_{th} will be continuously obtained.

with the no threshold, the fixed threshold and the random pilot reuse scheme is supposed to be the same as ω in the DPR scheme with the optimised threshold.

In Figure 3.2, the uplink achievable sum-rate is plotted versus the number of available pilots B with $\bar{K} = 32$, $S = 64$ and $M = 20$. As expected, the orthogonal pilot allocation scheme has the worst performance since no UEs are allowed to reuse the pilots. On the other hand, the performance of the DPR scheme with the optimised threshold outperforms the random pilot reuse scheme, the DPR scheme with fixed SINR thresholds (5 dB and 10 dB) and no threshold cases. The random selection of UE pairs to reuse their pilots in the random pilot reuse scheme may lead to a severe pilot contamination in pairs with low separation distances. Furthermore, a fixed threshold is generally less effective than the optimised one in the DPR scheme although all UEs guarantee their SINR requirements through the fixed threshold. The sum-rate performance at the threshold of 5 dB is better than the 10 dB as more UEs can be admitted in the case of 5 dB compared with the 10 dB as shown in Figure 3.3. Using the IGS method to continuously find the threshold that provides the maximum sum-rate gives the superiority to the DPR scheme when this threshold is adopted. However, additional computational complexity is needed due to the use of the IGS method compared with the fixed threshold.

Figure 3.3 shows the number of admitted UEs versus the number of available pilots B for the orthogonal pilot allocation and the DPR scheme with the optimised threshold, 5 dB and 10 dB thresholds when $\bar{K} = 32$, $S = 64$ and $M = 20$. The numbers of admitted UEs for the three cases increases with increasing the number of available pilots. However, the orthogonal pilot allocation scheme can serve the lowest number of UEs since no UEs are allowed to reuse the pilots. For the fixed threshold DPR scheme, the number of admitted UEs increases when the threshold decreases as more UEs can satisfy the SINR constraint. In the case of the optimised threshold DPR scheme, the number of admitted

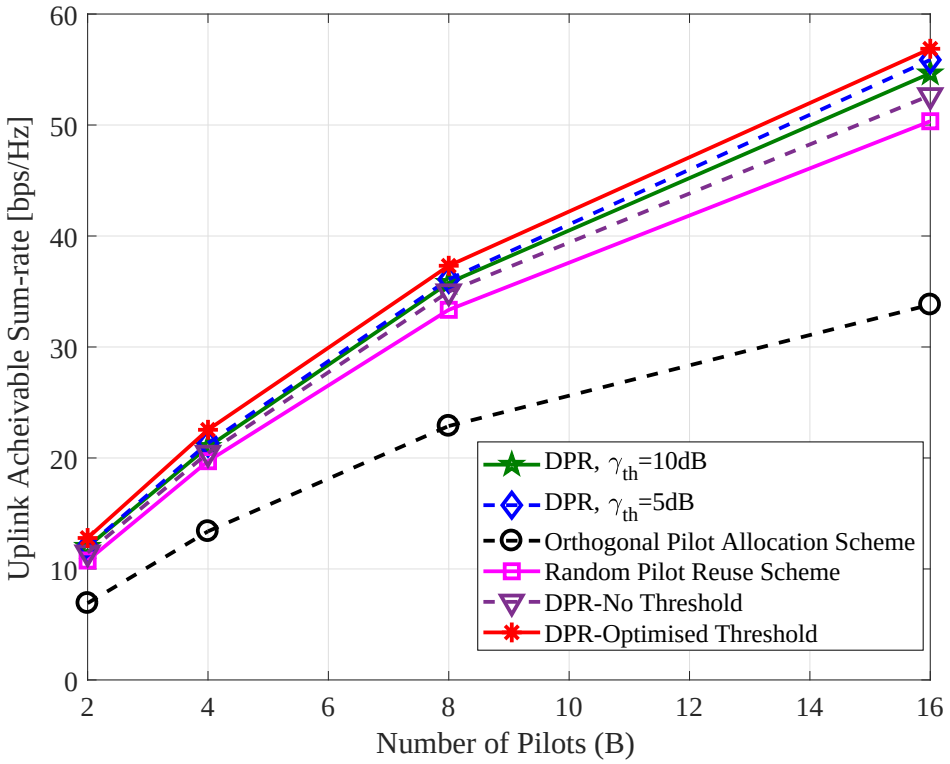

Figure 3.2: Uplink achievable sum-rate versus the number of pilots B.

UEs depends on the threshold itself, where the aim here is get the maximum sum-rate which does not guarantee a maximum number of admitted UEs.

The uplink achievable sum-rate is shown in Figure 3.4, by supposing $K = 16$, $B = 8$, $S = 64$ with $M = 10, 20, 50$ and 100. It is obvious that the sum-rate performance is continuously improved as M increases for all the reuse schemes owing to that a higher array gain can be obtained. This indicates that it is possible to reuse more pilots if a larger number of antennas is utilised as more UEs can satisfy the SINR constraint.

Figure 3.5 plots the uplink achievable sum-rate for the DPR scheme with the optimised threshold versus the number of pilots B with $\bar{K} = 32$, $S = 64$, $M = 20$ and for various sizes of serving cluster ($|\mathcal{N}_k| = 1, 2, 3$ and 4). The rate performance is generally improved as $|\mathcal{N}_k|$ increases, where more of the nearest RRHs will serve the UEs. Thus, more uplink signals for these UEs will be coherently detected by the CPU. However, when $|\mathcal{N}_k|$ is

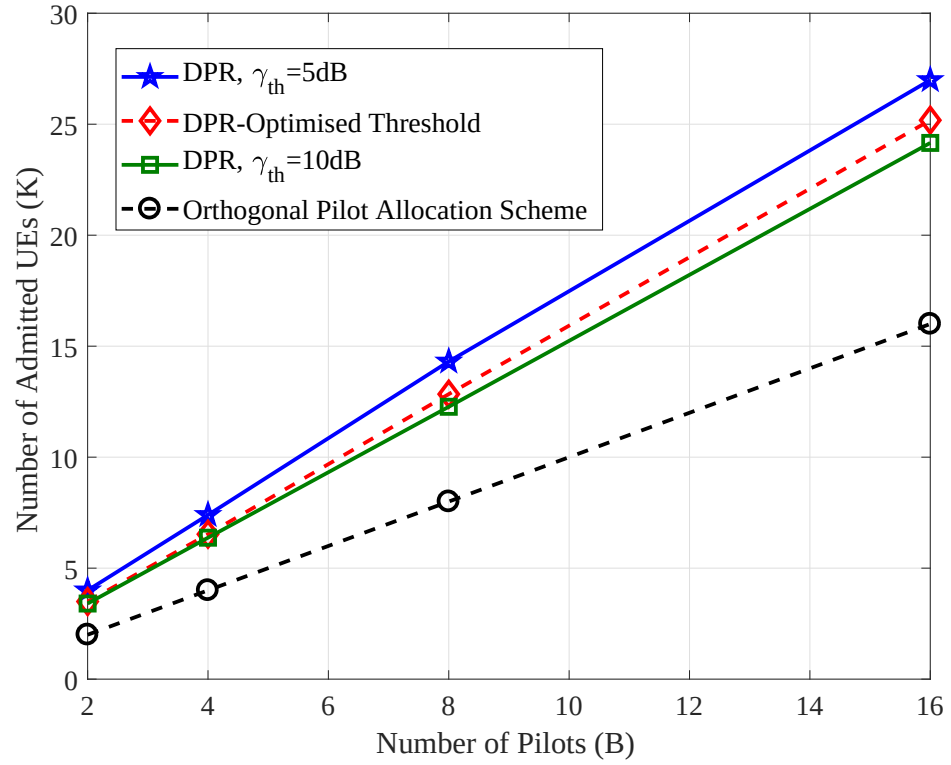

Figure 3.3: Number of admitted UEs versus the available pilots B.

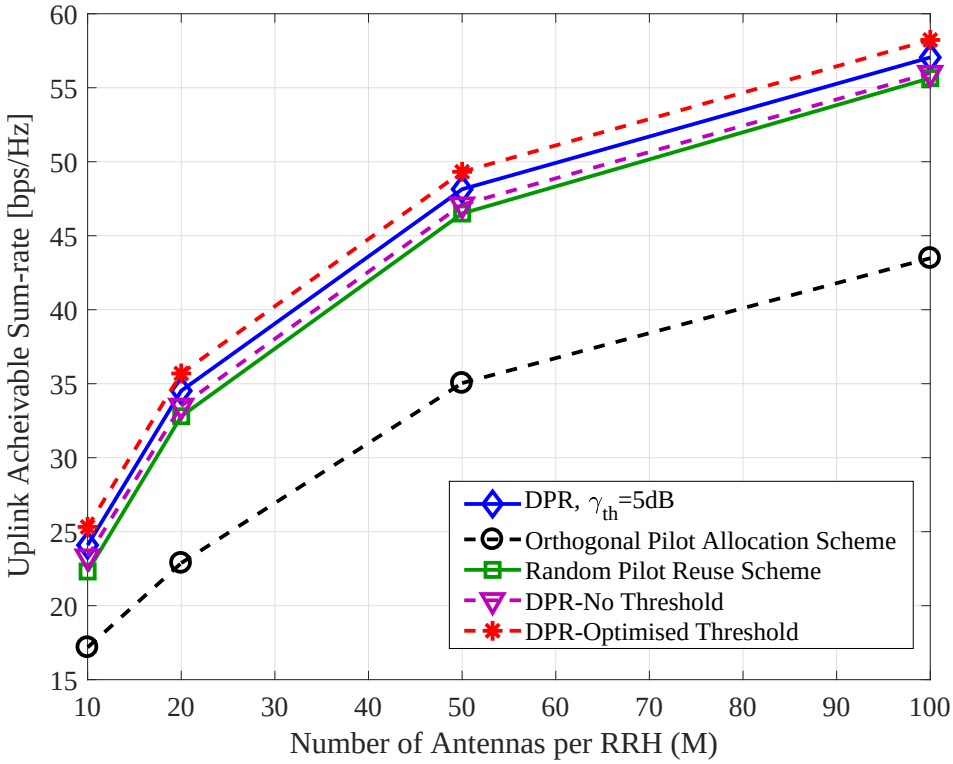

Figure 3.4: Uplink achievable sum-rate versus the number of antennas M.

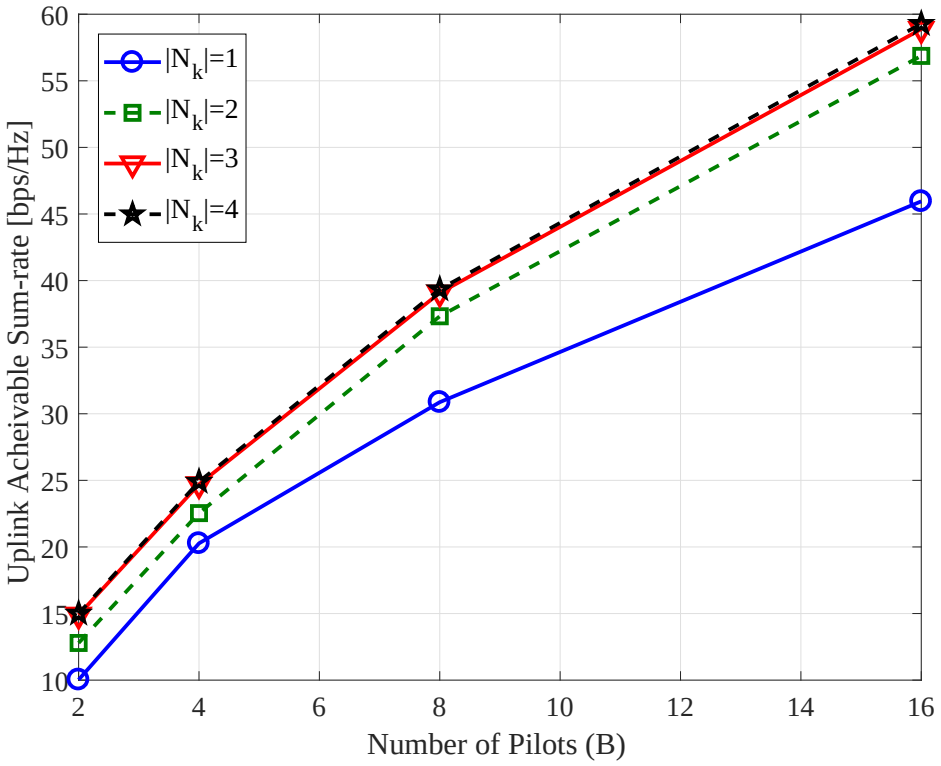

Figure 3.5: The impact of the size of $\mathcal{N}_k$ on the uplink achievable sum-rate.

greatly increased, such as when $|\mathcal{N}_k| = 3$ or 4, the two sets of $\mathcal{N}_k$ of a pair of UEs that share a single pilot will be closer to each other. Hence, higher pilot contamination could be received by RRHs located close to the second UE using the same pilot. This will negatively affect the sum-rate performance which will not be further improved.

Finally, the impact of changing the coherence block size S on the sum-rate performance of both the DPR scheme with the optimised threshold and the orthogonal pilot allocation scheme is shown in Figure 3.6 for different values of B. It is supposed here that $\bar{K} = 32$, $M = 20$, with three cases (S =32, 64 and 128). It is clear that the performance of the both two reuse schemes increases as S increases. The effect of the prelog-factor $(1 - \frac{B}{S})$ in (3.11) appears here. For a fixed B, the prelog-factor increases as S increases, where a greater part of the transmission block is employed for data transmission.

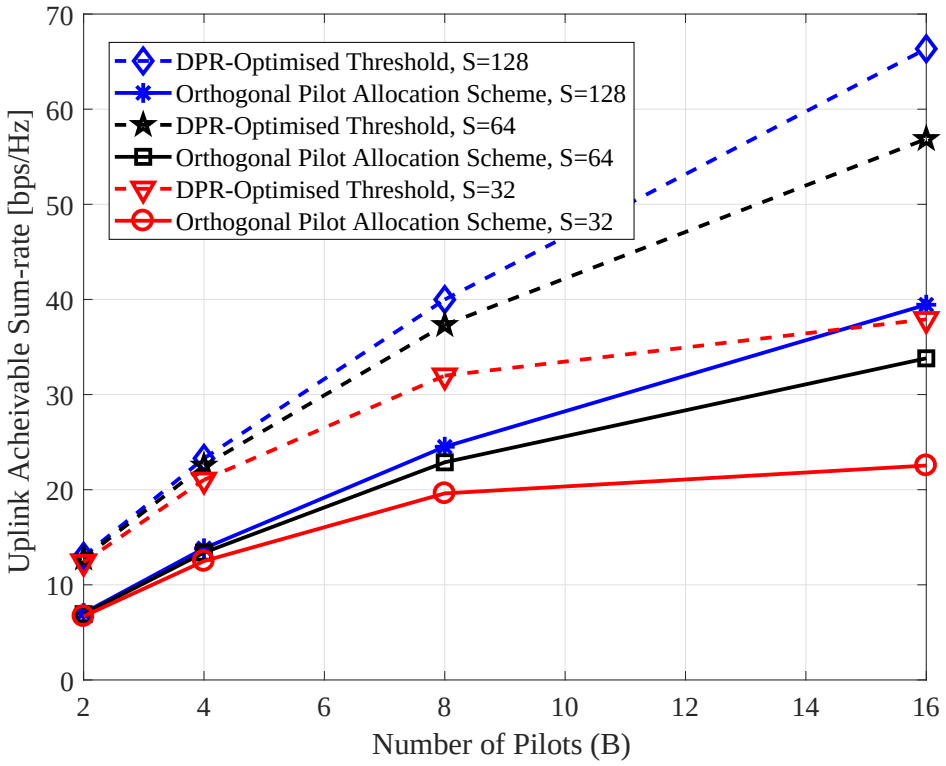

Figure 3.6: The effect of the transmission block size on the achievable sum-rate.

Chapter 4

Pilot Assignment in a CF massive MIMO System

In the previous chapter, the DPR scheme was presented assuming that a pilot can be shared by a pair of UEs located in a single cell of DM-MIMO. Although this scheme can be implemented in a CF massive MIMO system, reusing a pilot once can be impractical in the CF network that is supposed to cover a larger area than that of a single cell. In addition, a dense network was assumed in the previous scenario so a UE could has a high probability to obtain at least one nearby RRH being served this UE, thereby a good signal quality could be delivered. In this chapter, another pilot allocation design is presented that can be applied in CF networks of any size. This pilot reuse scheme is designed to specifically target the UEs suffering bad channel qualities, especially in non-dense networks in which some UEs might be far away from all the RRHs.

4.1 System Model

In this section, the network model for the CF massive MIMO is first presented. The signal model is then described together with the channel estimation method.

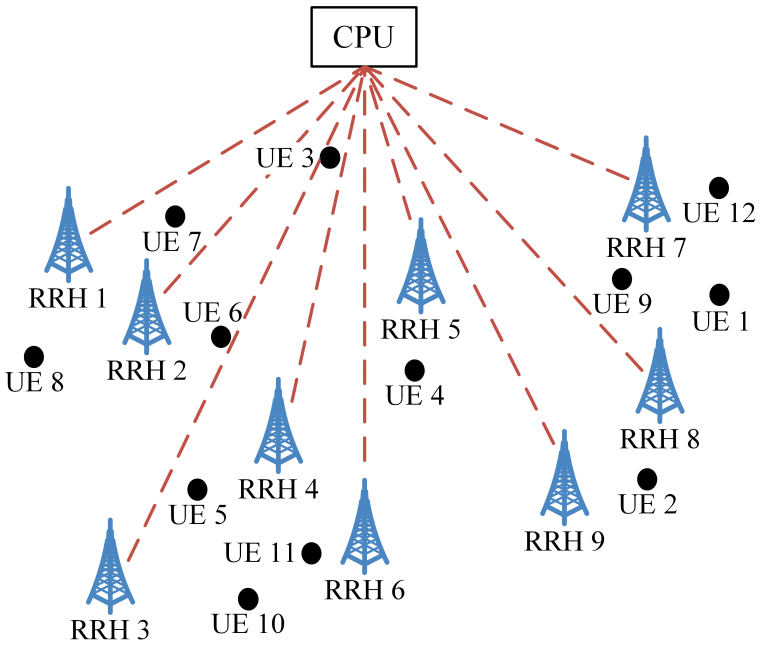

Figure 4.1: CF massive MIMO by supposing $\bar{K} = 12$.

4.1.1 Network Model

A downlink CF massive MIMO network is considered as shown in Figure 4.1. This network consists of $\bar{K}$ UEs and N RRHs, that simply transmit/receive radio signals. The set RRHs is denoted as $\mathcal{N} = \{1, \cdots, N\}$, and the set of UEs is denoted as $\bar{\mathcal{K}} = \{1, \cdots, \bar{K}\}$. It is supposed that K UEs are admitted in this network and the set of these UEs is denoted as $\mathcal{K} \subseteq \bar{\mathcal{K}}$. It has been presented in [15] that deploying a few multi-antenna RRHs in the CF massive MIMO is more beneficial than utilising many single-antenna APs from the channel hardening and spectral efficiency aspects. Increasing the number of antennas per RRH additionally means more array gain and less backhaul requirements [15]. Therefore, multiple antenna RRHs are assumed in this chapter, and each has M antennas. As shown in Figure 4.1, all RRHs are placed randomly in a large area and connected to a CPU via fronthaul links (the red dashed lines in Figure 4.1). The CPU has access to all UEs' CSI and data information. It is further assumed that UEs are equipped with single-antennas.

4.1.2 Signal Model

To reduce the computational complexity and data sharing overhead for the CF massive MIMO, the user-centric approach [22, 23] is adopted in this chapter as well. In this approach, a UE, for example UE k, only communicates with the nearest $\mathbb{N}$ RRHs, represented by the set $\mathcal{N}_k \subseteq \mathcal{N}$. Furthermore, the set of UEs served by RRH i is denoted as $\mathcal{K}_i \subseteq \mathcal{K}$. When applying the user-centric approach in the CF massive MIMO, the RRH sets for serving different UEs may overlap with each other. That is, for two UEs k and $k^{'}$, $\mathcal{N}_k \cap \mathcal{N}_{k'} \neq \varnothing$, $\forall k, k^{'} \in \mathcal{K}$. After applying the user-centric approach, the baseband received signal at UE k is modelled as

$$y_k = \underbrace{\sum_{i \in \mathcal{N}_k} \sqrt{\rho_{i,k}}\, \mathbf{h}_{i,k}^H \mathbf{w}_{i,k} s_k}_{\text{Desired Signal}} + \underbrace{\sum_{\substack{k' \in \mathcal{K} \\ k' \neq k}} \sum_{i \in \mathcal{N}_{k'}} \sqrt{\rho_{i,k'}}\, \mathbf{h}_{i,k}^H \mathbf{w}_{i,k'} s_{k'}}_{\text{Interference from other UEs}} + \underbrace{z_k}_{\text{Noise}}, \tag{4.1}$$

where $\mathbf{h}_{i,k} \in \mathbb{C}^{M \times 1}$ and $\mathbf{w}_{i,k} \in \mathbb{C}^{M \times 1}$ denote the downlink channel-vector and the precoding-vector from RRH i to UE k, respectively. s_k is the data symbol for UE k, and has unit power $\mathbb{E}\{|s_k|^2\} = 1$, and $\rho_{i,k}$ denotes the transmit power assigned to UE k from RRH i. Finally, $z_k \sim \mathcal{CN}(0, \sigma_k^2)$ stands for the additive complex white Gaussian noise (AWGN). The channel model includes the uncorrelated Rayleigh fading channel, which means that the channels are independent between UEs, RRH antennas and the coherence intervals. This assumption is based on the fact that the RRHs and the UEs are spread out over a wide area, therefore the scatterers for each RRH and each UEs are probably different [18]. The channel response vector $\mathbf{h}_{i,k}$ is assumed to follow $\mathcal{CN}(\mathbf{0}, \alpha_{i,k}\mathbf{I})$, where the variance $\alpha_{i,k}$ models the large-scale component that involves both the path-loss and the shadowing.

4.1.3 Uplink Channel Estimation for Intra-cluster CSI

Uplink and downlink transmissions in this scenario are executed by the TDD protocol. In addition to the uplink and downlink transmissions, each coherence interval includes a phase dedicated of uplink training. Since RRHs are considered as only simple radio units, the channel estimation of the uplink channels is assumed to be implemented in the CPU by utilising the pilot signals sent synchronously during the uplink training phase. It is not needed for RRHs to transmit pilots during the downlink transmission to measure the channel realisations. Alternatively, channel statistics are only needed due to the channel hardening phenomenon, as mentioned earlier [15, 18]. It is assumed that for a coherence interval of length S symbols, B symbols are dedicated for the uplink channel training. Then, the length of the pilot sequences that can be provided is B. The maximum number of the orthogonal pilot signal that can be available to serve the UEs is B as well. The remaining $S - B$ symbols of the coherence interval are devoted for data transmission. It is further assumed that B is smaller than the total number of UEs in the network, i.e., $B < K$. Consequently, without pilot reuse in CF massive MIMO, only B UEs can be served at the same time. In this chapter, the focus is on the case that $B < K$, and a proper pilot reuse scheme is proposed to enable UEs to share pilot sequences wisely in order to minimise the maximum estimation error for all UEs.

The available pilot set and their corresponding orthogonal pilot signals are denoted as $\mathcal{Q} = \{1, 2, \cdots, b, \cdots, B\}$ and $\mathbf{Q} = \{\mathbf{q}_1, \mathbf{q}_2, \cdots, \mathbf{q}_b, \cdots, \mathbf{q}_B\} \in \mathbb{C}^{B \times B}$, respectively. Each sequence in the matrix $\mathbf{Q}$ is mutually orthogonal with other sequences such that $\mathbf{Q}^H\mathbf{Q} = \mathbf{I}_B$. An arbitrary pilot reuse scheme with UEs set $\mathcal{K}$ and pilot set $\mathcal{Q}$ is denoted as $\mathcal{P}(\mathcal{K}, \mathcal{Q}) = \{(k, b_k) : k \in \mathcal{K}, b_k \in \mathcal{Q}\}$, where $(k, b_k) \in \mathcal{P}(\mathcal{K}, \mathcal{Q})$ denotes the pilot sequence $\mathbf{q}_{b_k}$ associated with the UE k. Furthermore, it is considered that $\mathcal{K}_b = \{k : b_k = b\}$ is the

group of UEs sharing the b^{th} pilot sequence.

During the training phase, each UE needs to transmit its assigned pilot to the RRHs to measure the CSIs. Given the pilot reuse scheme $\mathcal{P}(\mathcal{K}, \mathcal{Q})$, the received signal at RRH i arranged in a structure of size $M \times B$, is given by

$$\mathbf{Y}_{p,i} = \sqrt{\rho_p} \sum_{k \in \mathcal{K}} \mathbf{h}_{i,k} \mathbf{q}_{b_k}^H + \mathbf{N}_i, \tag{4.2}$$

where ρ_p is the transmit power for pilots, while $\mathbf{N}_i$ is the additive noise matrix received during the training phase with entries having the distribution $\mathcal{CN}(0, \sigma_p^2)$.

To estimate the channel-vector $\mathbf{h}_{i,k}$, where $i \in \mathcal{I}_k$, $\mathbf{Y}_{p,i}$ is first projected into $\mathbf{q}_{b_k}$ as

$$\begin{aligned} \mathbf{y}_{p,i,k} &= \frac{1}{\sqrt{\rho_p}} \mathbf{Y}_{p,i} \mathbf{q}_{b_k}, \\ &= \mathbf{h}_{i,k} + \sum_{k' \in \mathcal{K}_{b_k} \setminus \{k\}} \mathbf{h}_{i,k'} + \mathbf{n}_i, \end{aligned} \tag{4.3}$$

where $\mathbf{n}_i = \frac{1}{\sqrt{\rho_p}} \mathbf{N}_i \mathbf{q}_{b_k}$. The minimum mean square error (MMSE) estimate of channel $\mathbf{h}_{i,k}$ is given by

$$\hat{\mathbf{h}}_{i,k} = \alpha_{i,k} \Big(\sum_{k' \in \mathcal{K}_{b_k}} \alpha_{i,k'} + \hat{\sigma_p}^2 \Big)^{-1} \mathbf{y}_{p,i,k}, \tag{4.4}$$

where $\hat{\sigma_p}^2 = \sigma_p^2 / \rho_p$. Based on the property of MMSE estimation [55], the estimated channel $\hat{\mathbf{h}}_{i,k}$ is independent of the estimation error $\tilde{\mathbf{h}}_{i,k}$. Therefore, $\mathbf{h}_{i,k}$ can be decomposed as $\mathbf{h}_{i,k} = \hat{\mathbf{h}}_{i,k} + \tilde{\mathbf{h}}_{i,k}$, and both $\hat{\mathbf{h}}_{i,k}$ and $\tilde{\mathbf{h}}_{i,k}$ can be described as $\mathcal{CN}(\mathbf{0}, \theta_{i,k} \mathbf{I}_M)$ and $\mathcal{CN}(\mathbf{0}, \psi_{i,k} \mathbf{I}_M)$, respectively, where $\theta_{i,k}$ is expressed as [32, 56]

$$\theta_{i,k} = \frac{\alpha_{i,k}^2}{\sum_{k' \in \mathcal{K}_{b_k}} \alpha_{i,k'} + \hat{\sigma_p}^2}. \tag{4.5}$$

In addition, $\psi_{i,k}$ can be written as

$$\psi_{i,k} = \alpha_{i,k} - \theta_{i,k} = \frac{\alpha_{i,k} \big(\sum_{k' \in \mathcal{K}_{b_k} \setminus \{k\}} \alpha_{i,k'} + \hat{\sigma_p}^2 \big)}{\sum_{k' \in \mathcal{K}_{b_k}} \alpha_{i,k'} + \hat{\sigma_p}^2}. \tag{4.6}$$

Since the average channel estimation error will be considered later, a UE that is close to a RRH might have a very good channel where the estimation error $\psi_{i,k}$ will be large in absolute terms and will dominate over all the UEs having very weak channels to all RRHs. This can be addressed by utilising the normalised mean square error of the channel estimate (NMSE), where this metric will be employed in this chapter to compare the estimation quality of different pilot allocation schemes. NMSE can be defined as [21, 39]

$$\mathrm{NMSE}_{i,k} \triangleq \frac{\mathbb{E}\|\hat{\mathbf{h}}_{i,k} - \mathbf{h}_{i,k}\|^2}{\mathbb{E}\|\mathbf{h}_{i,k}\|^2} = \frac{\psi_{i,k}}{\alpha_{i,k}}. \tag{4.7}$$

Due to each UE being served by multiple RRHs, the aggregated NMSE per UE (ξ_k) needs to be generated. Therefore, the sum MSE for all the channels between the serving RRHs set ($\mathcal{N}_k$) and UE k divided by the sum of the variance of these channels is considered[1]. In other words, the NMSE per UE can be represented as

$$\xi_k = \frac{\sum_{i\in\mathcal{N}_k} \psi_{i,k}}{\sum_{i\in\mathcal{N}_k} \alpha_{i,k}}. \tag{4.8}$$

$\bar{\xi}$ will be additionally adopted to represent the average NMSE for all UEs in $\mathcal{K}$.

4.1.4 Downlink Sum-rate Performance

In this section, the downlink achievable sum-rate performance will be analysed for the CF massive MIMO network considering an arbitrary pilot assignment scheme along with the user-centric approach. The maximum-ratio transmission (MRT) precoding technique is assumed here. When the MRT precoding is used, the RRH i needs only $\hat{\mathbf{h}}_{i,k}$ to form the

[1]In calculating the total NMSE per user, averaging all the $\mathrm{NMSE}_{i,k}$ from the severing set $\mathcal{N}_k$ to the UE k is not recommended. If there is one RRH that is too close to UE k, a very low $\mathrm{NMSE}_{i,k}$ can be expected from this RRH. If the other RRHs are assumed to be far away from UE k, high $\mathrm{NMSE}_{i,k}$ are obtained from these RRHs. This creates a high total NMSE at UE k as the high values of $\mathrm{NMSE}_{i,k}$ dominate the one with low value, and this does not reflect the fact that UE k delivers a good performance as it is close to one of the RRHs. This has been also addressed in this chapter by using equation (4.8).

precoding vector for UE k. As a result, the MRT precoding is not affected by the local CSI approach as $\hat{\mathbf{h}}_{i,k}$ is always available, however this is not the case when the zero forcing (ZF) precoding is utilised. Under MRT representation, the precoding vector shown in (4.1) can be written as [56]

$$\mathbf{w}_{i,k} = \frac{\hat{\mathbf{h}}_{i,k}}{\sqrt{\mathbb{E}\{\|\hat{\mathbf{h}}_{i,k}\|^2\}}}. \tag{4.9}$$

The SINR analysis of the coherent transmission in [56] is employed in this chapter. The formula of the lower-bound SINR for UE k in [56] was derived in the scenario of multi-cell co-located massive MIMO with joint coherent transmissions as shown in ([56], Appendix F). In the following, this formula is modified to match the scenario of user-centric CF massive MIMO in this chapter as[2]

$$SINR_{k_{min}} = \frac{M\left(\sum_{i\in\mathcal{N}_k}\sqrt{\rho_{i,k}\theta_{i,k}}\right)^2}{M\sum_{i\in\mathcal{N}_k}\sum_{k'\in\mathcal{K}_{b_k}\setminus\{k\}}\rho_{i,k'}\,\theta_{i,k}+\sum_{i\in\mathcal{N}_k}\sum_{k'\in\mathcal{K}}\rho_{i,k'}\,\alpha_{i,k}+\sigma_k^2}. \tag{4.10}$$

In this chapter, it is assumed that each RRH distributes its power among the UEs served by this RRH based on the channel estimate strengths of these UEs. Thus, it is possible to describe $\rho_{i,k}$ as [23]

$$\rho_{i,k} = \frac{P_i|\hat{\mathbf{h}}_{i,k}|^2}{\sum_{l\in\mathcal{K}_i}|\hat{\mathbf{h}}_{i,l}|^2}, \tag{4.11}$$

where P_i is the total power transmitted by RRH i. The power control shown in (4.11) is similar to the maximum ratio combining approach for multipath diversity reception. For the SINR formula in (4.10), the numerator shows the signal power collected coherently from the set of serving cluster of RRHs, providing a better signal gain than utilising a single RRH. Benefiting from the array gain, the signal power increases with M. In the denominator of (4.10), the first term is the pilot contamination which increases with M.

[2]The derivation of this formula is presented in Appendix A.2.

The well designed pilot allocation scheme can provide a properly selected set of UEs sharing the same pilot which reduces $\psi_{i,k}$ and increases $\theta_{i,k}$ to enhance the SINR. The second term is the sum interference power from other UEs and the third term represents the power of noise. Finally, the lower-bound of the downlink ergodic achievable sum-rate of all admitted UEs is

$$R_{T_{min}} = (1 - \frac{B}{S}) \sum_{k \in \mathcal{K}} \log_2(1 + SINR_{k_{min}}). \tag{4.12}$$

4.2 Proposed Pilot Assignment Scheme

This section includes the proposed pilot allocation scheme aiming to achieve the objective of minimising the maximum estimation error with consideration of some practical constraints and a fixed number of pilot sequences.

4.2.1 Problem Formulation

In CF massive MIMO systems, as UEs with high pilot contamination limit system performance significantly [14], the pilot allocation in this chapter aims to minimise the maximum channel estimation error of all K UEs. Therefore, the problem of pilot allocation is formulated in the following

$$\mathcal{P}_e : \min_{\mathcal{P}(\mathcal{K}, \mathcal{Q})} \max_{\forall k \in \mathcal{K}} \xi_k, \tag{4.13a}$$

$$s.t. \, \mathcal{N}_k \cap \mathcal{N}_{k'} = \varnothing, \text{when } \mathbf{q}_{b_k} = \mathbf{q}_{b_k'}, \; k \neq k', \; \forall k, k' \in \mathcal{K}, \; \forall \mathbf{q}_{b_k} \in \mathbf{Q}, \tag{4.13b}$$

$$\max_b g_b \leq G, \; \forall b \in \mathcal{Q}. \tag{4.13c}$$

The constraint in (4.13b) indicates that it is required for the UEs sharing the same pilots to be associated with non-overlapped RRH clusters. In other words, the UEs served by the same RRH should be allocated with different orthogonal pilots for them. This

enables the CPU to differentiate the channels from UEs served by at least one common RRH. A similar idea is implemented in the cell-based scenarios where all UEs in the same macro-cell should be assigned orthogonal training sequences. In Figure 4.1, by allowing each UE is associated with its nearest two RRHs (i.e. $\mathbb{N} = |\mathcal{N}_k| = 2$, $\forall k \in \mathcal{K}$) based on the user-centric approach, UE 1, UE 2, UE 9 and UE 12 should utilise orthogonal pilots according to (4.13b) since the serving RRH clusters for all these UEs include one common RRH (RRH 8). Another constraint (4.13c) is employed to control the reuse times for each pilot sequence. In (4.13c), g_b is the number of times the l^{th} pilot sequence, $l \in \mathcal{Q}$ is used, and G is the limit of the number of times of reuse. This constraint is necessary to avoid high estimation error for some UEs, and to guarantee that there are no pilots that are extensively reused relative to other pilots.

The NMSE formula shown in (4.8) depends mainly on the large-scale fading coefficients $\alpha_{i,k}$ that vary at a slow rate, compared with the small-scale fading ones, and can be easily tracked by the CPU. Thus, the optimisation problem $\mathcal{P}_e$ can be rewritten as

$$\mathcal{P}_e : \min_{\mathcal{P}(\mathcal{K},\,\mathcal{Q})} \max_{\forall k \,\in\, \mathcal{K}} \frac{\sum_{i \in \mathcal{N}_k} \psi_{i,k}}{\sum_{i \in \mathcal{N}_k} \alpha_{i,k}}. \tag{4.14}$$

$$s.t.\ \text{(4.13b) and (4.13c)}.$$

To solve $\mathcal{P}_e$, the exhaustive search method can be utilised, in which all possible pilot allocation schemes are checked and the one that achieves the objective of minimising the maximum estimation error of all UEs while both (4.13b) and (4.13c) are satisfied is adopted. However, this is demanding computationally, especially in the case of a high number of UEs. In the subsequent section, a computation-feasible pilot allocation scheme is presented that can be suitably applied to improve the channel estimation error of UEs.

4.2.2 Pilot Assignment Scheme

In order to solve the optimisation problem $\mathcal{P}_e$, the following pilot allocation scheme is developed. Initially, the lower limit of $\psi_{i,k}$ can be easily obtained as provided in **Theorem 4.1**.

Theorem 4.1. *The minimum value of $\psi_{i,k}$ can be written as*

$$\psi_{i,k_{min}} = \frac{\alpha_{i,k}\ \hat{\sigma_p}^2}{\alpha_{i,k} + \hat{\sigma_p}^2}, \tag{4.15}$$

and $\psi_{i,k} = \psi_{i,k_{min}}$ can be obtained if and only if

$$\sum_{k' \in \mathcal{K}_{b_k} \backslash \{k\}} \alpha_{i,k'} = 0. \tag{4.16}$$

Proof. From (4.6), $\psi_{i,k_{min}}$ can be obtained

$$\psi_{i,k} = \frac{\alpha_{i,k}(\sum_{k' \in \mathcal{K}_{b_k} \backslash \{k\}} \alpha_{i,k'} + \hat{\sigma_p}^2)}{\sum_{k' \in \mathcal{K}_{b_k}} \alpha_{i,k'} + \hat{\sigma_p}^2} \tag{4.17}$$

$$\geq \frac{\alpha_{i,k}\ \hat{\sigma_p}^2}{\alpha_{i,k} + \hat{\sigma_p}^2}. \tag{4.18}$$

When $0 \leq \alpha_{i,l} \leq \alpha_{i,k}$, $l \in \mathcal{K}_{b_k} \backslash \{k\}$, $\psi_{i,k}$ will be increased monotonically when the set of UEs sharing the b_k^{th} pilot increases. Thus, if and only if $\alpha_{i,l} = 0$, $l \in \mathcal{K}_{b_k} \backslash \{k\}$, i.e., when UE k utilises unique pilot, the following can be satisfied

$$\sum_{l \in \mathcal{K}_{b_k}} \alpha_{i,l} = \alpha_{i,k}. \tag{4.19}$$

Plugging (4.19) into (4.17) will lead to (4.15). □

It can be seen that the minimum channel estimation error is achieved when a unique pilot is assigned to the UE, where noise will be the only contributor to the channel estimation error. However, as the pilot reuse is unavoidable when a large number of UEs (when $K > B$) have to be served, it is necessary to allocate pilots wisely to avoid having

a high channel estimation error. Inspired by the channel estimation error in (4.6), a series of parameters $\{\eta_k\}_{k=1}^{K}$ are declared to determine the statistical channel quality of the UEs in the network. These parameters can be defined as

$$\eta_k = \sum_{i \in \mathcal{N}_k} \alpha_{i,k},\ k = 1, 2, \cdots, K. \tag{4.20}$$

Furthermore, another set of parameters $\{\Upsilon_k\}_{k=1}^{K}$ is defined to evaluate the pilot contamination caused by UEs sharing the same pilot sequence with UE k as

$$\Upsilon_k = \sum_{k' \in \mathcal{K}_{b_k} \setminus \{k\}} \sum_{i \in \mathcal{N}_k} \alpha_{i,k'},\ k = 1, 2, \cdots, K. \tag{4.21}$$

It is assumed that $\mathcal{P}_u(\mathcal{K}_u, \mathcal{Q}_u) = \{(1, b_1^u), (2, b_2^u), \cdots, (K_u, b_K^u)\}$ is a particular pilot reuse scheme. The channel estimation error ψ_k defined in (4.6) for UE k that adopts the pilot b_k^u and RRH i is then determined by two aspects: the inter-group pilot contamination $\Upsilon_{b_k^u}$ caused by UEs sharing the same pilot with UE k, and the channel quality η_k. In order to minimise the maximum channel estimation error for all UEs in the network, high pilot contamination at the UEs having bad channel qualities should be avoided. A heuristic proposed pilot allocation scheme is then proposed based on this idea. At first, it is necessary to initially measure the minimum number of pilots (h) needed to serve all the UEs based on the constraints (4.13b) and (4.13b) and to remove some UEs when h is larger than the number of available pilots B. Thus, an initial stage is designed to identify the value of h while considering both (4.13b) and (4.13b) and to perform the UE selection if $h > B$. In the following, the two stages will be discussed:

4.2.2.1 Initial Stage

The aim of this stage is to calculate the minimum number of pilots h needed to serve all the UEs in the network and to achieve the UE selection. To fulfil the initial stage,

un undirected graph is generated, and the graph colouring mechanism utilised in [32] is adopted. This mechanism depends on the Dsatur algorithm [24, 32, 38], which requires low complexity. In order to create the indirected graph, and by following [32], a binary matrix $\mathbf{\Lambda}$ of size $K \times K$ is defined to satisfy (4.13b). In $\mathbf{\Lambda}$, the element $\lambda_{k,k'} \triangleq 1$ if the two UEs k and $k^{'}$ are served by at least one common RRH, i.e. $\mathcal{N}_k \cap \mathcal{N}_{k'} \neq \varnothing$, where $k \neq k^{'}$, otherwise $\lambda_{k,k'} \triangleq 0$. Based on $\mathbf{\Lambda}$, the undirected graph is generated, as shown in Figure 4.2, where the vertices denote UEs and the edges reflect the relationship between UEs governed by (4.13b) where any two UEs should be linked together if there is at least one RRH serves both of them. After generating the undirected graph, the graph colouring mechanism is applied, which allocates a minimum number of colours (equivalent to pilots) to all UEs. Colouring the vertices should ensure satisfying the constraint of the maximum number of reuse times G specified in (4.13c) and assigning different pilots to any pair of UEs connected with each other based on (4.13b) as illustrated in Figure 4.2. The minimum number of colours used in the graph colouring mechanism is equivalent to h. After identifying h, if the value of h is higher than B, some UEs need to be excluded to ensure that h is not higher than B. In the other case when $h \leq B$, all UEs can be served. If $h < B$, all B pilots will be exploited to serve UEs to further reduce the channel estimation error.

Algorithm 4.1 is presented here to reveal the procedures of how to measure h and achieve the UEs selection when $h > B$.

The full explanation of **Algorithm 4.1** can be described as follows:

1. *Initialization:* In line 1, the used pilot set is initialized as a null set, i.e., $\mathcal{Q}^{used} = 0$. Given $\alpha_{i,k}$, the matrix $\mathbf{\Lambda}$ can be calculated. In line 2, the first pilot is then allocated to UE 1 and $\mathcal{Q}^{used}$ is updated.

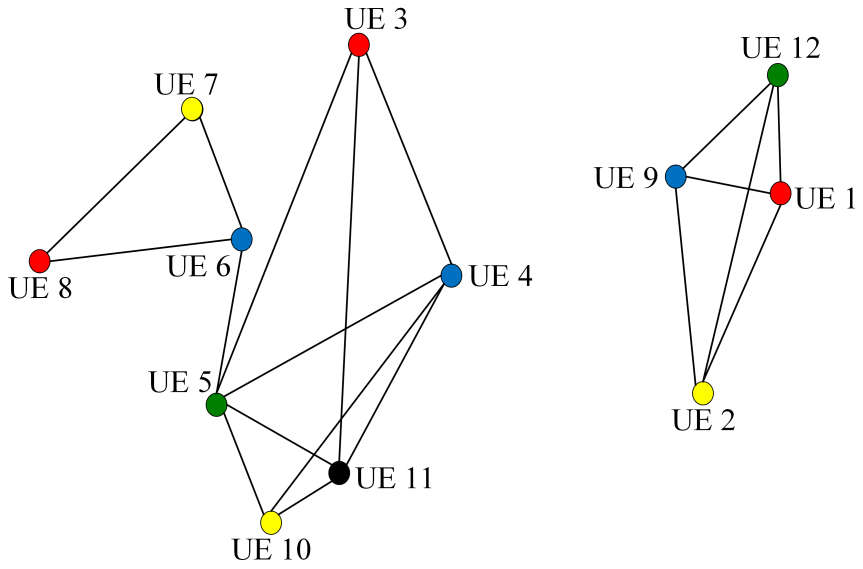

Figure 4.2: The indirected graph for the network in Figure 4.1 by assuming $\mathbb{N} = |\mathcal{N}_k| = 2$, $\forall k \in \bar{\mathcal{K}}$ after colouring its vertices by supposing $G = 3$.

2. *Loop Condition:* The rest of UEs in the set $\bar{\mathcal{K}}$ are assigned to their corresponding pilots in turn, and therefore the for loop in line 3 will go through all these UEs.

3. *Temporary Pilot Set:* To determine whether a new pilot or one of the previously used pilots is required, the set $\mathcal{Q}^{temp}$ is established in line 4. This set includes the pilots of any UE within the set {UE 1 to UE $k-1$} that has a link with the UE k in the undirected graph. A check is performed in line 5 on each UE k sequentially.

4. *A New Pilot Allocation Condition:* In the case when $\mathcal{Q}^{used} \cap \mathcal{Q}^{temp} = \mathcal{Q}^{used}$, this means that $\mathcal{Q}^{used} \cap \mathcal{Q}^{temp}$ includes all pilots that have already used $\mathcal{Q}^{used}$. Thus, a new pilot needs to be assigned to UE k and $\mathcal{Q}^{used}$ requires updating as illustrated in line 6.

5. *Unlinked Pilot Set:* In line 8, $\mathcal{Q}^{un}$ is further defined, which includes the set of pilots of the UE set {UE 1 to UE $k-1$} that is unlinked with UE k in the undirected graph.

6. *Reuse Times Condition:* $\mathcal{Q}^{un}$ is updated in line 9 to remove all pilots that have already been reused G times based on (4.13c). If all pilots are reused G times, i.e. $\mathcal{Q}^{un}$ is empty, a new pilot is allocated to UE k and $\mathcal{Q}^{used}$ is updated as in line 11. Otherwise, the pilot with the minimum index in $\mathcal{Q}^{un}$ is assigned to UE k (line 13). No need to update $\mathcal{Q}^{used}$ when a reused pilot is allocated to a UE. After colouring all the UEs, the cardinality of $\mathcal{Q}^{used}$ will be h.

7. *UE Selection:* If $h > B$, some UEs needs to be removed until $h = B$ is obtained. The UE with maximum connections in the undirected graph is first chosen to be removed, as all the connected UEs need to use different pilots from that utilised by this UE. It is necessary here to define $\aleph_k \triangleq \sum_{k' \neq k, k' \in \mathcal{K}} \lambda_{k,k'}$ as the number of connections that the UE k adopts with other UEs. If more than one UEs have the same maximum number of connections $\aleph_k$, among these UEs, the UE with the weakest channel quality η_k is first chosen to be removed. Afterwards, the matrix $\mathbf{\Lambda}$ is updated as shown in lines 17 to 19. Finally, a new h is calculated according to the new $\mathbf{\Lambda}$ and $\mathcal{Q}$ by repeating the steps in lines 1 to 16. The final set of $\bar{\mathcal{K}}$ will be $\mathcal{K}$.

4.2.2.2 Pilot Allocation Stage

After measuring h and determining the set of admitted UEs $\mathcal{K}$ through UE selection, the objective in $\mathcal{P}_e$ is achieved by adopting a further stage. In this stage, pilots are allocated to reduce the maximum channel estimation errors for all UEs. The channel gains for all UEs are already known through η_k in (4.20) by supposing that the large scale fading coefficients $\alpha_{i,k}$ are also known as well. The pilot interference information is also provided by Υ_k in (4.21). Although this pilot information is not available, the interference that a

Algorithm 4.1: Measuring h and UE selection

INPUT: System parameters: $\bar{\mathcal{K}}$, B, $\mathcal{Q}$, G, ξ_k, large-scale fading coefficients $(\alpha_{i,k})$.

OUTPUT: h and the set of admitted UEs $(\mathcal{K})$.

$\mathcal{Q}^{used} = 0$, calculate $\mathbf{\Lambda}$.

Part (1): Measuring h.

$b_1 = 1, \mathcal{K}_1 = \{1\}, \mathcal{Q}^{used} = \{1\}$.

for $k = 2$ to $|\bar{\mathcal{K}}|$ **do**

  $\mathcal{Q}^{temp} = \{b_k\}, \forall k$ such that $\mathbf{\Lambda}(k, 1:k-1) = 1$.

  if $\mathcal{Q}^{used} \cap \mathcal{Q}^{temp} = \mathcal{Q}^{used}$ **then**

    Allocate a new pilot, $b_k = |\mathcal{Q}^{used}| + 1, \mathcal{Q}^{used} \leftarrow \mathcal{Q}^{used} \cup \{|\mathcal{Q}^{used}| + 1\}$.

  else

    $\mathcal{Q}^{un} = \{\mathcal{Q}^{used} \setminus \mathcal{Q}^{temp}\}$.

    Update $\mathcal{Q}^{un} \leftarrow \mathcal{Q}^{un} \setminus \{t\}$, $\forall t$ such that $g_t > G$.

    if $\mathcal{Q}^{un} = \varnothing$ **then**

      Allocate a new pilot, $b_k = |\mathcal{Q}^{used}| + 1, \mathcal{Q}^{used} \leftarrow \mathcal{Q}^{used} \cup \{|\mathcal{Q}^{used}| + 1\}$.

    else

      Allocate a reused pilot, $b_k = \min\{\mathcal{Q}^{un}\}$.

    end if

  end if

end for

Part (2): UE selection when $h > B$.

while $h < B$ **do**

  Find $\grave{k} = \arg\max_{k \in \mathcal{K}} \aleph_k$. Select the UE with the weakest η_k if more than one UE have the same value of $\aleph_k$.

  Remove UE $\grave{k}$ from $\bar{\mathcal{K}}$, i.e., $\bar{\mathcal{K}}$=$\bar{\mathcal{K}}/\grave{k}$, and update matrix $\mathbf{\Lambda}$ with the new $\bar{\mathcal{K}}$.

  Go to step (1) to calculate the new h.

end while

UE receives can be controlled through the number of times the pilot associated with this UE is reused. Thus, the assignment of pilots in this section depends on the UEs with the low channel quality not receiving high pilot contamination. In other words, the UEs with the weakest channel quality will be allocated, as much as possible, with unique pilots or pilots with a low number of reuse times, while at the same time both (4.13b) and (4.13c) should continue to be satisfied.

The pilot allocation procedures are shown in **Algorithm 4.2**. The assignment of pilots requires a search within a number of possibilities of partitions of the UE set $\mathcal{K}$ obtained from the initial stage and choosing the partition that delivers a minimum average channel estimation error $\bar{\xi}$. In each partition, UEs are split into subsets equal to the number of available pilot sequences (B), and all the UEs in each subset will adopt an identical pilot sequence. The size of each subset should not be larger than G based on (4.13c), and there is no one common RRH serving the UEs in each subset simultaneously based on (4.13b). Despite the number of UEs in each subset, or the UEs sharing the same pilot being bounded at the upper limit by G, the allocations of pilots aims to assign a unique pilot or pilots with low number of reuse times to the UEs with the worst channel condition. UEs with the best channel quality are assigned with pilots reused more times. Although a huge number of UE set partitions can be initially obtained, applying all the above-mentioned constraints significantly limit the final number of partitions to be accepted for a search. This will be explained in detail in Section 4.4. The size of UE subsets in one UE set partition is generally depended on the ratio between K and B. To further clarify how the size of UEs subsets are decided and how pilots are allocated to UEs in each partition, the following two cases can be recognised.

1. When $K > 2B$, the number of UEs is much larger than the number of available

Algorithm 4.2: Pilot allocation algorithm

INPUT: System parameters: $\mathcal{K}$, B, N, h, G, η_k.

OUTPUT: Pilot allocation: $\mathcal{P}(\mathcal{K}, \mathcal{Q}) = \{(k, b_k) : k \in \mathcal{K}, b_k \in \mathcal{Q}\}$.

1: Find all possibilities of how the UEs set can be partitioned, denote the set of such partitions by $\mathcal{V} = [v_1, v_2, \cdots, v_f, \cdots, v_F]$, each partition in $\mathcal{V}$ should include B disjoint subsets. Assume for the $v_f{}^{th}$ partition, $\mathcal{L}_{v_f} = [l_1, l_2, \cdots, l_b, \cdots, l_B]$ are the subsets of this partition, the cardinal number of each subset l_b will be, $1 \leq |l_b| \leq G$, $\forall l_b \in \mathcal{L}_{v_f}$, $\forall v_f \in \mathcal{V}$. If $|l_b| \geq 2$, $\forall l_b \in \mathcal{L}_{v_f}, \forall v_f \in \mathcal{V}$, for (any) UE pair $\{k, k^{'}\}$ in this subset, (4.13b) should be satisfied, i.e. $\mathcal{N}_k \cap \mathcal{N}_k^{'} \neq 0$. The partitions in $\mathcal{V}$ should include UEs with the worst channel quality within the smallest subsets.

2: Find $v_{min} = \arg\min_{v \in \mathcal{V}} \bar{\xi}$.

3: **for** $b = 1$ to B **do**

4: For the partition v_{min}, assign the b^{th} pilot to all UEs in l_b, $b_k = b, \mathcal{K}_b = \{k\}, \forall k \in l_b, \forall l_b \in v_{min}$.

5: **end for**

pilots B. Each pilot therefore needs to be reused at least once and at most G as mentioned earlier. For instance, the case $K = 10$ with the following UEs ascending channel gain η_k order $[8, 2, 9, 6, 3, 1, 7, 5, 10, 4]$ is assumed; $B = 4$ and $G = 3$ are supposed in this example. For the partition 2 2 3 3, the two subsets of size 2 have to be filled, in any order, with any pair from the UEs $[8, 2, 9, 6]$ from the channel gain η_k vector as they have the weakest channel qualities. Then the remaining UEs $[3, 1, 7, 5, 10, 4]$ can be placed, in any order, into the remaining subsets of size 3. The partition at the end can be $[\{8, 2\}, \{9, 6\}, \{3, 1, 7\}, \{5, 10, 4\}]$, which represents an acceptable partition to be included in the search for UE partitions for the final pilot allocation. This supposes that the UEs in each subset in this partition satisfy (4.13b). As can be seen, this partition contains the UEs with the worst channel

quality in the subsets filled with a pair of UEs. The remaining UEs have been placed into the subsets of a larger size.

2. When $K \leq 2B$, the UEs with the weakest channel quality are able to utilise unique pilot sequences, while the UEs with good channel gains can be grouped so that more then one UE can share the same pilot. If it is assumed that six UEs have the following increasing channel quality η_k order $[2, 6, 3, 1, 5, 4]$, where UE 2 has the worst channel quality, by assuming $B = 4$ and $G = 3$, the examples of acceptable partitions that the search in **Algorithm 4.2** can include are $[2, 6, \{3, 1\}, \{5, 4\}]$ and $[2, 6, 3, \{1, 5, 4\}]$. In these two examples, and the same applies to all other possible UEs partitions, the UEs with worst channel quality will be allocated unique pilots. The rest of the UEs will share the rest of the pilots so that two or more UEs utilise the same pilot.

The proposed pilot allocation scheme can be achieved in the CPU. The assignment of pilot signal should be updated based on the rate at which the large-scale fading changes as the formula of NMSE in (4.8) is a function of the large-scale fading coefficients. It has been demonstrated that even in the case of high mobility, the large-scale fading varies slowly compared with the coherence interval, where it can be 40 times slower [18, 57]. This will reduce the complexity at the CPU. However, the undirected graph depends on the mobility of UEs. If the serving cluster of RRHs for an arbitrary UE has been changed due to moving this UE, the undirected graph will be changed under the constraint (4.13b) and hence the initial stage of calculating h and achieving the UE selection needs to be recomputed.

4.3 Channel Estimation Error Minimisation Problem

In the previous section, a pilot allocation scheme was presented with the objective of minimising the maximum channel estimation error. As the estimation error will affect the SINR in the data transmission, so as to the data-rate, in this section, the channel estimation error minimisation is linked with the SINR and the data-rate performance. Specifically, by adopting the same constraints of $\mathcal{P}_e$, problem $\mathcal{P}_s$ is further developed to allocate the pilots with the objective of minimising the average channel estimation error $\bar{\xi}$ with considering an additional constraint aiming to satisfy a SINR threshold (γ_{th}) per UE. This problem includes finding the minimum number of pilots (h_s) needed to serve all the UEs while satisfying both the objective and the constraints. It is necessary to mention here that the problem of minimising the training overhead while deploying the user-centric approach has been solved in both [24, 32] by utilising the graph colouring. However, the issue of delivering a particular quality of service (QoS) to the UEs and achieving the objective of minimising the average channel estimation error were not involved in [24, 32].

The problem described above can be formulated as

$$\mathcal{P}_s : \min_{\mathcal{P}(\mathcal{K},\,\mathcal{Q})} (\bar{\xi}, h_s) \tag{4.22a}$$

$$\text{s.t. } SINR_{k_{min}} \geq \gamma_{th},\ \forall k \in \mathcal{K}, \tag{4.22b}$$

$$\mathcal{N}_k \cap \mathcal{N}_{k'} = \varnothing, \text{when } \mathbf{q}_{b_k} = \mathbf{q}_{b_k'},\ k \neq k',\ \forall k, k' \in \mathcal{K},\ \forall \mathbf{q}_{b_k} \in \mathbf{Q}, \tag{4.22c}$$

$$\max_b g_b \leq G,\ \forall b \in \mathcal{Q}. \tag{4.22d}$$

This problem can be solved by utilising **Algorithm 4.3**, in which the graph colouring method in **Algorithm 4.1** is initially adopted to calculate the number of pilots h required to serve all the UEs in the network. By assuming $B \geq h$, all UEs can be served in this case and the UE selection is not required. This means that the second part of **Algorithm**

4.1 can be avoided when this algorithm is achieved. In this stage, **Algorithm 4.4** can be defined as being the same as of **Algorithm 4.2** except that each UE in each partition should satisfy the constraint (4.22b). If no partition meets the threshold in (4.22b), another pilot will be added to further improve the SINR of UEs and **Algorithm 4.4** will be repeated again. After updating the number of pilots, the constraint (4.22b) is tested again. If some partitions satisfy (4.22b) in addition to the other constraints, the partition with the minimum $\bar{\xi}$ will be chosen as the final pilot allocation scheme.

Algorithm 4.3: Solving $\mathcal{P}_s$

INPUT: System parameters: K, M, B, N, G, η_k, $q = 0$;

Large scale fading coefficients $\alpha_{i,k}$.

OUTPUT: $\mathcal{P}(\mathcal{K}, \mathcal{Q}), h_s$.

1: Apply **Algorithm 4.1** to find h.

2: Apply **Algorithm 4.4** by utilising h pilots, and denote the set of the partitions obtained from **Algorithm 4.4** as $\mathcal{V}_s = [v_1, v_2, \cdots, v_f, \cdots, v_F]$. Each partition in $\mathcal{V}_s$ should include h disjoint subsets. For the ${v_f}^{th}$ partition, $\mathcal{L}_{v_f} = [l_1, l_2, \cdots, l_q, \cdots, l_h]$ are assumed to be the subsets of this partition.

3: **if** $|\mathcal{V}_s| = \varnothing$ **then**

4: $h = h + 1$.

5: Go to step 2.

6: **else**

7: Find $v_{min} = \arg\min_{v \in \mathcal{V}_s} \bar{\xi}$.

8: $h_s = h$.

9: **end if**

10: **for** $q = 1$ to h **do**

11: For the partition v_{min}, assign the q^{th} pilot to all UEs in l_q, $b_k = q, \mathcal{K}_q = \{k\}, \forall k \in l_q, \forall l_b \in v_{min}$.

12: **end for**

4.4 Complexity Analysis

The computational complexity of the proposed algorithms is quantified in this section. For **Algorithm 4.1**, the computational complexity $\mathcal{O}(K^2)$ is required to operate the initial stage based on the Dsatur algorithm [26]. When some UEs need to be removed, the Dsatur algorithm should be executed also for at most K times to decide the final set of admitted UEs, and therefore the complexity has an upper limit of $\mathcal{O}(K^3)$ in this case.

In **Algorithm 4.2**, for the set of admitted UEs $\mathcal{K}$ with cardinality K, it is required to partition this set into B non-empty subsets. By assuming that $\bar{\mathcal{V}}$ is the set of these partitions, the number of ways $|\bar{\mathcal{V}}|$ of doing this is $\left\{ {K \atop B} \right\}$, where the notation $\left\{ \ \right\}$ indicates the Stirling number of the second kind. The explicit formula of $\left\{ {K \atop B} \right\}$ can be written as [58]

$$|\bar{\mathcal{V}}| = \left\{ {K \atop B} \right\} = \frac{1}{B!} \left(\sum_{i=0}^{B} (-1)^{B-i} \begin{pmatrix} B \\ i \end{pmatrix} i^K \right). \tag{4.23}$$

Due to constraint (4.13c), the illegal partitions that include any subset with the size $\widetilde{n}$, where $\widetilde{n} > G$, should be excluded from $\bar{\mathcal{V}}$. Since there are $\frac{K!}{\widetilde{n}!(K-\widetilde{n})!}$ possible ways to form the subset of size $\widetilde{n}$, the remaining $(B-1)$ subsets have to be filled with the rest of $(K-\widetilde{n})$ UEs. As there are $\left\{ {K-\widetilde{n} \atop B-1} \right\}$ ways to partition the remaining $(K-\widetilde{n})$ UEs into $(B-1)$ subsets, the restricted number of partitions $|\bar{\bar{\mathcal{V}}}|$ when the constraint (4.13c) is considered will be:

$$|\bar{\bar{\mathcal{V}}}| = |\bar{\mathcal{V}}| - \sum_{\widetilde{n}=G+1}^{K-B+1} \frac{K!}{\widetilde{n}!(K-\widetilde{n})!} \left\{ {K-\widetilde{n} \atop B-1} \right\}. \tag{4.24}$$

The upper limit of $\widetilde{n}$ shown in (4.24) is $\widetilde{n} = K - B + 1$. This can be obtained when a partition includes a subset of size $(K-B+1)$ and the remaining subsets contain single UEs.

In order to continue excluding the partitions that do not satisfy the constraint (4.13b) from $\bar{\bar{\mathcal{V}}}$, and also excluding the partitions that do not include the UEs with the weakest channel qualities in the subsets with the smallest size, a brute force method will be utilised in the next part to list the final set of acceptable partitions. The brute force method of calculating this includes:

1. Listing all the partitions of $\bar{\bar{\mathcal{V}}}$;
2. For each of these partitions, determining the number of set partitions of $\mathcal{K}$ into subsets, sizes of which correspond to the partition of K;
3. Summing the number of set partitions corresponding to each partition of K.

There is an explicit formula for step 2. The partition can be written as

$$\begin{pmatrix} a_1 & a_2 & \cdots & a_p \\ r_1 & r_2 & \cdots & r_p \end{pmatrix} \tag{4.25}$$

where the a_i's are the distinct numbers that appear in the partition and r_i is the number of times that a_i is repeated, so that $K = \sum_{i=1}^{p} r_i a_i$. For example, if $K = 15$ and $B = 7$, the partition 1 2 2 2 2 3 3 would be written as

$$\begin{pmatrix} 1 & 2 & 3 \\ 1 & 4 & 2 \end{pmatrix}$$

After this, the number of (unique) set partitions of K that this gives is [59]

$$\frac{K!}{\{(a_1!)^{r_1}(a_2!)^{r_2}\cdots(a_p!)^{r_p}\} \times (r_1!r_2!\cdots r_p!)}. \tag{4.26}$$

The next example shows how this approach would be used to calculate the number of ways of partitioning a set of $K = 12$ UEs into $B = 6$ non-empty subsets. The Stirling number of the second kind is $\left\{ {12 \atop 6} \right\} = 1323652$. For the brute force enumeration, 11

Table 4.1: Partition Sets When $K = 12$ and $B = 6$

Partition	Number of Possible Partitions
7 1 1 1 1 1	792
6 2 1 1 1 1	13860
5 3 1 1 1 1	27720
4 4 1 1 1 1	17325
5 2 2 1 1 1	83160
4 3 2 1 1 1	277200
3 3 3 1 1 1	61600
4 2 2 2 1 1	207900
3 3 2 2 1 1	415800
3 2 2 2 2 1	207900
2 2 2 2 2 2	10395

possible partitions are generated in Table 4.1 and the formula (4.26) has been applied for each. Summing the number of possible partitions for each case in Table 4.1 will give the Stirling number 1323652. By applying the constraint (4.13c), the brute force approach can easily be adopted by just excluding any partitions with any subset of a size larger than G. For the example in Table 4.1, when $G = 3$, the restricted list of partitions are illustrated in (Nsubsets1) in Table 4.2. The summation of these partitions is 695695.

In order to keep only the partitions that include UEs with the worst channel quality within the subsets with the smallest sizes as described earlier, the following formula needs to be applied in turn to the subsets of each size [59]

$$\prod_{i=1}^{p} \frac{(a_i r_i)!}{r_i!(a_i!)^{r_i}}. \tag{4.27}$$

For instance, the partition 3 3 2 2 1 1 is equivalent to $\begin{pmatrix} 1 & 2 & 3 \\ 2 & 2 & 2 \end{pmatrix}$, and the number of allowable subsets is

$$\frac{2!}{2!(1!)^2} \times \frac{4!}{2!(2!)^2} \times \frac{6!}{2!(3!)^2} = 1 \times 3 \times 10 = 30.$$

This can be applied similarly for all the partitions. The results are given in the third column (Nsubsets2) of Table 4.2. Note that the partition 2 2 2 2 2 2 has been excluded from Nsubsets2 as all its subsets have the same size, therefore there is no advantage for the UEs with the weakest channels when this partition is utilised.

Since the constraint (4.13b) refers to the fact that it is not possible for any set of UEs sharing the same pilot to be served by any common RRH. This additionally reduces the number of acceptable partitions. Any partition with a subset of UEs served by at least one common RRH should be excluded here. For N RRHs, and for the special case where each UE is served by the nearest two RRHs, the probability that a particular subset of 2 is allowable, in the sense that the two UEs in this subset have different nearest two RRHs is $\frac{(N-2)(N-3)}{N(N-1)}$. Furthermore, the probability that a subset of 3 or 4 includes UEs with non-overlapping serving RRH clusters is $\frac{(N-2)(N-3)(N-4)(N-5)}{(N(N-1))^2}$ and $\frac{(N-2)(N-3)(N-4)(N-5)(N-6)(N-7)}{(N(N-1))^3}$, respectively. For example, if there are 12 RRHs, the probability that a subset of three UEs will have different serving clusters, is 0.289. Thus, for the partition 3 3 3 1 1 1, all three sets of 3 need to be allowable, and the probability of this is $0.289 \times 0.289 \times 0.289 = 0.024$. After that, the number of partitions of the form 3 3 3 1 1 1 (given by Nsubsets2 in Table 4.2) is multiplied by this probability. The results are shown in the final column (Nsubsets3) of Table 4.2. The results of the final column do not provide the exact number in general, but the exact number depends on the spatial location of the UEs and the RRHs, so that the results here could be thought of as a sort

of average.

Table 4.2: Number of Partitions

	Number of Possible Partitions		
Partitions	Nsubsets1	Nsubsets2	Nsubsets3
3 3 3 1 1 1	61600	280	6.8
3 3 2 2 1 1	415800	30	1.2
3 2 2 2 2 1	207900	105	6.6
2 2 2 2 2 2	10395	–	–
Summation	695695	415	14.6

For **Algorithm 4.3**, the computational complexity comes from two steps. **Algorithm 4.1** is initially required to calculate h and that includes a complexity of $\mathcal{O}(K^2)$, where no UE selection is needed. After this, **Algorithm 4.4** is applied by utilising h pilots, which requires a similar complexity to that of **Algorithm 4.2** with $B = h$ by assuming it is required to search within all partitions of **Algorithm 4.2** to find the ones that satisfy the SINR constraint. Since it is needed to add a pilot when no partition meets the SINR condition, **Algorithm 4.4** should be repeated at most $(K - h)$ times, where h is incremented in each time. This means that the upper limit of the total complexity of **Algorithm 4.3** is $\mathcal{O}(K^2)$ plus $(K - h)$ times the complexity of **Algorithm 4.2**.

4.5 Simulation Results

The performance of the proposed algorithms is examined in this section. A CF massive MIMO network deployed in an area of 1km^2 is considered in this chapter. Both the UEs and RRHs are assumed to be randomly and uniformly distributed in this area. Each

RRH has 20 antennas and each UE has a single antenna. The coefficients of the large scale fading $\alpha_{k,i}$ can be modelled according to the 3GPP standard [32, 60]. First, the path-loss is $148.1 + 37.6 \log_{10} d_{i,k}$ (dB), where $d_{i,k}$ is the distance between the i^{th} RRH to the k^{th} UE measured in km. Then, the large scale fading $\alpha_{i,k}$ is calculated as $\alpha_{i,k} = -148.1 - 37.6 \log_{10} d_{i,k} + \wp_{i,k}$ (dB), where $\wp_{i,k}$ symbolises the shadow fading and possesses a lognormal distribution, which is represented by $10 \log_{10}(\wp_{i,k}) \sim \mathcal{CN}(0, \sigma^2_{shad})$. Based on the user-centric method, it is assumed that each UE chooses its nearest two RRHs, that is $\mathbb{N} = |\mathcal{N}_k| = 2$, $\forall k \in \mathcal{K}$. The other system parameters are summarised in Table 4.3. It is necessary to clarify here that since the results of the exhaustive search are included as it will be shown in the next paragraph, a relatively small CF network is considered in this simulation as larger networks imply unaffordable complexity of **Algorithm 4.2** in th case of the exhaustive search. The following results have been collected by averaging over 1000 independent trials, where UEs are randomly placed in each trial.

Table 4.3: Simulation Parameters

Parameter	Value
Number of RRHs (N)	10
Number of UEs ($\bar{K}$)	12
Shadow fading standard deviation (σ^2_{shad})	8 dB
Maximum number of pilot reuse times (G)	3
Noise variance for both σ_p^2 and σ_k^2	-96 dBm
Transmit power for pilots (ρ_p)	200 mW
RRH's maximum transmit power (P_i)	100 mW
Number of symbols per coherence block (S)	128

The performance of the proposed pilot reuse scheme obtained from **Algorithm 4.2**

is compared with that of the following three cases:

1. Exhaustive search: provides the optimal solution. It is the solution of the optimisation problem $\mathcal{P}_e$ when the exhaustive search is adopted. A complete search is fulfilled for all possibilities of how UE sets can be partitioned that meet only constraints (4.13b) and (4.13c).

2. Graph colouring: is obtained by allocating the pilots based only on the graph colouring as considered in [32].

3. Orthogonal pilot allocation (PA) scheme: includes assigning a unique orthogonal pilot to each UE. Therefore, there is no pilot contamination, and the channel estimation error is only caused by noise. This case requires a high pilot overhead especially when K is large.

In Figure 4.3, the average NMSE symbolised by $\bar{\xi}$ is plotted versus the number of available pilots B. The value of B is varied so that the performance of all the cases of the relationship between B and h can be tested, when all UEs can be served or only some of them. In addition, the two cases when $K \leq 2B$ or $K > 2B$ are shown, depending on the value of B. It can be seen from Figure 4.3 that the proposed scheme outperforms the graph colouring based allocation scheme, as in the latter, no channel information is exploited. Furthermore, the proposed pilot reuse scheme allocates the pilots with a lower number of reuse times to the UE with worst channel quality. The exhaustive search scheme gains a better performance compared with both the proposed scheme and the graph colouring as it always finds the best option among UE set partitions that can be served with the available set of pilots. However, a high computational complexity is needed to fulfil the exhaustive search as it will be shown later. As expected, the orthogonal pilot allocation (PA) scheme

achieves a small channel estimation error as UEs deliver zero pilot contamination in this case, and the channel noise is the only source of the error when the channels between UEs and RRHs are estimated. In order to serve all the 12 UEs assumed while generating Figure 4.3, the average value of h needs to generally be around 5.5 (as shown later in Figure 4.7). In Figure 4.3, when $B \leq 5$, h is mostly higher than B. This means that some UEs need to be removed, where the UEs with highest number of connections in the undirected graph and experience the weakest channels will be removed as illustrated in the UE selection part of **Algorithm 4.1**. The available pilots are reused intensively among the remaining UEs in all reuse schemes and a high pilot interference is expected. However, as the UEs with the highest number of connections and worst channel quality are removed, the remaining UEs mostly have good channels, thereby low average NMSE can be obtained. When $B = h$, at around $h = 5$, all UEs can be served and pilots are still highly reused and this leads to obtaining the maximum $\bar{\xi}$. As the average value of h needs to generally be around 5.5 based on Figure 4.7, when B is greater than 6, h is most probably less than B where all UEs can be served. The performance will be better as B increases, as a lower number of reuse for pilots can be performed. When $K > 2B$, unique pilots can be allocated to the UEs with the lowest channel quality so the performance of the proposed scheme approaches that of the optimal solution.

Figure 4.4 shows the number of admitted UEs K versus the number of pilots B for the proposed pilot allocation scheme, which is the same as the graph colouring based scheme and the exhaustive search method. As it is required to remove some UEs when $h > B$, it is not possible to serve all UEs when B is small. As B increases, K increases as well and more UEs can be admitted until all UEs can be served ($K = \bar{K}$) from $B = h$.

After studying the average NMSE ($\bar{\xi}$) in Figure 4.3, the actual NMSE ξ for every UE achieved by different algorithms is presented in Figure 4.5 for one randomly se-

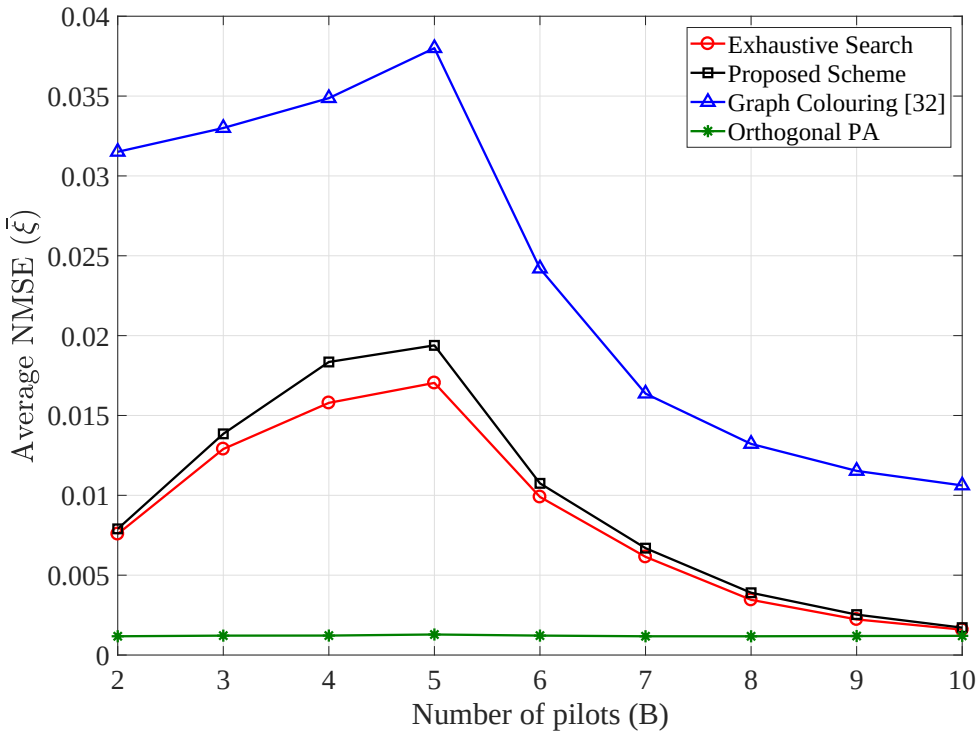

Figure 4.3: Average NMSE $\bar{\xi}$ versus the number of pilots B.

lected simulation trial. In this case, $B = 5$ and $G = 3$ are considered. The result of **Algorithm 4.1** shows that $h = 5$ is needed to serve all the UEs. Since $h = B$, all UEs can be admitted. In this trial, UEs have the following increasing channel quality η_k order $[7, 6, 12, 1, 11, 9, 10, 4, 8, 3, 5, 2]$, where UE 7 has the lowest channel quality. When the graph colouring is applied as illustrated in **Algorithm 4.1**, UEs shared the five pilots in the following manner, $[\{3\}, \{4, 2\}, \{7, 6, 1\}, \{12, 11, 9\}, \{10, 8, 5\}]$, where the UEs in each subset share one single pilot. As shown in Figure 4.5, the performance of the UEs with the worst channel quality is bad especially for UEs that their pilots have been reused two times, for example UE 7 and UE 6. The reason is that no channel information is exploited in **Algorithm 4.1**. In **Algorithm 4.2**, pilots with lower reuse times will be allocated to the UEs with lowest channel quality condition. The result of this allocation is $[\{1, 12\}, \{6, 11\}, \{7, 9\}, \{2, 3, 8\}, \{5, 4, 10\}]$. As illustrated, the

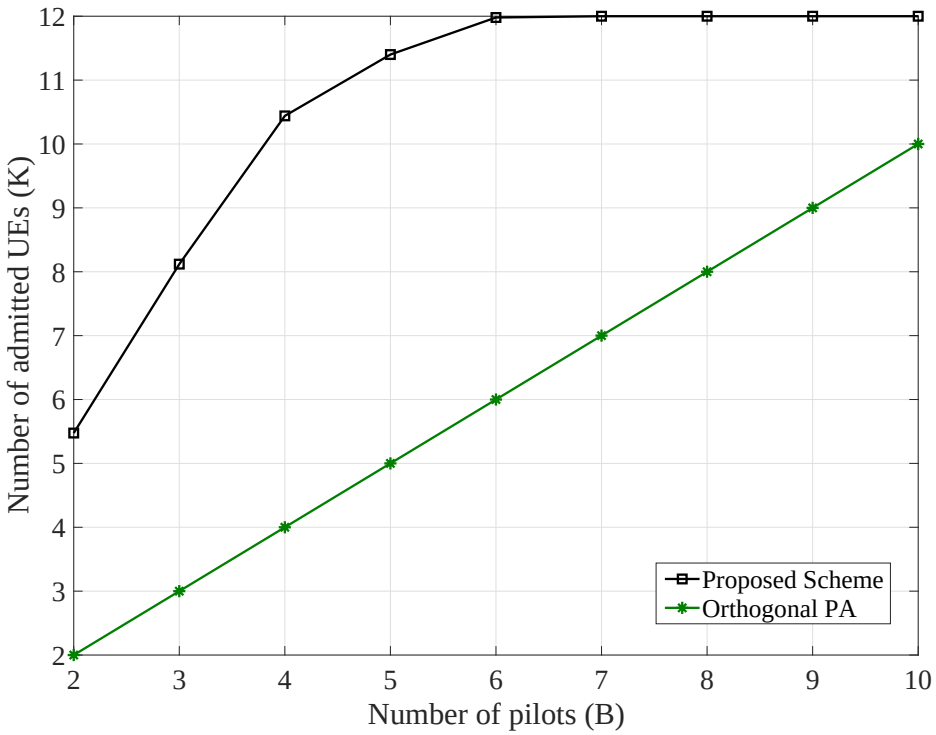

Figure 4.4: Number of admitted UEs K versus the number of pilots B when $\bar{K} = 12$.

performance generally improves in the case of the proposed scheme or **Algorithm 4.2**, especially for the UEs with the worst channel. Finally, the exhaustive search has a different result in how pilots are allocated, where pilots are assigned in the following way $[\{1, 8\}, \{2, 12\}, \{7, 6\}, \{3, 4, 9\}, \{5, 10, 11\}]$ which provides the best average estimation error. The objective of minimising the maximum channel estimation error is clearly shown here. UEs with bad channel quality, such as, UE 7, UE 6 and UE 12, deliver a better performance when **Algorithm 4.2** is considered.

Figure 4.6 plots the cumulative distribution function (CDF) curve of the maximum NMSE among all K UEs in the network when $B = 4$ and 8, respectively. It can be observed that the performance of all schemes improves when B increases as less pilot contamination is produced. The proposed pilot reuse scheme outperforms the graph colouring scheme with less error by about 0.13 when $B = 4$, and a lower amount of error

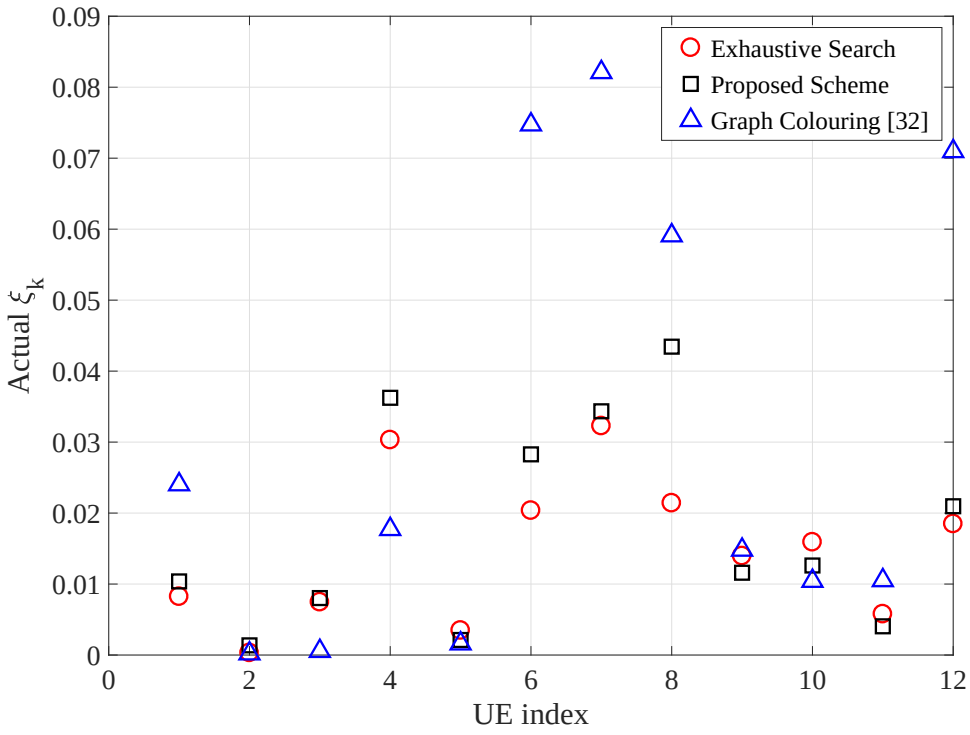

Figure 4.5: Actual estimation error ξ_k for a set of 12 UEs.

by about 0.03 can be achieved by the exhaustive search scheme. Moreover, as the number of pilots increases, i.e., when $B = 8$ is considered, the performance gaps among all pilot reuse schemes are further reduced.

In Figure 4.7, the average of the minimum number of pilots needed h is plotted for different numbers of UEs K and for various values of the maximum number of pilot reuse times G. In general, h increases as K increases, and this depends on the location of UEs in each simulation trail. Once the UEs are widely distributed within the coverage area, less h is needed as fewer connections among the vertices are obtained in the undirected graph based on constraint (4.13b). On the other hand, when UEs are densely placed on a small area, higher h is expected as more connections among the vertices are required. Another factor that affects h is the value of G. As G increases, fewer pilots are required and therefore a smaller h is obtained as shown in Figure 4.7. When G is greatly increased

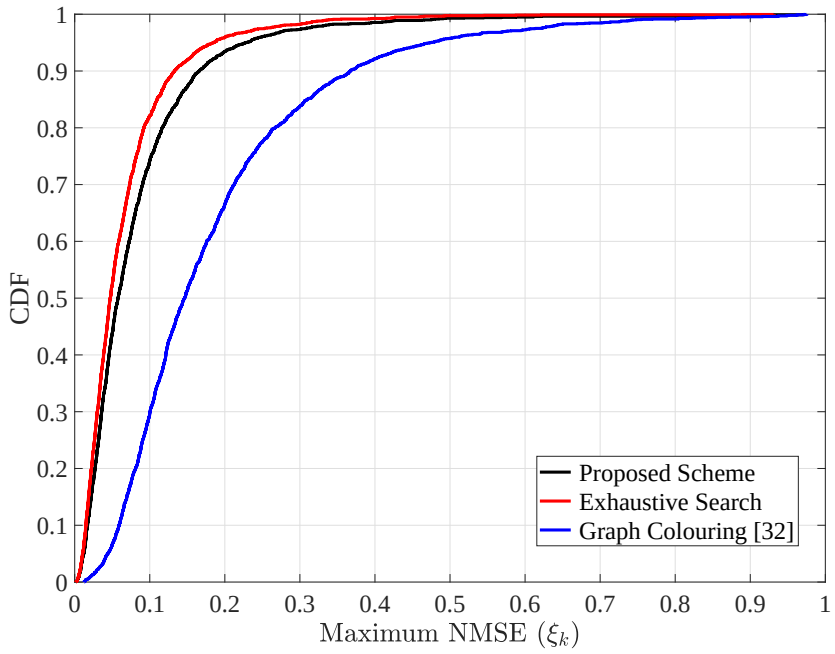

(a) $B = 4$

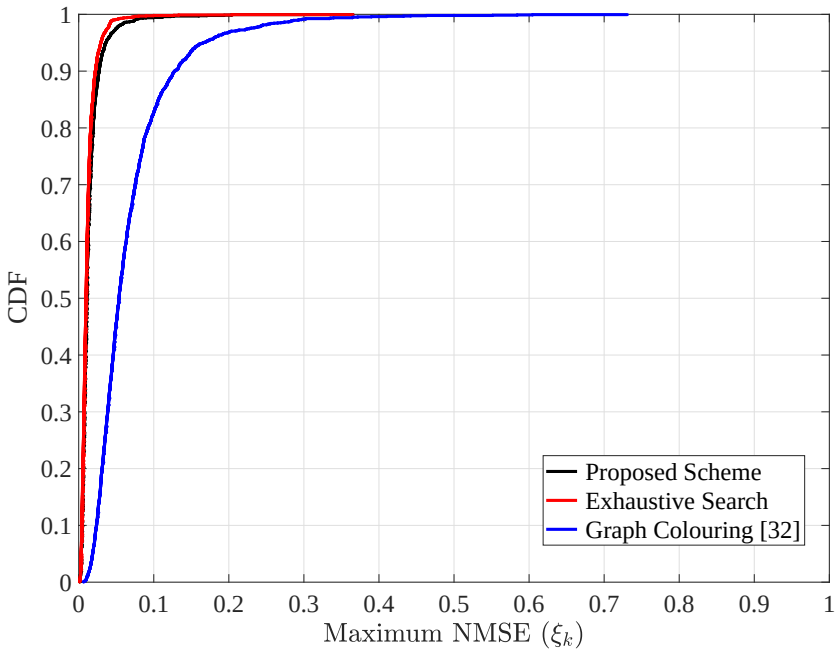

(b) $B = 8$

Figure 4.6: The CDF of the maximum NMSE when $K = 12$.

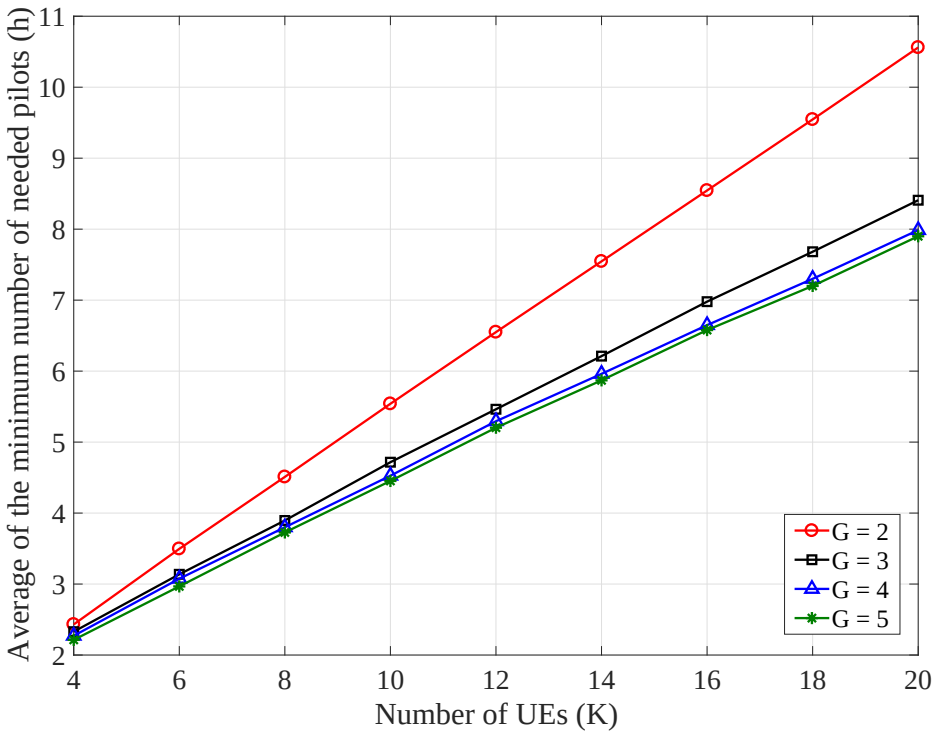

Figure 4.7: The average of the minimum number of pilots needed h for different number of UEs K.

as when $G = 4$ or $G = 5$, although a higher number of times of pilot reuse is allowed, it may only be possible to reuse the pilots a fewer number of times than G due to the need to satisfy the constraint (4.13b). Consequently, increasing the value of G to more than 4 will not affect the value of h.

The performance of the average NMSE of the proposed pilot reuse scheme for different number of pilots and values of G is presented in Figure 4.8. Increasing the value of G increases the NMSE for an arbitrary UE k as the set $\mathcal{K}_{b_k}$ in (4.8) expands. The same shape of the proposed scheme that was obtained in Figure 4.3 has appeared here too for all values of G. However, as h changes when G varies, as shown in Figure 4.7, the peak at which the maximum average NMSE is delivered changes as well, as the peak generally appears when $B = h$. As explained earlier, when B is greatly increased, the

proposed scheme allocates unique pilots to the UEs with the worst channel quality, which significantly reduces the estimation error whatever the value of G is.

Figure 4.9 shows how the proposed pilot reuse scheme affects the downlink minimum achievable sum-rate $R_{T_{min}}$ for different numbers of pilots B with $\bar{K} = 12$ when the MRT precoding is utilised. The orthogonal pilot allocation (PA) scheme delivers the worst sum-rate performance as the number of admitted UEs (K) here equals the number of pilots where it is not allowed for pilots to be reused among UEs. On the other hand, both the proposed scheme and the exhaustive search case provide almost the same superior performance compared with the graph colouring and the orthogonal pilot allocation schemes. This is due to the efficiency of the proposed reuse scheme in selecting the groups of UEs to share the same pilot. However, additional computational complexity is required by both the proposed scheme and the exhaustive search case because of the use of **Algorithm 4.2**. The graph colouring achieves lower performance than the proposed scheme especially when $h < B$. For all the reuse schemes, when $h < B$, the sum-rate performance is slightly reduced as B increases while K is fixed, as more resources for pilots signalling are utilised. This appears in the pre-log factor of (4.12), where this factor decreases as B increases and it has a greater impact on the sum-rate performance than the first term of the denominator of (4.10) that represents the pilot contamination.

The downlink minimum achievable sum-rate $R_{T_{min}}$ is illustrated in Figure 4.10, by supposing $B = 4$ and $M = 1, 10, 20, 50$ and 100. It is seen that for all the reuse schemes, the sum-rate performance is continuously enhanced when more antennas are added due to the effect of the array gain.

The impact of changing the number of RRHs N on the downlink minimum achievable sum-rate $R_{T_{min}}$ is plotted in Figure 4.11 when $B = 4$. It can be seen that the performance generally improves as N increases because UEs experience a better channel quality where

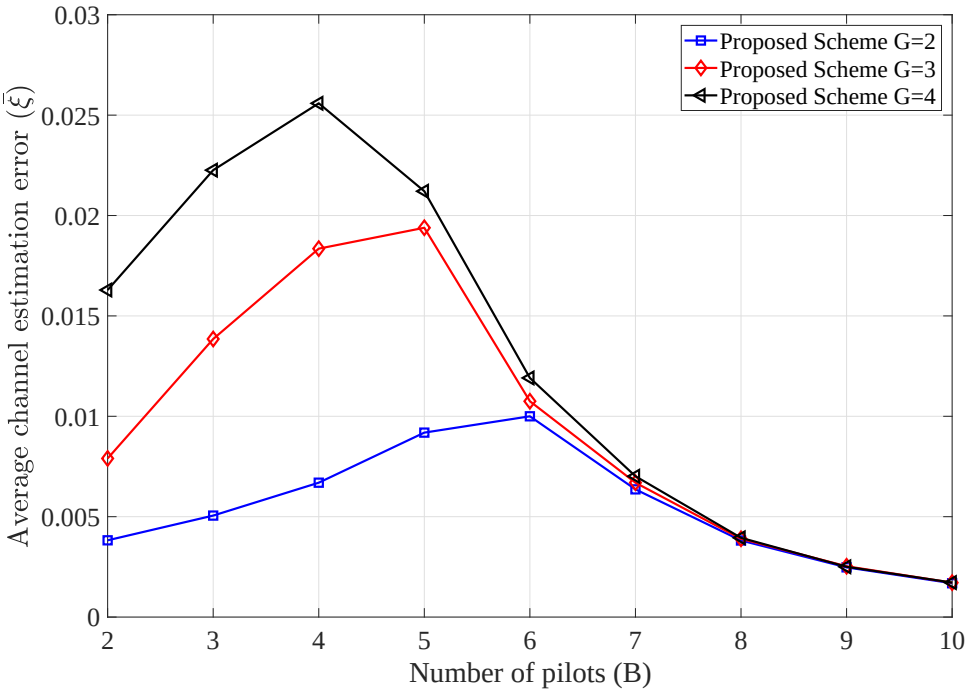

Figure 4.8: Average NMSE $\bar{\xi}$ for different number of reuse times G.

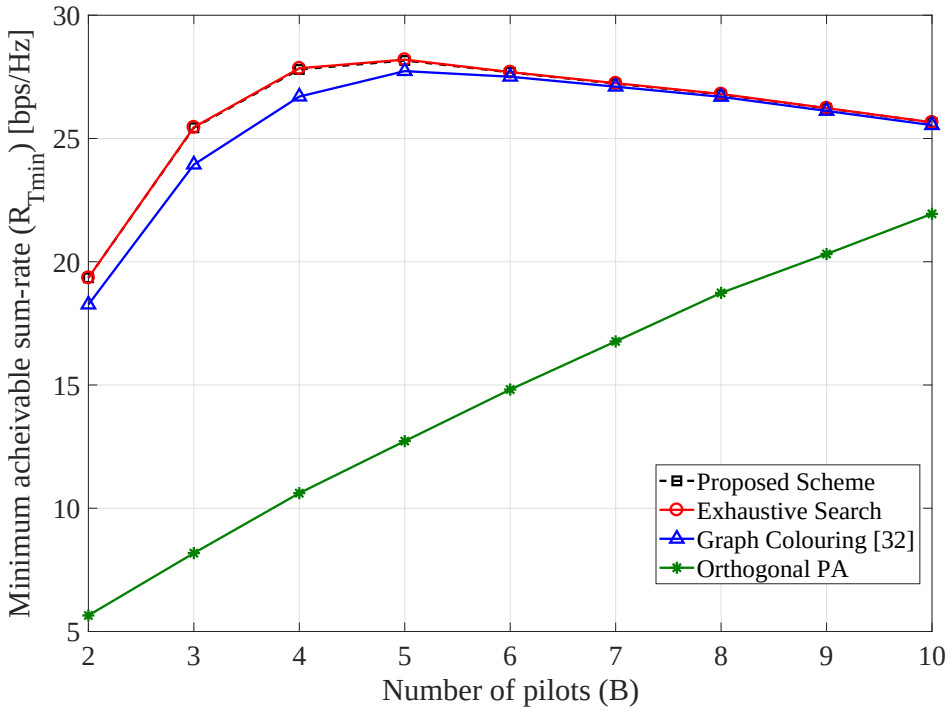

Figure 4.9: The downlink minimum sum-rate $R_{T_{min}}$ versus the number of pilots B.

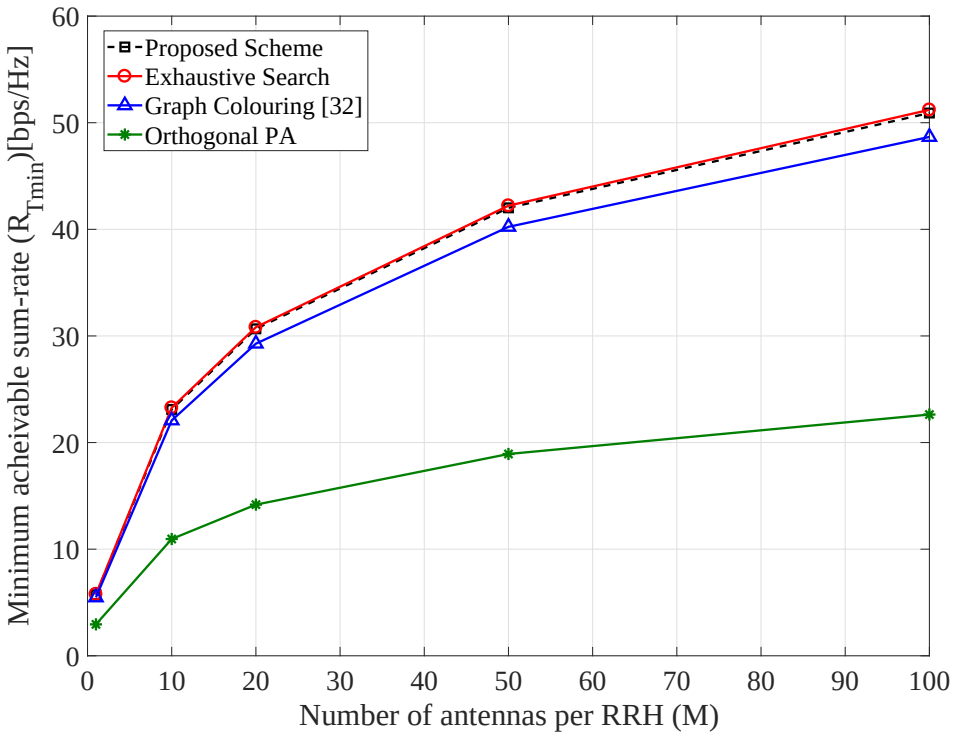

Figure 4.10: The downlink minimum sum-rate $R_{T_{min}}$ versus the number of antennas per RRH M.

RRHs will be closer to the UEs and this will reduce the channel estimation error.

The results of the complexity analysis of **Algorithm 4.2** is shown in Table 4.4 by assuming $\bar{K} = 12$ and $G = 3$. To evaluate the analysis of Section 4.4, the number of acceptable partitions obtained from the formulas of this section are compared with that obtained during the simulation. In the interest of balance, only the results of the case when all 12 UEs can be admitted are shown in Table 4.4. It can be seen that the results of the two cases are almost identical.

Another comparison is illustrated in Figure 4.12 to shed light on the complexity of the different algorithms presented in this chapter. The complexity of the exhaustive search, which solves $\mathcal{P}_e$ by utilising both **Algorithm 4.1** and **Algorithm 4.2**, is shown in Figure 4.12(b). It is required here to search in all the UEs partitions that satisfy only

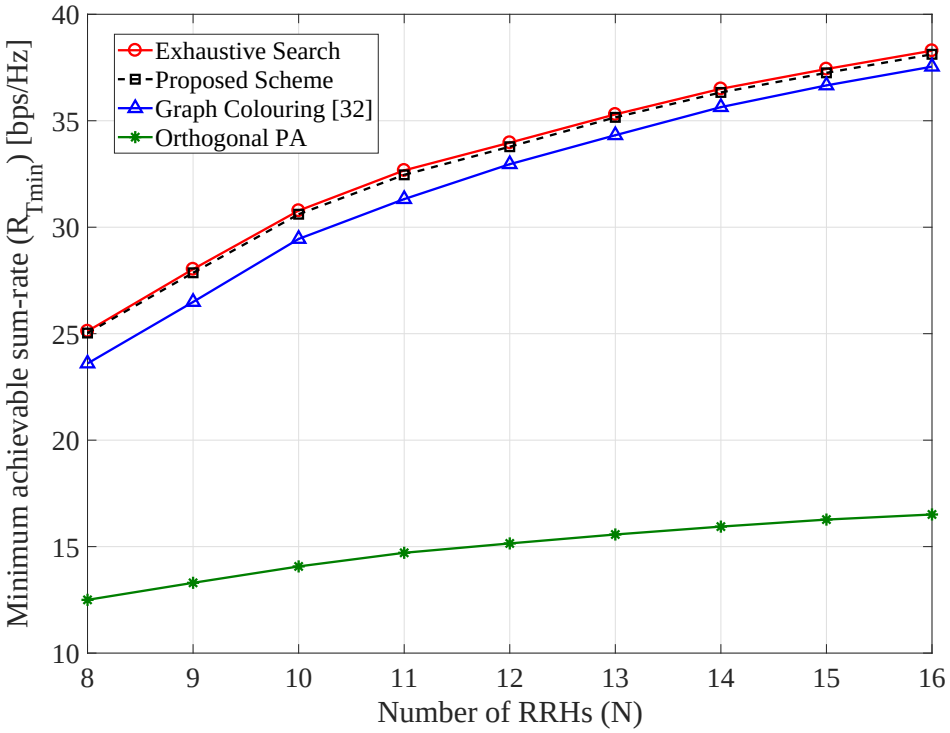

Figure 4.11: The downlink minimum sum-rate $R_{T_{min}}$ for various number of RRHs N.

Table 4.4: Complexity Comparison

B	Analytical Results	Simulation Results
6	7	7
7	207	220
8	24	22
9	5	6
10	2	1

the constraints (4.13b) and (4.13c) without considering the channel quality in selecting the partitions. The exhaustive search is very complex, as the number of partitions is too high. The complexity of the proposed scheme, the graph colouring and the orthogonal pilot allocation scheme are illustrated in Figure 4.12(a). Although the proposed scheme requires the use of both **Algorithm 4.1** and **Algorithm 4.2** as well, the number of partitions in this case is much lower than that of the exhaustive search as it is only necessary to choose the partitions that include the UEs with the worst channel quality in the subsets with the smallest size. This greatly reduces the number of acceptable partitions. For both the proposed scheme and the exhaustive search, a spike appears at $B = 7$. This depends on how many ways the set of UEs $\mathcal{K}$ can be partitioned into B subsets, where at $B = 7$, more ways of splitting $\mathcal{K}$ can be obtained compared with other values of B. In the graph colouring, it is necessary to perform only **Algorithm 4.1**, which has low-complexity. For small values of B, further operations are needed in **Algorithm 4.1** due to the UE selection. Therefore, greater complexity is delivered for all the algorithms in this case. Finally, the complexity of the orthogonal pilot allocation scheme is the lowest as it is equal to the number of pilots only.

For **Algorithm 4.3**, when **Algorithm 4.1** is initially applied, the complexity is 144 for 12 UEs. After this, when **Algorithm 4.4** is considered, by assuming that h is 6 and it is required to add 4 pilots to have $h_s = 10$, and by using the results in Table 4.4, the upper limit of the complexity of **Algorithm 4.4** will be 256, and the maximum total complexity of **Algorithm 4.3** will be 400.

Figure 4.13 and Figure 4.14 are presented to show the results of problem $\mathcal{P}_s$ with assuming that all UEs are served. In each iteration during the simulation, a different value of h is obtained based on the location of UEs in that iteration. Initially, $B = h$ is assumed. After that, more pilots are added to improve the SINR until the required SINR

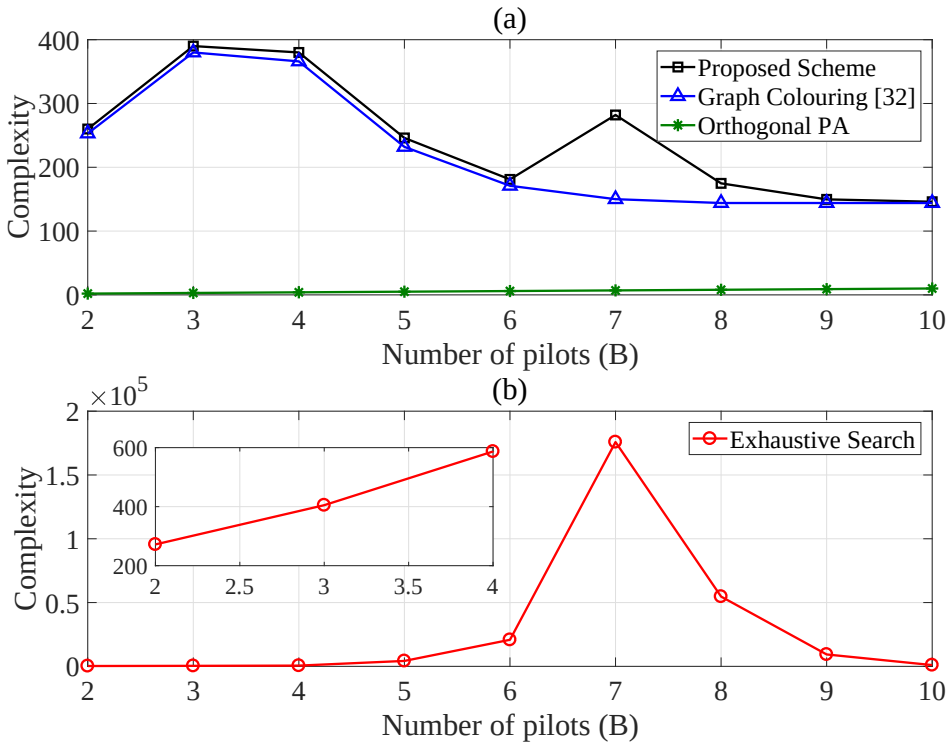

Figure 4.12: (a) The complexity of the proposed pilot allocation, graph colouring and the orthogonal pilot allocation schemes versus different values of B when $G = 3$. (b) The complexity of the exhaustive search case versus different values of B when $G = 3$.

threshold is met as explained in **Algorithm 4.3**. The upper subplot in Figure 4.13(a) shows the minimum number of pilots h_s needed for a particular SINR threshold to be satisfied by all UEs. It is evident that when the SINR threshold is initially increased, h_s increases linearly, where increasing the number of pilots improves the channel estimate and reduces the pilot contamination (the first term in the denominator of (4.10)). However, when the SINR threshold is increased to more than 8, the number of pilots h_s starts to increase rapidly. In addition, if the SINR requirement is higher than 8.3, it cannot be reached even if the number of pilots is highly increased as the effect of pilot contamination in this stage is insignificant, and consequently adding more pilots will be ineffective on the SINR. While obtaining the upper subplot of Figure 4.13(a), the minimum achievable

sum-rate is additionally measured as illustrated in the lower subplot of Figure 4.13(a). It is evident that the sum-rate is slightly reduced as h_s increases due to the utilisation of more resources by pilot signals while K is constant where the pre-log factor in (4.12) is decreased when more pilots are employed. Although increasing h_s improves the SINR (up to 8.3), the pre-log factor in (4.12) has a greater impact on the sum-rate. As it is not possible to obtain a SINR higher than 8.3, the minimum achievable sum-rate is further reduced when the SINR threshold is higher than 8. In Figure 4.14, the minimum average NMSE $\bar{\xi}$ obtained from using **Algorithm 4.3** is also illustrated. All the UE set partitions that meet the SINR threshold in **Algorithm 4.4** are tested and the one with the minimum average NMSE $\bar{\xi}$ is chosen. More pilots cause less $\bar{\xi}$; this continues until $\bar{\xi}$ approaches the case of no pilot reuse.

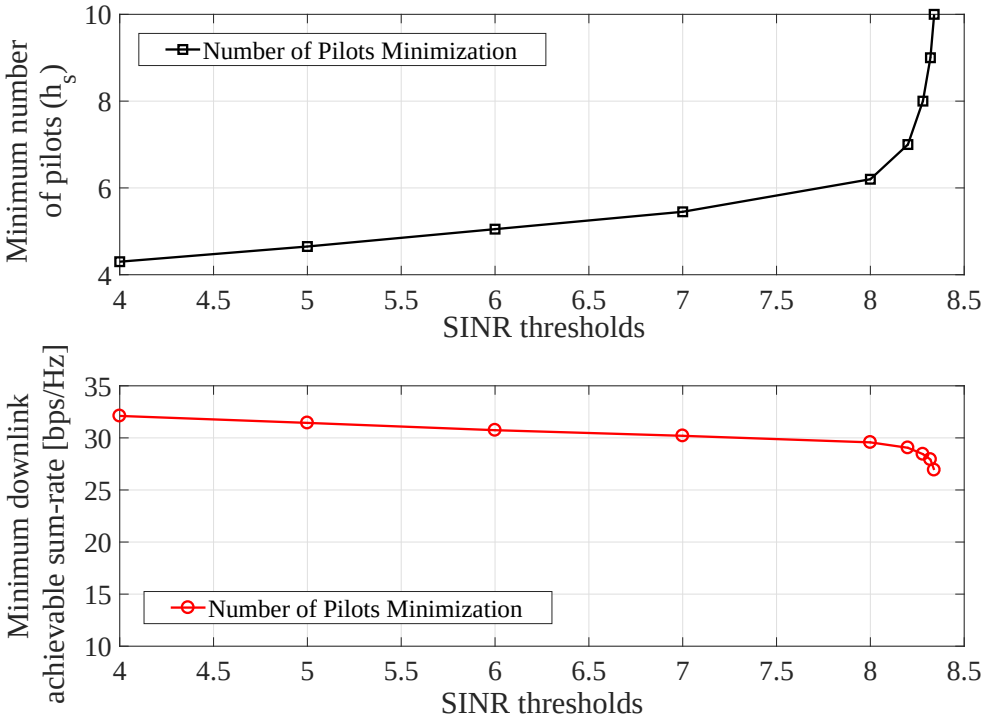

Figure 4.13: (a) Minimum number of pilots h_s obtained from $\mathcal{P}_s$ versus different values of SINR threshold. (b) Minimum downlink achievable sum-rate obtained from $\mathcal{P}_s$ versus different values of SINR threshold.

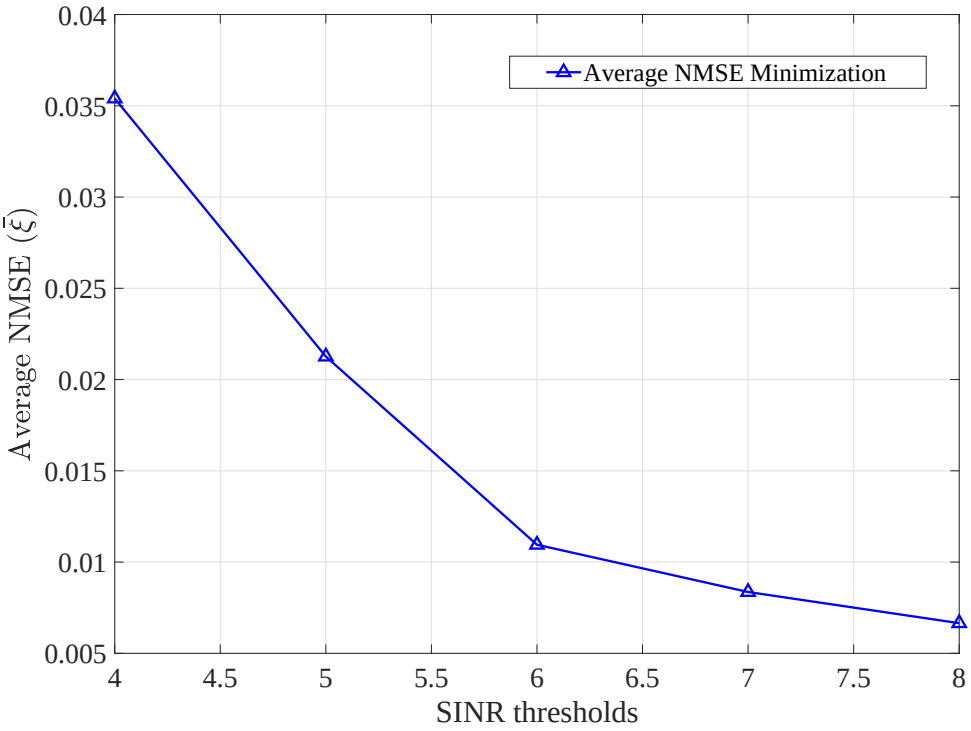

Figure 4.14: Minimizing the average NMSE $\bar{\xi}$.

Chapter 5

Conclusions and Future Work

5.1 Overall Conclusion

This thesis has investigated the challenging issue of the unaffordable channel training overhead in TDD distributed massive MIMO systems when the number of UEs being simultaneously served is higher than the number of available pilot sequences. Different pilot allocation schemes have been proposed in two different scenarios, a dense single cell DM-MIMO and a CF massive MIMO network. The key findings of each of these two scenarios is presented separately.

5.1.1 Pilot Allocation in DM-MIMO

The pilot reuse within the same cell in the dense TDD DM-MIMO is proposed in Chapter 3. Specifically, the DPR scheme is presented to allow a pair of UEs to share a single pilot sequence with the objective of maximising the sum-rate subject to a SINR constraint per UE. An expression of the SINR is firstly derived for any UE sharing its pilot with another by utilising both MMSE detection and channel estimation. A low-complexity algorithm is then proposed based on the separation distance between UEs. The iterative grid search (IGS) method is employed to find the threshold that can be utilised in the proposed

algorithm to maximise the sum-rate. Simulation results are presented to evaluate the uplink sum-rate performance of the proposed reuse scheme. The main conclusions are drawn as follows:

1. The DPR scheme with the optimised threshold can achieve the best uplink sum-rate performance compared with other pilot reuse schemes, such as the random pilot reuse scheme, the DPR scheme with fixed SINR thresholds (5 dB and 10 dB), and no threshold scheme. The superiority of the DPR scheme with the optimised threshold comes from employing the IGR method to find the optimal threshold. For the case of the DPR scheme with a fixed threshold, the sum-rate performance at a lower threshold, for instance, 5 dB is better than the performance at a higher threshold, for example, 10 dB, as more UEs can be admitted in the case of 5 dB than the case of 10 dB.

2. The number of admitted UEs in the DPR scheme relies on the SINR threshold value. Therefore, lower threshold values can achieve a higher number of admitted UEs as more UEs can be served. Using the optimised threshold does not guarantee that the maximum number of UEs are served as it aims to obtain the maximum sum-rate only.

3. Increasing the number of antennas per RRH is always beneficial for sum-rate performance of all the pilot reuse schemes. For the DPR scheme, more UEs can be satisfied with the SINR constraint when a higher number of antennas is adopted, as this improves UEs' SINR.

4. When more RRHs serve a UE based on the user-centric clustering method, the sum-rate performance is enhanced. However, when the size of the RRHs serving cluster

is greatly increased, to 4 RRHs for instance, more non-nearby RRHs are serving the UE. These RRHs contribute less to that UE's signal quality than the nearby RRHs, and are closer to the second UE sharing the same pilot with the desired UE. Thus, this leads to a higher pilot contamination received from these RRHs, and the sum-rate performance is unable to be further improved.

5. Increasing the coherence block size has a positive effect on the uplink sum-rate performance as greater resources need to be employed for data transmission.

5.1.2 Pilot Assignment in CF Massive MIMO

Another pilot allocation scheme is presented in Chapter 4 aiming to minimise the maximum channel estimation error for all UEs in the CF massive MIMO network subject to certain practical constraints. In this scheme, the UEs with the bad channel conditions are allocated with the pilots with a low number of reuse times, while the UEs with the best channel conditions adopt the pilots with higher reuse times. Two low-complexity algorithms are developed as two stages to perform this pilot reuse scheme. The first one utilises the graph colouring based on the Dsatur algorithm to determine the minimum number of pilots needed to serve all the UEs, and to achieve the UE selection in the case that there is not enough pilots to serve all the UEs. In the second algorithm, pilots are allocated based on the channel quality of UEs, as previously mentioned. The proposed scheme can be applied to any CF system whatever the number of antennas per RRH is. However, in this thesis, the performance of this scheme is evaluated in the context of CF massive MIMO system based on the average NMSE and the downlink sum-rate.

In order to link the channel estimation error with the sum-rate performance, a second problem is then developed to allocate the pilots with the objective of minimising both the

average channel estimation error and the number of pilots subject to the same constraints of the previous problem. In addition to these constraints, all UEs have to satisfy a particular SINR constraint. The main findings of the pilot allocation problems in CF massive MIMO are summarised below:

1. The average NMSE performance of the proposed scheme outperformed that of the graph colouring based scheme, and mostly approached the performance of the exhaustive scheme. In addition, the worst average NMSE was obtained by all the reuse schemes when all UEs were served with a minimum number of pilots, i.e. when $(B = h)$, where B is the total number of pilots and h is the minimum number of pilots needed to serve all the UEs. In the case of UE selection, i.e. when $B < h$, a better performance was delivered as the remaining UEs after the UE selection mostly had the best channel qualities. Finally, in the case when $B > h$, all UEs could be served, and a better average NMSE performance was obtained when more pilots were utilised.

2. The average value of h needed to serve a particular number of UEs depends on the value of the threshold of pilot reuse times G, and the distribution of UEs in the coverage area. When UEs are densely placed in a small area, higher h is obtained as more connections among the vertices of the indirected graph are needed. In addition, less h is required as G increases. However, having G larger than 4 did not affect h for 12 UEs, as satisfying the constraint of the non-overlapping RRHs prevented pilots being greatly reused.

3. The downlink minimum achievable sum-rate of the proposed scheme and the exhaustive search scheme when the maximum ratio transmission (MRT) was utilised had almost the same superiority performance compared with the graph colouring

scheme, especially with the case of a low number of pilots. For all the reuse schemes, when $h < B$, the sum-rate performance was slightly reduced as B increased while K was fixed, as more resources for pilots signalling were needed which reduced the pre-log factor of (4.12).

4. For the proposed pilot allocation scheme, an example showed that increasing the number of RRHs from 8 to 16 increased the minimum MRT achievable sum-rate by around 12 bps/Hz, as this improved the channel quality of UEs and reduced the channel estimation error. Furthermore, increasing the number of antennas per RRH from 1 to 100 increased the minimum achievable sum-rate by around 45 bps/Hz as higher array gain could be obtained.

5. Regarding the second problem $\mathcal{P}_s$, it was shown that increasing the number of pilots improved the SINR. However, increasing the number of pilots to more than 7 did not improve the SINR further as the impact of the pilot contamination was significantly reduced.

6. **Algorithm 4.1** had low complexity due to adopting the graph colouring mechanism based on the Dsatur algorithm. Similarly, the low complexity of **Algorithm 4.2**, **Algorithm 4.3** and **Algorithm 4.4** was obtained from the search within a limited number of UE set partitions. Although the number of partitions was initially huge especially for a large number of UEs, it was significantly reduced after removing the partitions that did not satisfy the constraints and the idea of allocating the pilots with low reuse times to the UEs with bad channel conditions.

5.2 Areas of Future Research

There are several open research directions in the distributed massive MIMO that still need to be explored to make it feasible to apply this in practice, as listed below:

1. The sum-rate analysis in Chapter 3 included the impact of intra-cell pilot contamination only. The effect of the inter-cell pilot contamination needs to be investigated as well when pilots are reused within the same cell by utilising the DPR scheme, and then among other cells too. Another stage can be added to the DPR scheme to perform an efficient pilot reuse among the cells.

2. For the sake of simplicity, in our research, the number of serving RRHs $\mathbb{N}$ was assumed to be fixed for all UEs in this thesis. However, $\mathbb{N}$ can be different for different UEs based on the particular needs of each UE. The impact of this should be investigated as well. Additionally, the set of RRHs serving a UE was selected in our work based on the nearest RRHs to that UE. Alternative RRH selection mechanisms can be further examined to see how they affect the proposed reuse schemes.

3. The local CSI approach means that not all the instantaneous CSI for all UEs can be available at the CPU. However, the CSI information is necessary in the ZF matrix to calculate $(\hat{\mathbf{H}}_i^H \hat{\mathbf{H}}_i)^{-1}$, where $\hat{\mathbf{H}}_i = [\hat{\mathbf{h}}_{i,1}, \hat{\mathbf{h}}_{i,2}, ..., \hat{\mathbf{h}}_{i,K}] \in \mathbb{C}^{M \times K}$ is the channel estimate matrix of RRH i. If the channel estimate is assumed be zero at the missing elements, then $\hat{\mathbf{H}}_i^H \hat{\mathbf{H}}_i$ will be non-invertible. Another approach is to compensate the missing elements by their corresponding large-scale fading coefficients, but when ZF aims to null the signals of unwanted UEs with missing the full CSIs, that will no longer be applicable. More investigation is needed to see how the ZF can work in this case,

and the impact of the local CSI on its sum-rate performance.

4. In the literature, the CF massive MIMO generally describes a network consisting of a massive number of single-antenna APs geographically distributed to jointly serve a set of UEs. It is interesting to compare the spectral efficiency performance of this scenario with that of this thesis, where few multi-antenna RRHs are deployed when the proposed reuse scheme and the user-centric approach are considered.

Appendix A

Appendices

A.1 Parameters of Equations (3.13) and (3.14)

The explicit formulas of the parameters of equations (3.13) and (3.14) are listed in this appendix. All these formulas are taken from ([54], Theorem 1, Theorem 2 and Theorem 3) with applying some modifications on them to match the scenario of a single cell DM-MIMO. First, $\mathbf{T}(\rho) \in \mathbb{C}^{M\mathbb{N}\times M\mathbb{N}}$, and for any $\rho > 0$ can be defined as

$$\mathbf{T}(\rho) = \left(\frac{1}{M\mathbb{N}} \sum_{k' \in \mathcal{K}} \frac{\bar{\mathbf{R}}_{k'}}{1 + \delta_{k'}(\rho)} + \mathbf{S} + \rho \mathbf{I}_{M\mathbb{N}} \right)^{-1}. \tag{A.1.1}$$

where $\mathbf{S} = \bar{\mathbf{Z}}/M\mathbb{N}$.

In addition, the elements of $\boldsymbol{\delta}(\rho) \triangleq [\delta_1(\rho) \cdots \delta_K(\rho)]^T$ are defined, where $\delta_k(\rho) = \lim_{t\to\infty} \delta_k^{(t)}(\rho)$, and for $t = 1, 2, \cdots$

$$\delta_k^{(t)}(\rho) = \frac{1}{M\mathbb{N}} \mathrm{tr} \bar{\mathbf{R}}_k \left(\frac{1}{M\mathbb{N}} \sum_{k' \in \mathcal{K}} \frac{\bar{\mathbf{R}}_{k'}}{1 + \delta_{k'}^{(t-1)}(\rho)} + \mathbf{S} + \rho \mathbf{I}_{M\mathbb{N}} \right)^{-1}, \tag{A.1.2}$$

with initial values $\delta_k^{(0)}(\rho) = 1/\rho, \forall k' \in \mathcal{K}$, where $\rho = M\mathbb{N}\rho_d$. Following this, $\bar{\mathbf{T}}$ can be defined as $\bar{\mathbf{T}} = \mathbf{T}(\frac{1}{M\mathbb{N}\rho_d})$ and $\bar{\boldsymbol{\delta}} = [\delta_1 \cdots \delta_K]^T = \boldsymbol{\delta}(\frac{1}{M\mathbb{N}\rho_d})$. Furthermore, $\mathbf{T}'(\rho) \in \mathbb{C}^{M\mathbb{N}\times M\mathbb{N}}$,

is defined as

$$\mathbf{T}^{'}(\rho) = \mathbf{T}(\rho)\mathbf{I}_{M\mathbb{N}}\mathbf{T}(\rho) + \mathbf{T}(\rho)\frac{1}{M\mathbb{N}}\sum_{k\in\mathcal{K}}\frac{\bar{\mathbf{R}}_k\delta_k^{'}(\rho)}{(1+\delta_k(\rho))^2}\mathbf{T}(\rho), \tag{A.1.3}$$

where $\bar{\boldsymbol{\delta}}^{'}(\rho) = [\delta_1^{'}(\rho)\cdots\delta_K^{'}(\rho)]^T$, and $\bar{\boldsymbol{\delta}}^{'}(\rho)$ can be calculated as

$$\bar{\boldsymbol{\delta}}^{'}(\rho) = (\mathbf{I}_K - \mathbf{J}(\rho))^{-1}\bar{\mathbf{v}}(\rho), \tag{A.1.4}$$

and $\mathbf{J}(\rho) \in \mathbb{C}^{K\times K}$, $\bar{\mathbf{v}}(\rho) \in \mathbb{C}^K$ can be calculated from

$$[\mathbf{J}(\rho)]_{kq} = \frac{\frac{1}{M\mathbb{N}}\mathrm{tr}\bar{\mathbf{R}}_k\mathbf{T}(\rho)\bar{\mathbf{R}}_q\mathbf{T}(\rho)}{M\mathbb{N}(1+\delta_q(\rho))^2}, \qquad 1\le k,q\le K \tag{A.1.5}$$

$$[\bar{\mathbf{v}}(\rho)]_k = \frac{1}{M\mathbb{N}}\mathrm{tr}\bar{\mathbf{R}}_k\mathbf{T}(\rho)\mathbf{I}_{M\mathbb{N}}\mathbf{T}(\rho), \qquad 1\le k\le K. \tag{A.1.6}$$

Finally, the following parameters are defined as

$$\mu_{\langle q,k\rangle} = \frac{1}{M\mathbb{N}}\mathrm{tr}\bar{\mathbf{R}}_k\mathbf{T}^{'} - \frac{2\vartheta_k^*\vartheta_{\langle q,k\rangle}^{'}(1+\delta_k) - |\vartheta_k|^2\delta_k^{'}}{(1+\delta_k)^2}, \tag{A.1.7}$$

$$\vartheta_k = \frac{1}{M\mathbb{N}}\mathrm{tr}\bar{\mathbf{R}}_k\mathbf{T}(1/\rho), \tag{A.1.8}$$

$$\vartheta_{\langle q,k\rangle}^{'} = \frac{1}{M\mathbb{N}}\mathrm{tr}\bar{\mathbf{R}}_k\mathbf{T}_q^{'}. \tag{A.1.9}$$

A.2 Derivation of Equation (4.10)

By using (4.1), and by applying the add-and-subtract technique shown in ([56], (43) and (44)), if the Gaussian noise is considered as the worst case distribution of the uncorrelated noise, a lower bound of the SINR of UE k can be presented as

$$SINR_{k_{min}} = \frac{\left|\sum_{i\in\mathcal{N}_k}\sqrt{\rho_{i,k}}\,\mathbb{E}\{\mathbf{h}_{i,k}^H\mathbf{w}_{i,k}\}\right|^2}{\sum_{k'\in\mathcal{K}}\mathbb{E}\left\{\left|\sum_{i\in\mathcal{N}_k}\sqrt{\rho_{i,k'}}\,\mathbf{h}_{i,k}^H\mathbf{w}_{i,k'}\right|^2\right\} - \left|\sum_{i\in\mathcal{N}_k}\sqrt{\rho_{i,k}}\,\mathbb{E}\{\mathbf{h}_{i,k}^H\mathbf{w}_{i,k}\}\right|^2 + \sigma_k^2}. \tag{A.1.10}$$

It is assumed that A_{NUM} and B_{DEN} are the numerator and the first term of the denominator of (A.1.10), respectively, where A_{NUM} and B_{DEN} are given as

$$A_{NUM} = \left| \sum_{i \in \mathcal{N}_k} \sqrt{\rho_{i,k}} \underbrace{\mathbb{E}\{\mathbf{h}_{i,k}^H \mathbf{w}_{i,k}\}}_{A_1} \right|^2, \tag{A.1.11}$$

$$B_{NUM} = \sum_{k' \in \mathcal{K}} \mathbb{E}\left\{ \left| \sum_{i \in \mathcal{N}_k} \sqrt{\rho_{i,k'}}\, \mathbf{h}_{i,k}^H \mathbf{w}_{i,k'} \right|^2 \right\}. \tag{A.1.12}$$

In order to simplify A_{NUM}, the independence between the channel estimates and the estimation errors can be utilised, and A_1 can be written as

$$A_1 = \mathbb{E}\{\mathbf{h}_{i,k}^H \mathbf{w}_{i,k}\} = \mathbb{E}\{\frac{\mathbf{h}_{i,k}^H \hat{\mathbf{h}}_{i,k}}{\sqrt{\mathbb{E}\{\|\hat{\mathbf{h}}_{i,k}\|^2\}}}\} = \sqrt{\mathbb{E}\{\|\hat{\mathbf{h}}_{i,k}\|^2\}} = \sqrt{M\theta_{i,k}}. \tag{A.1.13}$$

Thus, A_{NUM} can be finally simplified as

$$A_{NUM} = M\left(\sum_{i \in \mathcal{N}_k} \sqrt{\rho_{i,k}\theta_{i,k}} \right)^2. \tag{A.1.14}$$

In addition, B_{NUM} can be represented as

$$B_{NUM} = \underbrace{\sum_{k' \in \mathcal{K}_{b_k}} \mathbb{E}\left\{ \left| \sum_{i \in \mathcal{N}_k} \sqrt{\rho_{i,k'}}\, \mathbf{h}_{i,k}^H \mathbf{w}_{i,k'} \right|^2 \right\}}_{B_1} + \underbrace{\sum_{k' \notin \mathcal{K}_{b_k}} \mathbb{E}\left\{ \left| \sum_{i \in \mathcal{N}_k} \sqrt{\rho_{i,k'}}\, \mathbf{h}_{i,k}^H \mathbf{w}_{i,k'} \right|^2 \right\}}_{B_2}. \tag{A.1.15}$$

B_2 can be computed as the following

$$\begin{aligned} B_2 &= \sum_{k' \notin \mathcal{K}_{b_k}} \sum_{i \in \mathcal{N}_k} \rho_{i,k'} \mathbb{E}\left\{ \left| \mathbf{h}_{i,k}^H \mathbf{w}_{i,k'} \right|^2 \right\} = \sum_{k' \notin \mathcal{K}_{b_k}} \sum_{i \in \mathcal{N}_k} \rho_{i,k'} \frac{\mathbb{E}\left\{ \left| \mathbf{h}_{i,k}^H \hat{\mathbf{h}}_{i,k'} \right|^2 \right\}}{\mathbb{E}\left\{ \|\hat{\mathbf{h}}_{i,k'}\|^2 \right\}} \\ &= \sum_{k' \notin \mathcal{K}_{b_k}} \sum_{i \in \mathcal{N}_k} \rho_{i,k'} \frac{\alpha_{i,k} \mathbb{E}\left\{ \|\hat{\mathbf{h}}_{i,k'}\|^2 \right\}}{\mathbb{E}\left\{ \|\hat{\mathbf{h}}_{i,k'}\|^2 \right\}} = \sum_{k' \notin \mathcal{K}_{b_k}} \sum_{i \in \mathcal{N}_k} \rho_{i,k'} \alpha_{i,k}. \end{aligned} \tag{A.1.16}$$

Furthermore, B_1 can be computed as the following

$$B_1 = \sum_{k' \in \mathcal{K}_{b_k}} \mathbb{E}\left\{ \left| \sum_{i \in \mathcal{N}_k} \sqrt{\rho_{i,k'}}\, \mathbf{h}_{i,k}^H \mathbf{w}_{i,k'} \right|^2 \right\} = \sum_{k' \in \mathcal{K}_{b_k}} \mathbb{E}\left\{ \left| \sum_{i \in \mathcal{N}_k} \sqrt{\rho_{i,k'}}\, (\hat{\mathbf{h}}_{i,k}^H + \mathbf{e}_{i,k}^H) \frac{\hat{\mathbf{h}}_{i,k'}}{\sqrt{\mathbb{E}\{\|\hat{\mathbf{h}}_{i,k'}\|^2\}}} \right|^2 \right\}$$
$$= \underbrace{\sum_{k' \in \mathcal{K}_{b_k}} \mathbb{E}\left\{ \left| \sum_{i \in \mathcal{N}_k} \sqrt{\rho_{i,k'}}\, \frac{\hat{\mathbf{h}}_{i,k}^H \hat{\mathbf{h}}_{i,k'}}{\sqrt{\mathbb{E}\{\|\hat{\mathbf{h}}_{i,k'}\|^2\}}} \right|^2 \right\}}_{B_{11}} + \underbrace{\sum_{k' \in \mathcal{K}_{b_k}} \mathbb{E}\left\{ \left| \sum_{i \in \mathcal{N}_k} \sqrt{\rho_{i,k'}}\, \frac{\mathbf{e}_{i,k}^H \hat{\mathbf{h}}_{i,k'}}{\sqrt{\mathbb{E}\{\|\hat{\mathbf{h}}_{i,k'}\|^2\}}} \right|^2 \right\}}_{B_{12}}. \tag{A.1.17}$$

By utilising ([56], (12)), and by following the steps in ([56], (55)), both B_{11} and B_{12} can be written as

$$B_{12} = \sum_{k' \in \mathcal{K}_{b_k}} \sum_{i \in \mathcal{N}_k} \rho_{i,k'} (\alpha_{i,k} - \theta_{i,k}). \tag{A.1.18}$$

$$B_{11} = \sum_{k' \in \mathcal{K}_{b_k}} \mathbb{E}\left\{ \left| \sum_{i \in \mathcal{N}_k} \sqrt{\rho_{i,k'}}\, \frac{\alpha_{i,k}}{\alpha_{i,k'}} \frac{\|\hat{\mathbf{h}}_{i,k'}\|^2}{\sqrt{\mathbb{E}\{\|\hat{\mathbf{h}}_{i,k'}\|^2\}}} \right|^2 \right\} \tag{A.1.19}$$
$$= \sum_{k' \in \mathcal{K}_{b_k}} \sum_{i \in \mathcal{N}_k} \frac{\rho_{i,k'} \alpha_{i,k}^2 \mathbb{E}\{\|\hat{\mathbf{h}}_{i,k'}\|^4\}}{\alpha_{i,k'}^2 \mathbb{E}\{\|\hat{\mathbf{h}}_{i,k'}\|^2\}} + \sum_{k' \in \mathcal{K}_{b_k}} \sum_{i \in \mathcal{N}_k} \sum_{j \neq i \in \mathcal{N}_k} \frac{\rho_{i,k'} \alpha_{i,k} \alpha_{j,k}}{\alpha_{i,k'} \alpha_{j,k'}} \sqrt{\mathbb{E}\{\|\hat{\mathbf{h}}_{j,k'}\|^2\} \mathbb{E}\{\|\hat{\mathbf{h}}_{i,k'}\|^2\}}$$
$$= \sum_{k' \in \mathcal{K}_{b_k}} \sum_{i \in \mathcal{N}_k} \frac{\rho_{i,k'} \alpha_{i,k}^2}{\alpha_{i,k'}^2} (M-1) \theta_{i,k'} + \sum_{k' \in \mathcal{K}_{b_k}} \sum_{i \in \mathcal{N}_k} \sum_{j \neq i \in \mathcal{N}_k} \frac{\rho_{i,k'} \alpha_{i,k} \alpha_{j,k}}{\alpha_{i,k'} \alpha_{j,k'}} M \sqrt{\theta_{i,k'} \theta_{j,k'}}$$
$$= \sum_{k' \in \mathcal{K}_{b_k}} (\sum_{i \in \mathcal{N}_k} \sqrt{M \rho_{i,k'} \theta_{i,k}})^2 - \sum_{k' \in \mathcal{K}_{b_k}} \sum_{i \in \mathcal{N}_k} \rho_{i,k'} \theta_{i,k} \tag{A.1.20}$$

Finally, both B_1 and then B_{NUM} can be reformed as

$$B_1 = B_{11} + B_{12} = \sum_{k' \in \mathcal{K}_{b_k}} (\sum_{i \in \mathcal{N}_k} \sqrt{M \rho_{i,k'} \theta_{i,k}})^2 + \sum_{k' \in \mathcal{K}_{b_k}} \sum_{i \in \mathcal{N}_k} \rho_{i,k'} (\alpha_{i,k} - \theta_{i,k}). \tag{A.1.21}$$

$$B_{NUM} = B_1 + B_2 = \sum_{k' \in \mathcal{K}_{b_k}} (\sum_{i \in \mathcal{N}_k} \sqrt{M \rho_{i,k'} \theta_{i,k}})^2 + \sum_{k' \in \mathcal{K}} \sum_{i \in \mathcal{N}_k} \rho_{i,k'} \alpha_{i,k}. \tag{A.1.22}$$

By substituting (A.1.13) and (A.1.22) in (A.1.10), the SINR formula of (4.10) can be obtained.

References

[1] Ericsson, "Ericsson mobility report," technical report, Ericsson, 2018.

[2] E. Björnson, J. Hoydis, and L. Sanguinetti, *Massive MIMO Networks: Spectral, Energy, and Hardware Efficiency*. Foundations and Trends(r) in S, Now Publishers, 2017.

[3] J. G. Andrews, S. Buzzi, W. Choi, S. V. Hanly, A. Lozano, A. C. K. Soong, and J. C. Zhang, "What will 5G be?," *IEEE Journal on Selected Areas in Communications*, vol. 32, pp. 1065–1082, June 2014.

[4] M. Shafi, A. F. Molisch, P. J. Smith, T. Haustein, P. Zhu, P. D. Silva, F. Tufvesson, A. Benjebbour, and G. Wunder, "5G: A tutorial overview of standards, trials, challenges, deployment, and practice," *IEEE Journal on Selected Areas in Communications*, vol. 35, pp. 1201–1221, June 2017.

[5] K. T. Truong and R. W. Heath, "The viability of distributed antennas for massive MIMO systems," in *2013 Asilomar Conference on Signals, Systems and Computers*, pp. 1318–1323, Nov. 2013.

[6] M. Sadeghi, C. Yuen, and Y. H. Chew, "Sum rate maximization for uplink distributed massive MIMO systems with limited backhaul capacity," in *2014 IEEE Globecom Workshops (GC Wkshps)*, pp. 308–313, Dec. 2014.

[7] R. Sabbagh, C. Pan, and J. Wang, "Pilot allocation and sum-rate analysis in cell-free massive MIMO systems," in *2018 IEEE International Conference on Communications (ICC)*, pp. 1–6, May 2018.

[8] R. Raoof, C. Pan, H. Zhu, and J. Wang, "Dynamic pilot reuse in distributed massive MIMO systems," in *2017 IEEE 85th Vehicular Technology Conference (VTC Spring)*, pp. 1–5, June 2017.

[9] H. Zhu, "Performance comparison between distributed antenna and microcellular systems," *IEEE Journal on Selected Areas in Communications*, vol. 29, pp. 1151–1163, Jun. 2011.

[10] J. Wang, H. Zhu, and N. J. Gomes, "Distributed antenna systems for mobile communications in high speed trains," *IEEE Journal on Selected Areas in Communications*, vol. 30, pp. 675–683, May. 2012.

[11] W. Ali, J. Wang, H. Zhu, and J. Wang, "Distributed antenna system based frequency switch scheme evaluation for high-speed railways," in *2017 IEEE International Conference on Communications*, pp. 1–6, May 2017.

[12] W. Ali, J. Wang, H. Zhu, and J. Wang, "An expedited predictive distributed antenna system based handover scheme for high-speed railway," in *GLOBECOM 2017 - 2017 IEEE Global Communications Conference*, pp. 1–6, Dec 2017.

[13] S. Firouzabadi and A. J. Goldsmith, "Downlink performance and capacity of distributed antenna systems," *CoRR*, vol. abs/1109.2957, 2011.

[14] T. L. Marzetta, "Noncooperative cellular wireless with unlimited numbers of base station antennas," *IEEE Transactions on Wireless Communications*, vol. 9, pp. 3590–3600, Nov., 2010.

[15] Z. Chen and E. Björnson, "Channel hardening and favorable propagation in cell-free massive MIMO with stochastic geometry," *IEEE Transactions on Communications*, pp. 1–1, 2018.

[16] R. Sabbagh, H. Zhu, and J. Wang, "Pilot allocation and sum-rate analysis in distributed massive MIMO systems," in *2017 IEEE 86th Vehicular Technology Conference (VTC-Fall)*, pp. 1–5, Sept 2017.

[17] E. Nayebi, A. Ashikhmin, T. L. Marzetta, and H. Yang, "Cell-free massive MIMO systems," in *2015 49th Asilomar Conference on Signals, Systems and Computers*, pp. 695–699, Nov 2015.

[18] H. Q. Ngo, A. Ashikhmin, H. Yang, E. G. Larsson, and T. L. Marzetta, "Cell-free massive MIMO versus small cells," *IEEE Transactions on Wireless Communications*, vol. 16, pp. 1834–1850, March 2017.

[19] T. H. Nguyen, T. K. Nguyen, H. D. Han, and V. D. Nguyen, "Optimal power control and load balancing for uplink cell-free multi-user massive MIMO," *IEEE Access*, vol. 6, pp. 14462–14473, 2018.

[20] H. Q. Ngo, L. Tran, T. Q. Duong, M. Matthaiou, and E. G. Larsson, "On the total energy efficiency of cell-free massive MIMO," *IEEE Transactions on Green Communications and Networking*, vol. 2, pp. 25–39, March 2018.

[21] E. Björnson, J. Hoydis, and L. Sanguinetti, *Massive MIMO Networks: Spectral, Energy, and Hardware Efficiency*. Foundations and Trends(r) in S, Now Publishers, 2017.

[22] E. Björnson and E. Jorswieck, *Optimal Resource Allocation in Coordinated Multi-Cell Systems*, vol. 9. Now Publishers, Jan. 2013.

[23] S. Buzzi and C. D'Andrea, "Cell-free massive MIMO: User-centric approach," *IEEE Wireless Communications Letters*, vol. 6, pp. 706–709, Dec 2017.

[24] Z. Chen, X. Hou, and C. Yang, "Training resource allocation for user-centric base station cooperation networks," *IEEE Transactions on Vehicular Technology*, vol. 65, pp. 2729–2735, April 2016.

[25] E. Bjornson, R. Zakhour, D. Gesbert, and B. Ottersten, "Cooperative multicell precoding: Rate region characterization and distributed strategies with instantaneous and statistical CSI," *IEEE Transactions on Signal Processing*, vol. 58, pp. 4298–4310, Aug 2010.

[26] D. Brélaz, "New methods to color the vertices of a graph," *Commun. ACM*, vol. 22, pp. 251–256, Apr. 1979.

[27] A. Paulraj, R. Nabar, and D. Gore, *Introduction to Space-Time Wireless Communications*. New York, NY, USA: Cambridge University Press, 1st ed., 2008.

[28] V. Saxena, "Pilot contamination and mitigation techniques in massive MIMO systems," *Ph.D. dissertation, Department of Electrical and Information Technology, Lund University, Lund, Sweden,*, Feb. 2014.

[29] T. L. Marzetta, E. G. Larsson, H. Yang, and H. Q. Ngo, *Fundamentals of Massive MIMO*. Cambridge University Press, 2016.

[30] E. G. Larsson, O. Edfors, F. Tufvesson, and T. L. Marzetta, "Massive MIMO for next generation wireless systems," *IEEE Communications Magazine*, vol. 52, pp. 186–195, Feb. 2014.

[31] A. Tolli, M. Codreanu, and M. Juntti, "Cooperative MIMO-OFDM cellular system with soft handover between distributed base station antennas," *IEEE Transactions on Wireless Communications*, vol. 7, pp. 1428–1440, April 2008.

[32] C. Pan, H. Mehrpouyan, Y. Liu, M. Elkashlan, and N. Arumugam, "Joint pilot allocation and robust transmission design for ultra-dense user-centric TDD C-RAN with imperfect CSI," *IEEE Transactions on Wireless Communications*, vol. 17, pp. 2038–2053, March 2018.

[33] S. M. Kay, *Fundamentals of Statistical Signal Processing: Estimation Theory*. Upper Saddle River, NJ, USA: Prentice-Hall, Inc., 1993.

[34] O. Y. Bursalioglu, C. Wang, H. Papadopoulos, and G. Caire, "RRH based massive MIMO with "on the fly" pilot contamination control," in *2016 IEEE International Conference on Communications (ICC)*, pp. 1–7, May 2016.

[35] G. Interdonato, H. Q. Ngo, E. G. Larsson, and P. Frenger, "How much do downlink pilots improve cell-free massive MIMO?," in *2016 IEEE Global Communications Conference (GLOBECOM)*, pp. 1–7, Dec 2016.

[36] L. Wang and Q. Liang, "Optimization for user centric massive MIMO cell free networks via large system analysis," in *2016 IEEE Global Communications Conference (GLOBECOM)*, pp. 1–1, Dec 2016.

[37] H. Yang and T. L. Marzetta, "Performance of pilot reuse in multi-cell massive MIMO," in *2015 IEEE International Black Sea Conference on Communications and Networking (BlackSeaCom)*, pp. 157–161, May 2015.

[38] X. Zhu, L. Dai, and Z. Wang, "Graph coloring based pilot allocation to mitigate pilot contamination for multi-cell massive MIMO systems," *IEEE Communications Letters*, vol. 19, pp. 1842–1845, Oct. 2015.

[39] H. Yin, D. Gesbert, M. Filippou, and Y. Liu, "A coordinated approach to channel estimation in large-scale multiple-antenna systems," *IEEE Journal on Selected Areas in Communications*, vol. 31, pp. 264–273, Feb. 2013.

[40] K. Upadhya, S. A. Vorobyov, and M. Vehkapera, "Superimposed pilots are superior for mitigating pilot contamination in massive MIMO," *IEEE Transactions on Signal Processing*, vol. 65, pp. 2917–2932, June 2017.

[41] J. Ma and L. Ping, "Data-aided channel estimation in large antenna systems," *IEEE Transactions on Signal Processing*, vol. 62, pp. 3111–3124, June 2014.

[42] F. Fernandes, A. Ashikhmin, and T. L. Marzetta, "Inter-cell interference in non-cooperative TDD large scale antenna systems," *IEEE Journal on Selected Areas in Communications*, vol. 31, pp. 192–201, Feb. 2013.

[43] X. Yan, H. Yin, M. Xia, and G. Wei, "Pilot sequences allocation in TDD massive MIMO systems," in *2015 IEEE Wireless Communications and Networking Conference (WCNC)*, pp. 1488–1493, Mar. 2015.

[44] H. Huh, G. Caire, H. C. Papadopoulos, and S. A. Ramprashad, "Achieving massive MIMO spectral efficiency with a not-so-large number of antennas," *IEEE Transactions on Wireless Communications*, vol. 11, no. 9, pp. 3226–3239, 2012.

[45] Q. Sun, J. Wang, S. Jin, C. Xu, X. Gao, and K. K. Wong, "Rate analysis and pilot reuse design for dense small cell networks," in *IEEE International Conference on Communications (ICC)*, pp. 2845–2850, Jun. 2015.

[46] L. You, X. Gao, X. G. Xia, N. Ma, and Y. Peng, "Pilot reuse for massive MIMO transmission over spatially correlated rayleigh fading channels," *IEEE Transactions on Wireless Communications*, vol. 14, pp. 3352–3366, Jun. 2015.

[47] Q. He, L. Xiao, X. Zhong, and S. Zhou, "Increasing the sum-throughput of cells with a sectorization method for massive MIMO," *IEEE Communications Letters*, vol. 18, pp. 1827–1830, Oct. 2014.

[48] H. Huang, M. Trivellato, A. Hottinen, M. Shafi, P. J. Smith, and R. Valenzuela, "Increasing downlink cellular throughput with limited network MIMO coordination," *IEEE Transactions on Wireless Communications*, vol. 8, pp. 2983–2989, June 2009.

[49] F. Boccardi and H. Huang, "Limited downlink network coordination in cellular networks," in *2007 IEEE 18th International Symposium on Personal, Indoor and Mobile Radio Communications*, pp. 1–5, Sep. 2007.

[50] A. Tolli, M. Codreanu, and M. Juntti, "Cooperative MIMO-OFDM cellular system with soft handover between distributed base station antennas," *IEEE Transactions on Wireless Communications*, vol. 7, pp. 1428–1440, April 2008.

[51] S. Kaviani and W. A. Krzymien, "Multicell scheduling in network MIMO," in *2010 IEEE Global Telecommunications Conference GLOBECOM 2010*, pp. 1–5, Dec 2010.

[52] S. Buzzi and C. D'Andrea, "User-centric communications versus cell-free massive MIMO for 5G cellular networks," in *WSA 2017; 21th International ITG Workshop on Smart Antennas*, pp. 1–6, March 2017.

[53] E. Björnson, E. G. Larsson, and M. Debbah, "Massive MIMO for maximal spectral efficiency: How many users and pilots should be allocated?," *IEEE Transactions on Wireless Communications*, vol. 15, pp. 1293–1308, Feb. 2016.

[54] J. Hoydis, S. ten Brink, and M. Debbah, "Massive MIMO in the UL/DL of cellular networks: How many antennas do we need?," *IEEE Journal on Selected Areas in Communications*, vol. 31, pp. 160–171, Feb. 2013.

[55] T. Kailath, B. Hassibi, and A. H. Sayed, *Linear estimation*. Upper Saddle River, NJ: Prentice-Hall; London: Prentice-Hall International, 2000.

[56] T. V. Chien, E. Björnson, and E. G. Larsson, "Joint power allocation and user association optimization for massive MIMO systems," *IEEE Transactions on Wireless Communications*, vol. 15, pp. 6384–6399, Sept 2016.

[57] T. Rappaport, *Wireless Communications: Principles and Practice*. Upper Saddle River, NJ, USA: Prentice Hall PTR, 2nd ed., 2001.

[58] R. L. Graham, D. E. Knuth, and O. Patashnik, *Concrete Mathematics: A Foundation for Computer Science*. Boston, MA, USA: Addison-Wesley Longman Publishing Co., Inc., 2nd ed., 1994.

[59] R. Hankin and L. West, "Set partitions in R," *Journal of Statistical Software, Code Snippets*, vol. 23, no. 2, pp. 1–12, 2007.

[60] "Evolved Universal Terrestrial Radio Access (E-UTRA); Further advancements for E-UTRA physical layer aspects (Release 9)," *3GPP Tech. Rep. 36.814*, March 2010.